A Re-Evaluation of the Evolved Stars in the Globular Cluster M13[1]

Eric L. Sandquist, Mark Gordon, Daniel Levine

Department of Astronomy, San Diego State University, San Diego, CA 92182

Michael Bolte

UCO/Lick Observatory, University of California, Santa Cruz, CA 95064

ABSTRACT

We have analyzed photometry from space- and ground-based cameras to identify *all* bright red giant branch (RGB), horizontal branch (HB), and asymptotic giant branch (AGB) stars within $10'$ of the center of the globular cluster M13.

We identify a modest (7%) population of HB stars redder than the primary peak (including RR Lyrae variables at the blue end of the instability strip) that is somewhat more concentrated to the cluster core than the rest of the evolved stars. We find support for the idea that they are noticeably evolved and in the late stages of depleting helium in their cores. This resolves a disagreement between distance moduli derived from the tip of the red giant branch and from stars in or near the RR Lyrae instability strip. We identified disagreements between HB model sets on whether stars with $T_{\rm eff} \lesssim 10000$ K (near the "knee" of the horizontal branch in optical CMDs) should evolve redward or blueward, and the differences may depend on the inclusion of diffusion in the stellar interior. The sharp cut at the red end of M13's HB provides strong evidence that stars from the dominant HB group must still be undergoing blue loops, which implies that diffusion is being inhibited. We argue that M13's HB is a somewhat pathological case — the dominant HB population occurs very near the "knee" in optical CMDs, and evolved stars exclusively appear redward of that peak, leading to the incorrect appearance of a continuation of the unevolved HB.

We identify two stars as "blue hook" star candidates — the faintest stars in optical bands that remain significantly subluminous in the shortest ultraviolet wavelength photometry available. M13 also has a distinct group of stars previously identified with the "second U jump". Based on far UV photometry, we find that these stars have genuinely high temperatures (probably 26000 K $\lesssim T_{\rm eff} \lesssim$ 31000 K), and are not produced by a jump in brightness at lower temperature ($T_{\rm eff} \approx 22000$ K) as previously suggested. These stars are brighter

than other stars of similar color (either redder or bluer), and may be examples of "early hot flashers" that ignite core helium fusion shortly after leaving the red giant branch. We used ultraviolet photometry to identify hot post-HB stars, and based on their numbers (relative to canonical AGB stars) we estimate the position on the HB where the morphology of the post-HB tracks change to $I \sim 17.3$, between the two peaks in the HB distribution.

Concerning the possibility of helium enrichment in M13, we revisited the helium-sensitive R ratio, applying a new method for correcting star counts for larger lifetimes of hot horizontal branch stars. We find that M13's R ratio is in agreement with theoretical values for primordial helium abundance $Y_P = 0.245$ and inconsistent with a helium enhancement $\Delta Y = 0.04$. The brightness of the horizontal branch (both in comparison to the end of the canonical HB and to the tip of the red giant branch) also appears to rule out the idea that the envelopes of the reddest HB stars have been significantly enriched in helium. The absolute colors of the turnoffs of M3 and M13 may potentially be used to look for differences in their mean helium abundances, but there are inconsistencies in current datasets between colors using different filters that prevent a solid conclusion.

The numbers of stars on the lower red giant branch and in the red giant bump agree very well with recent theoretical models, although there are slight indications of a deficit of red giant stars above the bump. There is not convincing evidence that a large fraction of stars leave the RGB before undergoing a core helium flash.

Subject headings: stars: AGB and post-AGB — stars: evolution — Hertzsprung-Russell and C-M diagrams — stars: horizontal branch — globular clusters: individual (M13) — ultraviolet: stars

1. Introduction

M13 was one of the first globular clusters identified as having unusually blue horizontal branch (HB) stars, and it remains one of the prototypes of the "long blue tail" with stars

[1]Based on observations made with the NASA/ESA Hubble Space Telescope, obtained from the data archive at the Space Telescope Science Institute. STScI is operated by the Association of Universities for Research in Astronomy, Inc. under NASA contract NAS5-26555.

approaching the main sequence for helium stars. As Smith (2005) notes, differences between stars on both giant branches and stars on the horizontal branch can be discerned from data in papers as early as Barnard (1909, 1914). Along with the nearby, massive, and little reddened cluster M3, M13 forms half of the best known "second parameter" pair. The chemical composition of the hydrogen envelopes of HB stars affects their observable properties via opacity and mean molecular weight. The "first parameter" is heavy element content, where higher metallicity produces higher envelope opacity and generally redder stars. Because M3 and M13 have nearly the same iron abundances ($\langle$[Fe/H]$\rangle = -1.53$ for M13 versus $\langle$[Fe/H]$\rangle = -1.45$ for M3; Sneden et al. 2004) but M3 has a much redder HB including a huge number of RR Lyrae variable stars, a second parameter is needed. In addition to the color shift between the HBs of M3 and M13, the HB stars in M13 show a bimodal distribution that is not present in M3. On its own, this fact implies that the HB stars were produced by at least two different populations of cluster stars or involve different methods of producing HB stars. M3 and M13 share a number of similarities beyond iron abundance, and we tabulate some of their characteristics in Table 1.

Many theories have been proposed to explain the HB differences, and two of the main goals of this paper are to 1) assemble a large and complete set of photometric data for M13, and 2) use the photometric data to examine questions bearing on the production of M13's horizontal branch stars. Because of the complexity of the HB, it is very doubtful that one explanation can cover all of its aspects. Before we describe our results, we briefly summarize the main hypotheses we will examining, and the primary reasons they are viable. We emphasize that they are not mutually exclusive.

The Δt Hypothesis. Early models showed that as the mass of the hydrogen-rich envelope of an HB star is decreased, the surface temperature increases with relatively little change in luminosity. In this hypothesis, age differences between populations of stars lead to differences in mass between stars leaving the main sequence and between stars reaching the HB. While it is natural to expect that clusters in the Milky Way were born at different times, age differences are hard to prove except for clusters that are much younger than the average. Rey et al. (2001) compared M13 with M3 and found that turnoff-to-giant branch color differences and changes in HB morphology were consistent with an age difference $\Delta t = 1.7 \pm 0.7$ Gyr (with M13 older). Catelan (2009) finds that the age differences implied by differences in the cluster CMDs near the turnoff can explain the HB morphology as long as M3 is younger than about 12 Gyr and the EHB stars in M13 are presumed to arise from a process that is unrelated to the age. However, there are aspects of M13's population that cannot be explained in this hypothesis. For example, neither of the studies above could reproduce the bluest HB stars in M13 in synthetic HB simulations using the same chemical composition and dispersion in stellar mass used for M3.

The ΔY Hypothesis. Variations in helium content (Y) result in differences in position on the HB, largely because greater helium abundance allows lower mass stars to leave the main sequence at the present day (D'Antona & Caloi 2008b). Johnson & Bolte (1998) proposed that a helium abundance difference $\Delta Y \sim 0.05$ (with M13 the more helium rich) could be responsible for many of the unusual features of the color-magnitude diagram (CMD), including an interesting difference in the slopes of the subgiant branch. Caloi & D'Antona (2005) also examined data for M3 and M13, finding the luminosity of the red giant bump and RR Lyrae stars relative to the cluster turnoff are consistent with an enhancement $\Delta Y \sim 0.04$. This picture has been taken very seriously with the discovery of multiple stellar populations in some clusters. For example, NGC 2808 was found to have at least three identifiable main sequences (Piotto et al. 2007), while ω Cen has a blue main sequence (Bedin et al. 2004) that appears to be helium enriched (Piotto et al. 2005). ω Cen and NGC 2808 are among the most massive clusters known in the Milky Way, which may enable them to retain gas that has been processed and released by a first generation of stars.

While the helium abundance is very difficult to measure except in limited circumstances, spectroscopic observations of other heavy element species lead to the belief that helium was probably enriched in some clusters. Stars in M13 are well-known to have star-to-star abundance differences in O and Na that can be traced from the giant branch (Smith & Briley 2006; Yong et al. 2006; Johnson et al. 2005; Smith et al. 2005; Sneden et al. 2004) to the main sequence turnoff (Cohen & Meléndez 2005; Briley et al. 2004). O depletion and Na enrichment can only be accomplished in hydrogen-fusion regions where significant production of helium is accomplished (Denisenkov & Denisenkova 1989; Langer et al. 1993), and star-to-star variations on the main sequence require that they must have been present in the gas forming the stars.

The ΔY hypothesis is attractive for M13 because it may explain the blueward shift of the main body of HB stars compared to M3's population, and the bimodality of the HB (as an additional population within the cluster). D'Antona & Caloi (2008b) conducted a fit to M13's HB using helium-enriched models, and found that a fit required 70% of the population to be enriched to $0.27 < Y < 0.35$ (a mean $\Delta Y \approx 0.04$), and the remaining 30% to be enriched to $Y \sim 0.38$. There are some difficulties with this picture though. In the D'Antona & Caloi models of M13, they still needed to assume a rather large (but constant) total mass loss on the RGB ($0.18 M_{\odot}$). Because M13 has few HB stars in the instability strip or redward (where M3's HB is heavily populated), *virtually all* of M13's HB stars must also be more helium rich than M3's. This is in striking contrast to more massive clusters that show strongly bimodal HB star distributions in which the redder HB population is interpreted as a first generation of stars formed from primordial material, while subsequent generations have varying degrees of enrichment and are bluer. The massive clusters that are inferred

to have such large spreads in Y generally also have multiple main sequence or subgiant branch populations, whereas M13 has shown no sign of multiple populations to date. There is also not a clear bimodality in the spectroscopic abundances and a definite connection has never been made between the abundances and HB morphology (although see Carretta et al. 2007, for indications that the maximum $T_{\rm eff}$ extent of the HB is correlated with the extent of observed Na-O anticorrelations). Rey et al. (2001) attribute some of Johnson & Bolte's conclusions to slight missteps in the implementation of their relative age comparison.

The $\dot{M}$ Hypothesis. From early models, it was recognized that a significant amount of mass loss is needed, probably on the red giant branch (RGB), to produce the colors of the majority HB populations in most clusters. Dispersion in colors was then taken to mean that there are star-to-star differences in mass loss, although a mechanism to produce these differences has not been identified.

Independent of the majority of HB stars, there is a population that seems to *require* strong mass loss: the "blue hook" stars (Castellani & Castellani 1993; D'Cruz et al. 1996; Castellani et al. 2006a; Miller Bertolami et al. 2008). In ultraviolet color-magnitude diagrams of some of the most massive clusters (D'Cruz et al. 2000; Brown et al. 2001), stars are found fainter and redder than the zero-age HB (ZAHB) at its blue end, meaning that they must have almost no hydrogen envelope. If a star loses virtually all of its hydrogen envelope before reaching the tip of the RGB, it can leave the RGB without igniting core helium fusion. As the star contracts onto the He white dwarf cooling curve, a late He flash can be ignited that drives a convection zone that reaches hydrogen rich layers (Brown et al. 2001).

The Evolution Hypothesis. As relatively cool HB stars convert He into carbon and oxygen, they are expected to eventually evolve brightward and redward toward the asymptotic giant branch (AGB). Depending on the distribution of stars on the HB, evolving HB stars could be mistaken for fainter, more slowly evolving HB stars, thereby misrepresenting the brightness of the HB. Clusters with large blue HB populations (like M13) are most susceptible to this effect because evolutionary tracks may nearly parallel the ZAHB at the blue end of the HB distribution where the relative number of unevolved stars drops rapidly. Because the HB is a frequently used standard candle in astronomy, it is worth studying the degree to which this affects stellar populations.

Evolutionary effects have been inferred from the pulsation properties of RR Lyrae stars. For example, Jurcsik et al. (2003) used magnitudes and periods to identify RR Lyraes in different stages of their HB evolution. Cacciari et al. (2005) identified mean lines in the period-amplitude diagram for different subsets of M3 variables, and labeled them as regular or "well-evolved". They showed that in at least some other clusters, the majority of variables

could be identified with one group or the other.

For the purposes of this paper we focused on post main-sequence evolution. Using datasets from telescopes and instruments having a wide range in spatial resolution and field size, we attempted to completely survey the evolved stars from the center far into the outskirts of the cluster. We discuss the observational material and the analysis of the photometry in §2. In §3, we describe the steps used to identify the evolutionary status of the evolved cluster stars. We examine the red giant branch and horizontal branch populations in greater detail in §4 and §5, respectively. In §6 we look at population ratios and their relationship to the evolution timescales for stars in different stages. Finally in §7 we discuss the body of evidence involving second parameter effects (cluster to cluster variations) and intracluster differences between stars.

2. Datasets

2.1. Archival Hubble Space Telescope Imaging

We used WFPC2 images taken in three different studies and ACS images from one additional study for photometric measurements. The principal investigators and filters used are listed in Table 2. The images from proposal 8174 were composed of three partially overlapping fields that were reduced separately and later combined.

All of the WFPC2 images were processed using the HSTPhot[2] package (version 1.1.7b), which was described by Dolphin (2000a). Star positions for each set of processed data were derived using the IRAF task METRIC, which we used to convert the HSTPhot pixel coordinates to RA and DEC. METRIC positions often have absolute errors of up to $0\farcs5$, but absolute errors are not important for our purposes. The RA and DEC coordinates were converted to a system relative to the cluster center (Fig. 1). The data for each star, including coordinates, flight system magnitudes, and errors, were extracted from each dataset and merged into one master file. In cases where a star had multiple measurements in the same filter, the values were averaged using weights derived from the measurement errors. This master dataset was used to construct CMDs that we used to identify post-MS stars. The F160BW images were reduced separately because the filter distorts star positions relative to the rest of the images, complicating the matching of stars within HSTPhot. After completing the photometry, we were then able to match all of the stars with previously identified HB and AGB stars.

[2]`http://purcell.as.arizona.edu/hstphot/`

The ACS Wide Field Camera (WFC) images were processed using the DOLPHOT[3] package with its module for ACS data. DOLPHOT tasks mask bad pixels, correct for effective pixel area, and do point-spread function photometry. Individual frames (prior to drizzling in the ACS pipeline) were obtained from the HST Archive in order to get photometry on stars covering the widest possible dynamical range (including stars that were saturated on long exposures) and to avoid the pixel resampling that goes along with the drizzling process.

Because the WFC sits far from the optical axis of *HST*, there is significant geometric distortion of these images. For the purposes of the photometry, the differences in effective pixel area were corrected within DOLPHOT through the use of a pixel area map provided on the ACS website[4]. DOLPHOT, however, does not currently correct pixel positions to sky coordinates. For the purposes of *relative* astrometry, we used the fourth-order polynomial corrections provided in the most recent IDCTAB file for the dataset (qbu1641sj_idc.fits). These corrections reduce distortions to about 0.1 pixels, which is more than adequate for our purposes. The star positions were later put on a common coordinate system with photometry from WFPC2 images as described below.

2.2. Archival CFHT Images

The Hubble Space Telescope is very effective at resolving the core of the cluster, but its approximately $3'$ by $3'$ field of view is insufficient to capture most of the cluster stars. We thus turned to the archive of the Canada-France-Hawaii Telescope (CFHT) CFH12K camera for data covering the majority of the globular cluster (Fig. 1), with data collected by J.-H. Park, Y.-J. Sohn, and S. J. Oh in Feb. 2001 using B, V, and Cousins I filters. This camera is composed of a mosaic of 12 CCD's, of which we only used numbers 11 and 12 because these two chips covered the most heavily populated parts of the cluster. Each chip covers a roughly $7'$ by $14'$ area of sky. The images we obtained from the CFHT archive were already bias-subtracted and flat-fielded. For the photometry, we used the DAOPHOT II/ALLSTAR packages (Stetson 1987). Star positions in the CFHT images, like the HST images, needed to be transformed from pixel coordinates into angular offsets from the cluster center. We cross-identified stars from the USNO A2.0 catalog, covering an approximately $18.3'$ by $16.7'$ area of sky around the cluster that encompassed the CFHT field. These catalog stars were used to convert the CFHT pixel positions into RA and DEC coordinates relative to the core of M13. In regions of overlap, the HST datasets were placed on the same

[3]`http://purcell.as.arizona.edu/dolphot/`

[4]`http://www.stsci.edu/hst/acs/analysis/PAMS`

coordinate system.

2.3. KPNO 0.9m Imaging

We also reduced imaging the KPNO 0.9 m telescope taken in B, V, and Cousins I filters by Bolte and Sandquist on two nights in May 1995. The camera used a single 2048 × 2048 CCD with a scale of $0\farcs68$ per pixel, for a field of view $23\farcm2$ on a side. The photometry was done similarly to the CFHT dataset, and coordinates were transformed to the CFHT system.

2.4. Proper Motion (PM) Studies

We cross identified all stars from the proper motion studies of Cudworth & Monet (1979) and Cudworth (1979). The field covered by these studies is similar in size to that of the KPNO images. For the brightest stars, membership probabilities were available to within about $1'$ of the cluster center, while for fainter stars the innermost $2 - 3'$ was effectively excluded. Their photometry had a faint limit at $V \sim 15.6$, which is about 0.5 mag fainter than the red end of the HB. As a result, the proper motion membership probabilities were useful primarily for identifying bright stars that would otherwise contaminate post-HB and giant star samples.

2.5. Archival UIT Imaging

The archive of the Ultraviolet Imaging Telescope contains aperture and point-spread function photometry of M13 produced following the procedures described in Stecher et al. (1997), and the images involved have previously been discussed by Parise et al. (1994). However, in examining the UIT images, we found a large number of sources that were not recorded by Parise et al. or in the UIT archive file, and these match up with horizontal branch stars identified with optical photometry. It appears that the earlier photometry had an unnecessarily high faint limit.

We therefore rereduced the two longest exposure far UV images (using the B5 filter with central wavelength 1620 Å) taken on the Astro 2 mission (fuv2418, 192.5 s; fuv2419, 953.5

s). We downloaded archived IDL reduction routines called MOUSSE[5] for use on linearized, flat-fielded digitizations of the original photographic images. The *uit_find* routine identifies significant sources using an algorithm based on DAOPHOT, and determines centroided positions for each. The *uit_aper* routine conducts aperture photometry. We used a 3 pixel radius aperture recommended by Parise et al. (1994) and verified that the measurements matched the archived aperture photometry to within 0.01 mag for sources in common. The shorter fuv2418 exposure was analyzed to allow the brightest sources to be incorporated, as they were saturated on the longer exposure.

Many sources could be identified in the core of the cluster because crowding is relatively mild in the far UV. However, crowding does significantly modify the photometry, so we will generally restrict our discussion to stars more than $120''$ from the cluster center, as did Parise et al. (1994). This partly resulted from the pixel scale (pixels in the digitized photographs have a scale of about $1\farcs14$) and tracking inaccuracy in the longer fuv2419 exposure. We identified a few instances of blending in the UIT observations outside this radius when stars on the blue tail of the HB were close enough together on the sky. We rated UIT detections by hand based on the apparent degree of contamination, and will only plot stars with the best ratings.

We note that only in one case (ID 72) did we find a star that was very likely to be a proper motion nonmember, and in two other cases (UIT source 568; ID 3904) did we find stars that could not be identified as HB or AGB stars. ID 72 has optical photometry that places it only about 0.2 mag brighter than the HB level. We found no clear counterpart to UIT source 568 ($m_{1620} = 15.98$), and hypothesize that it might be related to the faint UV sources found in HST photometry by Ferraro et al. (1997). Source (ID 3904) corresponds to a bright blue straggler star in optical photometry.

2.6. Photometry Calibration

2.6.1. CFHT

We calibrated the BVI PSF photometry from CFHT to the standard system using standard stars from M13 described in Stetson (2000). These standard stars are rigorously matched to the same photometric system as the earlier Landolt (1992) study. We obtained the 2 May 2005 update star list from the CADC website[6]. The conditions for the CFHT

[5]http://archive.stsci.edu.uit/analysis.html

[6]`http://cadcwww.dao.nrc.ca/standards/`

observations did not appear to be photometric, so the magnitude zeropoints for each image were free parameters in the calibration.

Standard stars in the Stetson field cover almost the entire range of colors for evolved stars: from stars at the faint end of the HB distribution to a giant star within 0.5 V mag of the RGB tip. Three redder stars (probably field) were included to extend the color calibration closer to the color of the tip ($B - I \approx 3.1$). We found it necessary to calibrate the two CFHT12k CCD samples separately because of significant differences in color terms. (This is consistent with the results of other studies — for an example, see Kalirai et al. 2001.) Using the CCDSTD (e.g., Stetson 1992) program, the standard star transformation equations were found to be:

$$b = B + a_i + (-0.025 \pm 0.006)(B - I) + (0.0084 \pm 0.0029)(B - I)^2$$

$$v = V + b_i + (-0.0038 \pm 0.0026)(B - I)$$

$$i = I + c_i + (-0.0079 \pm 0.0025)(B - I)$$

for chip 11, and

$$b = B + a_i + (-0.030 \pm 0.004)(B - I) + (-0.0173 \pm 0.0018)(B - I)^2$$

$$v = V + b_i + (-0.0084 \pm 0.0013)(B - I)$$

$$i = I + c_i + (-0.0011 \pm 0.0012)(B - I)$$

for chip 12, where b, v, and i are instrumental magnitudes, B, V, and I are standard magnitudes, and a_i, b_i, and c_i are the zero points for individual frames. The $(B - I)$ color was chosen primarily for its wide wavelength spacing, which helps minimize the importance of photometric errors in B or I. We compared the final calibrated measurements with the Stetson standard values, as shown in Fig. 2. The comparisons include 417 stars from chip 11 and 286 stars from chip 12. The median residuals ΔB, ΔV, ΔI, and $\Delta(B - I)$ were all less than 0.003 mag for the samples from both CCDs, and consistent with zero. There do not seem to be significant systematic trends at the extremes of the color range either.

2.6.2. HST

For most purposes, we preferred to leave the HST datasets in flight system magnitudes using the VEGAMAG zeropoints in order to maintain the relative precision of the original photometry and to make it possible for others to use improved transformations to a standard system in the future. However, to produce uniform samples of stars from photometric datasets in different regions of the cluster, we did need to derive some transformations.

Because the CFHT photometry appears to be accurately matched to the standard system and because the CFHT images had good spatial resolution in the cluster core, we use this dataset to examine the calibration of the ACS WFC photometry in V and I. The comparison involves HB and faint RGB stars because stars high on the RGB were heavily saturated even on the shortest exposures. In comparing the ACS flight system magnitudes to the CFHT photometry, it was clear that second-order color terms in color were needed to transform the F606W observations, but a first order term seemed sufficient to transform the F814W observations. This is in agreement with the transformations derived by Sirianni et al. (2005). However, we found that when we used the Sirianni et al. transforms, the RGB stars were systematically too faint by about 0.04 mag. We therefore derived our own transformations. It was necessary to iterate the process, eliminating stars with large positive residuals (most likely due to blending in the CFHT dataset). The following transformations were derived from 437 stars:

$$m_{606} = V + (0.010 \pm 0.004) + (-0.0592 \pm 0.0174)(V-I) + (-0.1553 \pm 0.0207)(V-I)^2$$

$$m_{814} = I + (-0.005 \pm 0.004) + (0.0290 \pm 0.0053)(V-I)$$

Fig. 3 shows the comparison between the CFHT photometry and the ACS photometry calibrated to VI.

For a small number of stars, WFPC2 images were the primary source for photometry, thanks to crowding and/or gaps in sky coverage. We used WFPC2 photometry in the VEGAMAG system, but have calibrated measurements in the F555W and F785LP bands to V and I. We first used the standard calibration of Dolphin (2000b), but found that there were large color-dependent residuals. As a result, we determined new transformation equations using 153 RGB and HB stars in common with the CFHT data (eliminating stars that were most likely to be blended, as we did with the ACS data):

$$m_{555} = V + (0.065 \pm 0.009) + (0.0860 \pm 0.0364)(V-I) + (0.0207 \pm 0.0498)(V-I)^2$$

$$m_{785} = I + (0.051 \pm 0.010) + (0.1346 \pm 0.0413)(V-I) + (-0.2869 \pm 0.0557)(V-I)^2$$

The transformed WFPC2 and CFHT datasets are compared in Fig. 4. Although the formal errors on the quadratic term for the m_{555} equation imply it has low significance, it was our qualitative judgement that it improved the transformation at the red end of the color range.

For a small number of stars at the faint end of the RGB in the cluster core, the only reliable near-infrared measurements were in the WFPC2 field of proposal 8278, and so this was also calibrated to CFHT measurements using a sample of 87 RGB and HB stars:

$$m_{555} = V + (0.052 \pm 0.011) + (0.0538 \pm 0.0428)(V-I) + (-0.0378 \pm 0.0629)(V-I)^2$$

$$m_{814} = I + (0.021 \pm 0.012) + (0.3233 \pm 0.0481)(V - I) + (-0.3328 \pm 0.0688)(V - I)^2$$

In the color range covered by the stars with WFPC2 photometry, the two calibrations typically agree to better than 0.05 mag.

2.6.3. KPNO

We observed Landolt standard fields on one photometric night from the KPNO run, and a standard star calibration using these data was used in calibrating cluster data from previous studies (Hargis et al. 2004; Pollard et al. 2005; Fekadu et al. 2007). In this paper we have opted to calibrate the KPNO photometry directly against the well-observed Stetson (2000) standards in the M13 field used to calibrate the CFHT data. To ensure the calibration of the evolved populations, we restricted the standard star sample to 343 stars brighter than the approximate turnoff of the cluster ($V < 19$). The transformation equations are

$$b = B + a_i + (-0.0279 \pm 0.0018)(B - I)$$

$$v = V + b_i + (-0.0002 \pm 0.0017)(B - I)$$

$$i = I + c_i + (-0.0130 \pm 0.0020)(B - I)$$

The residuals of the calibration are shown in Fig. 5. The median residuals in all cases (B, V, I, $B-V$, and $V-I$) are less than 0.005 mag, and well within the uncertainty in the fit. There may be some small systematic trends at the extreme ends of the color range for the standard stars: $(B-V) \lesssim -0.1$ and $(B-V) > 1.2$. After additional experiments though, we found that second-order color terms or changes to the standard star sample (fewer main sequence turnoff standard stars, so that the giant and horizontal branch stars carried more weight) did not significantly improve the fits.

For most of the scientific applications later in the paper, the relative precision of photometric measurements within one dataset is most important. However, for the discussion of HB and RGB luminosity functions, it is important that there are not large systematic errors between the datasets we have merged together. The luminosity functions will employ the I-band measurements, so particular attention should be focused on that filter. Figures 6 and 7 show comparisons between the KPNO photometry and the CFHT photometry from chip 11 and chip 12. There appear to be signs of systematic residuals in various places [notably some small offsets in V and I in chip 11, and a trend in $\Delta(B-V)$ versus $(B-V)$ for chip 12]. However, for the great majority of stars, the residuals are quite small ($\lesssim 0.04$ mag). In the KPNO-CFHT comparisons, the I-band measurements seem to be well calibrated.

3. Identification of Evolutionary Status

Our first step was to first identify all known variable stars (RR Lyrae, BL Her, bright giants) from Kopacki et al. (2003) in order to eliminate stars that might confuse classifications. Our subsequent procedure for separating stars by evolutionary stage involved all of the datasets described above (from widest area coverage to smallest: PM, KPNO, CFHT, HST ACS, and HST WFPC2). We relied primarily on the observations with the highest available spatial resolution for each portion of the field.

The main CMDs used to identify giant stars (RGB and AGB) are shown in Fig. 8. For the outermost portion of the field, the KPNO dataset was used along with proper motion information. The CFHT dataset was used for the bright RGB and AGB samples even within the core, driven by the fact that the brightest cluster stars were saturated in the HST images (with the exception of some exposures in the ultraviolet). Crowding effects were minor for the CFHT images, which were taken with good seeing and with a high resolution camera ($0\farcs2$ pixels). Because giant stars (RGB and AGB) were all observed in BVI filters and because the $B-I$ color covers the widest wavelength range, we used $B-I$ as their primary discriminant. For fainter RGB stars ($I > 14.5$), HST photometry was available in the core, and so ACS WFC photometry was used when available, and WFPC2 photometry for all other stars falling between WFC chips or outside the WFC field.

The HB and AGB manqué are comprised of hotter stars, so we relied on the shortest wavelength filters to identify them. For the portions of the core observed in the ultraviolet, the F160BW, F255W, and F336W filters on HST are particularly good discriminants (see Fig. 9), with the F160BW observations effectively selecting *only* the hottest HB stars and a handful of manqué stars. Otherwise the HST ACS observations were the primary source for identifications for the bluest horizontal branch stars in the core. HB candidates in the core were selected based on CMD position, but derived χ^2, sharpness, and crowding values were used to flag candidates that might be spurious. Questionable candidates were also examined by eye, and stars that clearly fell on chip defects or very close to brighter stars were rejected. The crowding parameter in DOLPHOT (the change in measured brightness if close neighbors had not been simultaneously fit with point-spread functions) was very effective at flagging spurious stars. We found that a change of 0.4 mag indicated a spurious star in nearly all cases. The optical CMDs used in the HB star selections are shown in Fig. 10.

Just outside the observed HST fields, there is noticeable scatter in the photometry measured from the CFHT images, as can be seen in the lower right panel of Fig. 10. To reliably identify blue HB stars in this region, we made use of UIT observations. UIT observations cover almost the entire field discussed in this paper, and even though blending sometimes made accurate photometry a problem in the core, the UIT observations allowed

us to identify blue HB stars even there. As a result, we believe we have virtually all of the faint HB stars in our sample, all the way from the cluster center out to the edge of our large ground-based fields.

AGB manqué stars also deserve discussion. In optical CMDs these stars (post-HB stars that will not reach the traditional AGB) are predicted to evolve almost parallel to the zero-age HB (ZAHB), and the hottest ones can sometimes be hard to distinguish from normal HB stars. Ultraviolet-optical CMDs can flatten out the blue HB and make it possible to identify AGB manqué stars by their relative brightness. For the majority of the field we identified candidates from the HB sample in the highest resolution optical CMD first. We subsequently used observations in F160BW and F255W for the core, and the wide-field UIT observations elsewhere to validate most of the candidates. We found that nearly all of the bluest candidates selected from the optical CMDs were verified with the ultraviolet observations, but 5 additional manqué stars were identified first in the UV. For the UV observations, we defined stars to be manqué if they were more than about 0.8 mag brighter than the faintest HB stars at the same color. (This criterion is based on where theoretical tracks predict evolution slows again after core He exhaustion.) The UIT observations were subject to blending in the central regions and some candidates were rejected based on high-resolution optical photometry, but in all cases it was possible to identify the stars that were the primary UV sources based on other photometry. In addition, some of the Whitney et al. (1995) sources did not appear to have cluster counterparts at the tabulated positions. We do not have an explanation for this. Two stars (HB 72 and 295) present reasonably strong cases in optical CMDs for being manqué, but are not discernibly unusual in the UV, so we have left them as HB stars. Finally, two manqué stars (AGB 12 and 26) were identified using only optical photometry because they fell outside the HST ultraviolet observations, but in a region of the cluster where the UIT images were too crowded to yield reliable measurements. All of our cross identifications are given in Table 3. The photometry for the identified stars can be found in Tables 4-7. With the use of the UV observations, we believe we have isolated nearly all AGB manqué stars from the HB sample.

4. The Red Giant Branch

We assembled a comprehensive tabulation of the bright RGB stars in M13 from the tip of the RGB to the base of the RGB, where it meets the subgiant branch. As described in §3, we eliminated AGB stars from the sample using the best photometry available (see Fig. 8). This is a relatively easy task in M13 because the AGB is well-separated in color from the RGB except near the bright end.

In a study of the cluster core using the HST Planetary Camera, Cohen et al. (1997) previously found evidence that there was an excess of bright giants compared to models. Though their photometry was not precise enough to separate AGB and RGB stars, the excess appeared to be too large to be explained by the AGB star population. To examine the evolution rates of the bright giants, we followed the procedure described by Sandquist & Martel (2007). In this method theoretical cumulative luminosity functions in I band are shifted in magnitude so that the tip of the giant branch matches the brightest giant, and the luminosity function is then normalized to the total number of stars found brighter than the RGB bump. Sandquist & Martel found that this has the benefit of making the comparison extremely insensitive to chemical composition and age, which makes it possible to test the physics of the upper giant branch in clusters with large giant populations. In that study, Sandquist & Martel found that the giant population in NGC 2808 was significantly depleted relative to the model predictions, and hypothesized that this could be due to underestimated neutrino emission rates or loss of the giant envelope (causing some giants to leave the RGB before undergoing a normal helium flash). We have therefore tested whether M13's very blue HB morphology is reflected in the character of the giant population. Sandquist & Hess (2008) recently examined a large sample in the core of the distant cluster NGC 2419 (another cluster with a long blue HB tail), which showed only weak signs of a depleted bright giant population.

To conduct the test for M13, we shifted Victoria-Regina (VandenBerg et al. 2006) and Teramo (Cassisi et al. 2004) models to the I magnitude of the brightest giant. We need to be careful because almost all of the brightest giants in M13 are known to vary irregularly on timescales of more than 40 d (Kopacki et al. 2003). The variability itself should be a relatively small effect based on the variation amplitudes observed by Kopacki et al. (2003): $0.07 < \Delta V < 0.38$ for the 12 stars studied, with most having amplitudes toward the low end of that range. We identified all of the known RGB variables, and find that V11 appears to be the brightest ($I \approx 10.3$) in our study and most others. (Our V-band measurements appear to have been made in brighter periods in the star's variation. According to Kopacki et al., the star's mean V magnitude is only a few hundredths of a magnitude different from other bright giants.)

Fig. 11 shows the comparison for a model having [Fe/H] $= -1.41$ and [α/Fe] $= +0.3$. We tested models with different metallicity, but as described earlier, the exact value does not significantly affect the results. In addition, the Victoria-Regina and Teramo models agree well with each other. The plotted Victoria-Regina model shows the best agreement with the observed position of the RGB bump. We conducted Kolmogorov-Smirnov (K-S) tests with the observed and theoretical luminosity functions using different faint cutoffs for the RGB sample. (Because the RGB sample increases exponentially with increasing magnitude, this

was necessary to ensure that deviations on the less-populated bright RGB are not washed out.) The test results are presented in Table 9. The probability P that the observed stars are consistent with being drawn from the theoretical distribution reaches a minimum of about 5% when the cutoff is at $I = 12.76$ in response to a clump of stars at $I \approx 12$ (see below). Otherwise, the probabilities remain greater than 15%, and the overall impression from the test is that there is at most a slight deficit of stars compared to the model predictions, in contrast to the Cohen et al. (1997) results.

As discussed by Sandquist & Martel (2007), this method of comparing with models is insensitive to chemical composition for [Fe/H] $\lesssim -1$, which means that it should be possible to combine samples from different clusters to improve the statistical significance of the comparisons. M5 has a readily available sample of RGB stars (Sandquist & Bolte 2004), and issues related to combining the two samples are minimal. For example, M5 and M13 have very similar distance moduli [$(m-M)_{0,M13} - (m-M)_{0,M5} \approx 0.06$, Ferraro et al. 1999; -0.02, Recio-Blanco et al. 2005; -0.08, Carretta et al. 2000] and reddening [E$(B-V)_{M13}$−E$(B-V)_{M5} = -0.01$, Harris 1996; -0.02, Recio-Blanco et al. 2005] values, and their metallicities are similar (with M13 universally identified as more metal poor by about 0.2 dex). The M5 sample is similar in size to the M13 sample as well. In the comparisons below we use a model with a compromise [Fe/H] $= -1.31$, although once again the composition choice is not critical. In light of the similar and relatively well-determined distance moduli, we have chosen to combine the samples after correcting for the small difference in distance modulus. This is probably superior to shifting the cluster samples so that the brightest giants in each cluster match because i) many of the brightest giants in M13 are variable, and ii) statistically speaking, the brightest giants may fall at different brightness levels fainter than the tip of the red giant branch (TRGB).

The combined sample is shown in Fig. 12. K-S test probabilities only go below 10% in small ranges of magnitude (for example, $P = 0.05$ for a cutoff at $I - I_{TRGB} = 3.00$). Overall, we regard the agreement with the models as good, and a confirmation of the most recent plasmon neutrino emission rates (Haft et al. 1994; Itoh et al. 1996), which influence the evolution rates near the TRGB. There are variations in counts around the theoretical predictions, but are not significant at more than a 2σ level. With these samples, we see no reason to consider particles beyond the standard model with very large mean free paths (such as axions and WIMPS) that could affect cooling of the degenerate core (e.g. Catelan et al. 1996).

The evolution rates for fainter giants can also be examined using star numbers. Using a sample covering a smaller portion of the cluster, Cho et al. (2005) found that M13 appeared to have "extra" stars in and slightly fainter than the RGB bump. On the other hand, in

their study of the bumps of a large sample of clusters, Riello et al. (2003) found that M13 appeared to have a lower than expected number of bump stars (stars with V within ± 0.4 mag of the bump center) compared to giant stars between 0.5 and 1.5 V magnitudes fainter than the bump. Both Riello et al. and Bono et al. (2001) found M13 had a lower value than the mean for their whole sample of clusters, and in the case of Riello et al. the value was almost 3σ lower. Using $V_{bump} = 14.75$, our M13 samples are more than twice as large as the ones tabulated by Riello et al. We find $R_{bump} = 297/609 = 0.487 \pm 0.034$, which is quite consistent with the mean value found by Riello et al. and with theoretical predictions (Riello et al. 2003; Bjork & Chaboyer 2006). The slope of the lower giant branch in the cumulative luminosity function (which is related to the evolution timescale) for M13 is also in very good agreement with the predictions of the Victoria-Regina and Teramo models. Based on our large sample, the M13 giants are evolving at the rate predicted by models.

As mentioned above, the CLF of M13 also shows a slight enhancement in the number of RGB stars at $I \approx 12.0$ or $V \approx 13.15$. This feature can be seen by eye in some of the CMDs (for example, see Fig. 13). This is reminiscent of the "heap" feature seen in NGC 2808 by Bedin et al. (2000), which was identified about 1.4 V magnitudes brighter than the RGB bump. This feature falls approximately where the RGB and AGB begin to overlap. While there have been quite a number of spectroscopic studies of M13, there is not an unambiguous spectroscopic signature to separate AGB stars from RGB stars. For example, Smith & Briley (2006) find that photometrically-identified AGB stars had uniformly weak CN bands, indicative of O$\longrightarrow$N conversion. However, there is a significant group of CN-weak RGB stars even fainter than the level where they could reasonably be confused for AGB stars.

We present the differential luminosity function for the bright end of the RGB in Fig. 14. As Bedin et al. found for NGC 2808, the heap is not statistically significant. Its appearance in the CMD comes largely from the contrast with slightly fainter RGB stars, which appear to be less common than predicted theoretically. In our M13 sample (which is close to as large as it will get for this cluster), the heap appears to be significant at about the 2.5σ level based on K-S tests on the cumulative luminosity function.

To summarize, after gathering the largest possible sample of giant stars in the cluster, we see at most low-significance deviations from theoretical luminosity functions. We emphasize that our luminosity function comparisons have been done in a relative sense, by forcing agreement between the brightness of the observed and theoretical TRGB. In contrast to the case for NGC 2808 (but in agreement with NGC 2419), we do not see evidence of large numbers of stars leaving the RGB early that could account for the bluest HB stars in the cluster.

5. The Horizontal Branch

5.1. Brightness and Radial Distributions

M13 possesses a horizontal branch comprised mainly of stars bluer than the instability strip (Fig. 10). Before we turn to comparisons of the HB population with other post-main-sequence samples, we will first examine the distribution of HB stars in the CMD and as a function of radius in the cluster.

Our dataset has been derived from a wide-range of source material, but V photometry is common to all of the sources, and I photometry is available for all but one of the sources (the proper motion data of Cudworth & Monet 1979). We use I photometry to describe the relative positions of stars on the HB because it is an *observable* quantity, and HB stars grow monotonically fainter in I with decreasing mass. The relationship between I magnitude and mass results from competition between decreasing radius and increasing surface temperature as the mass of the star's envelope decreases, and from the rapidly increasing bolometric corrections that result. The use of a directly observable coordinate for HB position also reduces the difficulties in comparing models and observations (Vargas Álvarez & Sandquist 2007).

Because of the potential influence of blending, we drew the I magnitude of a star from the photometric dataset with the highest spatial resolution: ACS WFC, CFHT, and KPNO. Five stars fell in the gap between the two ACS WFC chips, and their photometry was derived from WFPC2 observations in F785LP (§2.6). In Fig. 15, we show a histogram of the HB star distribution in I, clearly showing the well-known bimodality. For conceptual purposes, we have broken the HB into three parts: $I < 16.25$ (the bright peak, hereafter P1), $16.25 < I < 18$ (intermediate stars), and $I > 18$ (the faint peak, hereafter P2). The break at $I = 18$ corresponds to gap G3 identified by Ferraro et al. (1998), while the break at $I = 16.25$ is slightly fainter than their gap G1 and at approximately the same position as the "u jump" identified by Grundahl et al. (1998). Grundahl et al. (1999) tentatively identified this as the place on the HB where radiative levitation of heavy elements becomes important, and spectroscopic studies (Behr 2003; Fabbian et al. 2005; Pace et al. 2006) confirmed a change in the atmospheric abundances of heavy elements at similar positions in a number of other clusters. The gap G1 appears to correspond to a local minimum in the HB distribution at $I \approx 15.7$. There is no doubt that Ferraro et al. (1998) saw clear evidence of gap G1 in their dataset, but the gap in their data was fairly wide and it is difficult to assign a precise location using their smaller dataset.

Because the well-studied cluster M3 shows a clear change in HB morphology with distance from the center (Catelan et al. 2001), we examined the distribution for signs of radial

variations. In the top panel of Fig. 15, we see that the HB and RGB distributions are essentially identical. In the lower panel, we plot the HB distributions for samples with $r < r_h$ and $r > r_h$ (380 and 404 stars, respectively). There appear to be slight differences between the sample distributions, with the second peak at the end of the blue tail becoming less prominent in the outer portion of the cluster. As shown in the cumulative radial distributions in the bottom panel of Fig. 16, there are modest differences in the innermost $140''$ of the cluster, with the intermediate HB stars being the least centrally concentrated and the faint peak stars being the most centrally concentrated. However, for this global comparison, a Kolmogorov-Smirnov test indicates that there is still a 21% chance that those two distributions could be drawn from the same parent population. When the comparison is restricted to $r < r_c$ or r_h, the probability does not change significantly.

Table 8 shows the number counts for different radial samples. The counts show a tendency for stars in the faint peak to be more centrally concentrated. They are almost as abundant as bright peak stars in the very center of the cluster ($r < r_c/2$), but the fraction drops quickly so that for $r \gtrsim r_c$, they are consistently about as abundant as the intermediate group. There is a marginal trend in the fraction of HB stars in the faint blue peak (f_{P2}) as a function of distance, but a significant change in the difference in the fractions in the bright red and faint blue peaks ($f_{P1} - f_{P2}$).

Cohen et al. (1997) found that the blue HB stars in M13 appear to be centrally depleted relative to other types of stars for their sample with $r < 60''$. We believe the difference is probably due to incompleteness at the faint end of their horizontal branch sample. The appearance of the horizontal branch in their Fig. 4 clearly shows the bright peak, but there is little or no sign of the faint peak (most stars in $18 < V < 19$), which falls near the completeness limit of their dataset.

5.2. Notable Stars

Only nine RR Lyrae stars are known in the entire cluster, but there are stars redder than the instability strip. We find a conspicuous group of eight stars just bluer than the RGB but approximately 0.5 mag fainter than the AGB clump (seven are seen in Fig. 17). A star at the red end of the theoretical ZAHB locus plotted in Fig. 17 has a mass of $0.8M_{\odot}$, so HB stars in this part of the CMD would be more massive than stars at the cluster turnoff (the HB is theoretically expected to curve back toward higher temperature and luminosity for more massive stars). We believe that these stars are probably evolved counterparts to blue straggler stars, as originally proposed by Fusi Pecci et al. (1992). This possibility could be tested by comparing the number to the size of the sample of cluster stragglers (and

thereby comparing their relative lifetimes), but this is beyond the scope of the current work. Although field stars are relatively common in this part of the CMD, five of the eight stars have proper motions indicating that they are high probability members (Cudworth 1979). The remaining three stars are all within 45″ of the cluster center. Only one of the stars (HB 532) has UV observations — in the F255W passband it is significantly brighter than the RGB but fainter than hotter HB stars, which rules out an optical blend of a hot HB and an RGB star.

From careful examination of the photometry, we identified three additional stars that we believe may be red HB stars. HB 314 has proper motion information that identifies it as a high probability member and photometry that places it at V magnitude nearly identical to stars blueward of the instability strip. The two remaining stars do not have proper motion information, and their CMD positions give them greater probabilities of being field stars. HB 793 has a V magnitude placing it at the cluster HB level, and it is fairly blue compared to the known field stars of similar brightness, but it is outside the proper motion field ($r = 625''$). HB 133 is closer to the cluster center ($r = 103''$), but has a V magnitude placing it about 0.3 mag fainter than the cluster's HB. However, there are no other stars near it in the CMD, and there is a small possibility that it is an undetected variable star, although it was within the field studied by Kopacki et al. (2003) using a sensitive image subtraction method.

Although quite a few globular clusters have long blue horizontal branch tails (NGC 6752, M2, and M80 are examples), M13 is somewhat unusual in having a secondary peak in its distribution of stars that falls near the theoretically-predicted blue end of the HB. Clusters that have blue hook stars (such as ω Cen, NGC 2808, and NGC 2419) have blue HB tails in optical CMDs that extend to fainter magnitudes. As a result, we have looked at the faintest HB stars in the optical to gauge whether there are any blue hook stars present.

Sandquist & Hess (2008) noted that the M13 HB largely terminates at the approximate position of a gap in the EHB population of NGC 2419 when the HBs are aligned at their brightest points in B. In CMDs employing B, F439W, or F336W filters, we identified a handful of candidates that were fainter than the faint HB peak P2. However, ultraviolet CMDs must be used in conjunction with the optical CMDs in order to get a full picture of the spectral output of the stars. In Fig. 9, we present our UV CMDs for M13. As we progress from the near UV (F336W and F255W) to the far UV (B5 and F160BW), bolometric corrections become less severe for the hottest stars, and the hottest HB stars match the rest of the blue HB in brightness. Although the WFPC2 F160BW and UIT B5 filters cover similar portions of the spectrum, and produce similar CMDs in Fig. 9, the F160BW filter reaches peak sensitivity more than 100 Å shorter than the B5 filter. We believe this is responsible for the slight upturn near the blue end of the HB in F160BW. In

CMDs using even shorter wavelength observations, the hottest HB stars would continue to change their configuration.

D'Cruz et al. (2000) found a large group of blue hook stars in ω Cen that were subluminous in an (F160BW, F160BW-V) CMD compared to other stars at the end of the HB. A similar structure does not exist in Fig. 9 near F160BW−F555W≈ -3.5, but there are two stars that meet the typical definition of the blue hook: fainter than the ZAHB in the far UV. The optical measurements for these two stars put them significantly fainter than the predicted hot end of the HB. The UIT source (HB 2) is approximately 0.7 mag fainter than the hot end of the HB in the B5 filter, and 1 magnitude fainter in B. (It is the faintest HB source in the KPNO panel of Fig. 10.) HB 431 is among the faintest sources in the three WFPC2 UV filters, but is faintest only in F160BW. (It is the second faintest HB source in the ACS WFC panel of Fig. 10.)

Nine other stars are fainter than the EHB in optical bands and sit at the extreme blue/faint end of the HB in ultraviolet bands (although fairly close to the extrapolated zero-age HB), and so we flag them as potentially interesting stars. The UIT sources are HB 8, 56, 73, 86, and 757, while the WFPC2 sources are HB 373, 485, 611, and 636.

5.3. Evolution of HB Stars

With a large sample of HB stars, the sample of evolved HB stars also grows, making it possible to trace post-HB evolution. The two most densely populated portions of the HB contain 75% of the stars, and so to first order, post-HB stars will trace the evolution of these two groups.

In Fig. 18 and 19, we show a comparison between theoretical models of Pietrinferni et al. (2006, hereafter, Teramo) and Dotter et al. (2007, hereafter, DSEP) and our ground-based photometry in $(V, B-I)$ for $r > 200''$. To gauge the edges of the HB distribution, we used zero-age and central helium depletion ($Y_c = 0.05$ or 0.10) CMD positions as a function of mass. Because there is some uncertainty about the precise chemical composition of M13 (e.g., Johnson & Bolte 1998), we fitted the HB band to the photometric data in order to better identify evolved stars in a differential sense. We emphasize, however, that the fit does not completely validate the models. In fact, there are mismatches between observation and theory that we will examine below.

5.3.1. The Reddest BHB Stars

Because M13 has a blue HB, traditional photometric indicators of distance (M_V^{HB}), age (ΔV_{TO}^{HB}, for example) and helium ($R = N_{HB}/N_{RGB}$) that have the V magnitude of the HB in their definitions cannot be used without corrections of uncertain accuracy. As a result, redder stars may better define the brightness of the HB if they can be proven to reside near the ZAHB in the CMD.

As shown in Fig. 20, we identified 55 stars redward of the most heavily populated part of the HB (the bright peak P1; 308 stars in $16.25 > I \gtrsim 14.9$). The stars stretch to the instability strip ($0.10 < V - I < 0.22$), and it is likely that at least some of the RR Lyrae stars belong to the same group. These stars have largely been ignored in previous studies of M13 because many (but not all) are found in the cluster core. The evidence of a small gap at $V - I \approx 0.10$ between the reddest BHB stars and the bright peak makes it worth considering whether they represent a separate population and what their evolutionary status is. For the purpose of this section, we restrict ourselves to comparisons with theoretical models, delaying additional discussion of the luminosity of the HB to §7.2.2.

In examining recent stellar models from different research groups, we found that there is still a great deal of variation in the morphology of evolution tracks for stars that start their HB lives with $T_{\rm eff} \approx 10000$ K. This is an important question because it affects the interpretation of the reddest BHB stars in M13. Sweigart (1987) asserted that the relative importance of the helium-fusion luminosity (L_{He}/L) is the main influence on whether the evolution is primarily blueward or redward. Stars that have strong hydrogen fusion shells significantly increase the helium core mass during the HB phase, leading to higher L_{He}/L and blueward evolution. As the helium becomes depleted, the importance of core fusion is reduced and stars tend to evolve redward, becoming more giant-like. For similar compositions, some models predict a modest blueward loop before the approach to the AGB (e.g. Sweigart 1987; Dorman 1992; Yi et al. 1997) for HB evolution starting with $T_{\rm eff} \approx 10000$ K, while the most recent models (e.g. DSEP, Pietrinferni et al. 2006) predict stars evolve redward (see Fig. 21). For the Teramo (Pietrinferni et al. 2006) models, slightly cooler HB stars (ones starting among the reddest blue HB stars) have short blue loops. However, in the case of DSEP models, stars with $-2 \leq$ [Fe/H] ≤ 0 *all* evolve strongly redward from the start, and remain close to the ZAHB during much of the HB phase. Consistent with Sweigart's discussion, core helium burning remains significantly stronger than the hydrogen fusion shell in DSEP models, even for stars starting quite close to the giant branch. If the DSEP models are good representations of actual evolution, even the evolved HB stars in M13 could be reasonable indicators of where the ZAHB is. Clearly there are significant differences between these models that may help us to identify important physics.

Although there are many small differences between the physics inputs in the DSEP and Teramo models, we believe the likely cause is diffusion. Diffusion was consciously disabled in the Teramo models, while the DSEP models stop diffusion in the outermost $0.05M_{\odot}$ of stars and linearly ramp their diffusion algorithm to full strength at $0.10M_{\odot}$ below the surface. As seen in more metal poor $0.73M_{\odot}$ models with diffusion by Michaud et al. (2007), the introduction of diffusion produces redward evolution for a star that would otherwise evolve blueward. There is clear evidence of diffusive processes in the surface compositions of bluer HB stars in globular clusters (e.g. Moehler et al. 2003; Moni Bidin et al. 2009), but not among stars like the reddest BHB stars. Still, the surface layers are less likely to show chemical signatures due to near-surface convection. The DSEP models may be demonstrating that diffusion in the interior can be constrained by observations — processes such as rotationally-induced mixing could inhibit the action of diffusion.

The numbers of stars can also constrain the models — because the early stages of core helium fusion take the longest, the initial direction of the evolution in color should have a big effect on how many stars are found to the red of peak P1. Fig. 22 shows a representative synthetic horizontal branch generated from DSEP web tools[7] with a number of stars in the primary peak comparable to observations. We did not attempt to fully model the fainter parts of the primary peak because most of those stars are expected to exhaust their core helium before entering into the color range we are considering, becoming too bright to be considered HB stars (see §5.3.3). Even so, the number of stars actually observed is *considerably smaller* than predicted by the synthetic HB simulation. The models predict that the red population ($I < 14.9$) should be approximately 28% the size of the primary peak population, whereas the M13 population is only about 19%. Small variations in chemical composition (helium or heavy elements) also do not affect this conclusion. Whatever the reason, the DSEP evolutionary tracks do not seem to be accurately representing the evolution of stars from the primary peak. A small amount of blueward evolution would relieve the discrepancy.

Teramo tracks produce a somewhat better fit to the M13 data, but the observations appear to need blueward evolution to continue at slightly higher temperatures to explain the appearance of the rather sharp red edge at $(V - I) = 0.07$ (pure redward evolution would tend to smear out such a feature in color). When the ZAHB and $Y_c = 0.05$ lines are fit to the magnitude extent of the primary peak, the reddest BHB stars and RR Lyrae stars fall near the $Y_c = 0.05$ line, implying they are significantly evolved (see Fig. 23).

[7]http://stellar.dartmouth.edu/ models/shb.html We used "empirical" color transformations as these appear to do a better job than "synthetic" transformations in reproducing photometry in and around the subgiant branch (Dotter et al. 2007; Sarajedini et al. 2007).

While the Teramo models come close to explaining the appearance of the sharp red edge of the HB distribution, the underlying question remains *why* there should be such a sharp edge for M13's population. Increased envelope mass, as well as increased helium and metal abundance are known to encourage blueward evolution. Helium enrichment has a significant effect on the HB luminosity and some effect on the evolution of red HB stars. For modestly helium-enriched ($Y = 0.30$) Teramo models in Fig. 24 (consistent with the δY hypothesis), a large (and probably unrealistic) distance modulus of about 14.75 is required, and the evolution of stars at the red end of the bright peak P1 goes too bright to explain the reddest BHB stars. In fact these stars can't be satisfactorily reproduced in the current helium-enhanced models.

Pietrinferni et al. (2009) recently computed HB models for "extreme" CNONa abundance mixtures in which the sum of CNO elements is approximately a factor of two higher at a given [Fe/H] than for a typical α-enhanced mixture. The mixture is intended to be representative of pollution resulting from intermediate mass AGB stars, and N is by far the most abundant heavy element due to nuclear processing. An extreme CNONa mixture could realistically produce blueward evolution for the dominant HB population. However, measurements of oxygen abundances among the cool HB stars in M13 all indicate [O/Fe] is normal for globular clusters and super-solar (Peterson et al. 1995). Smith et al. (1996) and Cohen & Meléndez (2005) also found that [(C+N+O)/Fe] did not seem to vary significantly within their samples of CN-strong and CN-weak giants, and the CNO elements do not show "extreme" enhancement (the average was about 0.3 dex). Similar results have been found for relatively unevolved stars in other clusters (Carretta et al. 2005), although stars in NGC 1851 show a significant 0.57 dex spread (Yong et al. 2009).

From the theoretical comparisons above, our preferred explanation is that the reddest BHB stars are stars with unenriched compositions that evolve somewhat to the blue after reaching the ZAHB. However, it must be admitted that the theoretical models disagree to a greater extent than we would like. We return to the discussion of these stars in §7.2.2.

5.3.2. Ultraviolet Bright Stars

We next identified hotter ultraviolet-bright stars (the brightest cluster stars in U band, but optically identifiable) from the study of Zinn et al. (1972). ZNG 1 (Barnard 29) is a post-AGB star (Conlon et al. 1994; Moehler et al. 1998; Thompson et al. 2007), and is the brightest star in the UV by almost 3 mag (see the UIT panel of Fig. 9).

In the lower left panel of Fig. 9, ZNG 2, ZNG 6, and ZNG 7 sit at the cool side of a

group of stars we identify as AGB manqué stars, which are hot stars that are significantly brighter than the hot HB (see §5.3.3). ZNG 2 (G 43) was observed spectroscopically by Moehler et al. (2003), and its low gravity ($\log g \approx 3$) clearly identifies it as being a post-HB star. ZNG 7 falls slightly bluer than the "knee" of the HB in the upper right panel of Fig. 10, but is quite bright in the ultraviolet. ZNG 6 is the only one of the UV bright stars that has HST ACS observations, which again places it significantly brighter than the HB (see the lower left panel of Fig. 10).

In optical CMDs, ZNG3 and ZNG 4[8] are about a magnitude brighter than the knee of the HB, and part of a small group of stars seeming to parallel the HB. ZNG 3 and 4 are among the reddest objects with reliable photometry detected using UIT (see Fig. 9). ZNG4 was observed spectroscopically by Ambika et al. (2004), who identified chemical signatures of diffusion, which only shows up among blue HB stars with $T_{\rm eff} \gtrsim 11000$ K. A likely explanation is that ZNG 4 ($T_{\rm eff} = 8500$ K) was once a hot blue HB star that evolved, and the chemical signature is leftover from the earlier phase. A significant convective envelope is not likely to appear until the star reaches lower $T_{\rm eff}$. We identify both stars as supra-HB stars, which probably trace evolution from midway on M13's HB, as discussed in the next subsection.

5.3.3. Hot Post-HB Stars

The origin and evolutionary behavior of the hottest HB stars has implications beyond stellar evolution — these stars contribute to, and perhaps dominate, the ultraviolet light from old stellar populations in galaxies (Dorman et al. 1993). Recently, Brown et al. (2008) used a STIS UV CMD of the dwarf elliptical M32 to study the main stellar contributors in the ultraviolet: the hot HB, the AGB manqué, and the post-AGB. The authors found that the CMD could constrain the chemical evolution of the population, but that the post-HB evolution did not seem to be in good agreement with models. Although galactic populations provide better leverage on the shortest stages of post-HB evolution, a massive globular cluster with a simpler population and precise photometry should also constrain theoretical models.

Using a combination of ultraviolet and optical CMDs, we attempted to identify all stars that have evolved away from the hotter parts of the HB. As discussed in §5.3.1, theoretical HB models (Dotter et al. 2007; Pietrinferni et al. 2006) with no helium enrichment agree that stars originating from the primary peak in the HB distribution produce AGB stars exclusively — the evolution of the stars keeps them within about 0.2 mag of the HB until shortly before central He exhaustion. Core helium exhaustion occurs over a large portion of the star's

[8]For completeness, ZNG 5 is a non-member according to proper motions, and is not considered here.

core due to convection during helium fusion, causing a star to adjust its structure rapidly (in about a Kelvin-Helmholtz timescale) and move to the AGB clump. However, during the time leading up to core exhaustion, the core convection zone is decreasing in size, leaving behind a composition gradient. In typical AGB stars, almost half of the AGB lifetime is taken up while the new He fusion shell eats through this composition gradient. During this time the star's evolution pauses, producing a fairly well populated AGB clump about 1 V mag brighter than the HB (Ferraro et al. 1999). Figs. 19 and 18 show illustrative theoretical tracks and synthetic HB populations from DSEP and Teramo using canonical physics and reasonable choices for chemical composition (nearly primordial helium abundance, for example). The top rows in both plots show tracks for stars which evolve near the HB and have normal AGB phases including an AGB clump.

The middle rows in Figs. 19 and 18 show stars that produce stars that spend part of their lives as somewhat bluer than average AGB stars, but do not have an AGB clump phase. For these stars, the evolution as the He fusion shell consumes the composition gradient take longer (more than a Kelvin-Helmholtz timescale) and occurs at higher surface temperature. Most of these stars can be put into one of two categories based on whether they have colors bluer or redder than the "knee" of the HB in optical CMDs ($B - I \approx -0.1$). One group of stars sitting approximately 1 mag above what would be the horizontal part of the normal HB ($14 < B < 14.5$ in Fig. 10; $V \approx 14.1$) corresponds to "supra-HB" stars previously identified by Strom et al. (1970) and Zinn (1974). This group includes ZNG 3 (AGB 75) and ZNG 4 (AGB 8), as well as AGB 27, 32, and 33 (detected in F160BW using HST, and the reddest post-HB star marked in the upper left panel of Fig. 9), 50 (also detected in HST F160BW), 81, and two of the known BL Her pulsating variable stars (V1 and V6; Kopacki et al. 2003). Type II Cepheids (a group that includes BL Her stars) are only found among stellar populations having a significant blue HB component, as was noted by Wallerstein (1970) and Smith & Wehlau (1985). As reviewed by Wallerstein (2002), the great majority of well-studied Type II Cepheids show no period change or increasing period, consistent with evolution toward the red and larger size.

Even hotter post-HB stars are harder to identify in optical CMDs because of the steepness of the HB in magnitude. Relatively small color errors can cause normal HB stars to overlap stars that have evolved significantly in luminosity from hotter on the HB. When ultraviolet observations are used, these stars are much more easily separated by brightness (see Fig. 9). So-called AGB manqué stars fall in this category — they are stars that have evolved away from the HB that will not reach the traditional AGB because the star's envelope does not have enough mass to produce a giant-like structure. Observationally, this definition is hard to use because it requires reliable knowledge of the star's future evolution in the CMD. However, theoretical calculations imply that there is a big change in track

morphology on the blue HB. The bottom rows of Figs. 19 and 18 show stars that would not have an identifiable AGB phase.

The main difference in the models with total mass less than about 0.54 $M_{\odot}$ at M13's metallicity is that hydrogen shell fusion is unable to provide much of the luminosity even during the core contraction following helium exhaustion. It appears that if L_H at maximum does not surpass L_{He} after the H fusion shell has reignited and stabilized, the star will remain at high temperature during the relatively slow helium shell adjustment.

The supra-HB and AGB manqué stars in M13 identified with crosses generally fall more than a magnitude above the faint envelope of HB stars. So for a fairly standard chemical composition, models predict that the only evolution tracks that produce hot post-HB stars come from bluer than some point between the two HB peaks in M13. Observationally, there is an apparent gap between two sets of "UV-bright" stars in the UIT CMD in Fig. 9. While individual optical CMDs in Fig. 10 may leave the impression of color gaps between groups of hot post-HB stars, the union of the optical CMDs (see Fig. 23) indicates that there is a thin, fairly uniformly populated band paralleling the HB from its bluest to its reddest colors with a couple of post-HB stars even closer to the AGB clump. There are a few stars in the ACS field without UV photometry that will partially fill the gap between the two groups of "UV bright" stars in the UIT CMD. As a result, we believe these stars are tracing out the slowest phase of post-HB evolution for stars that do not follow traditional AGB tracks. A relatively small change in envelope mass leads to a drastic change in the morphology of the tracks for these stars. Because M13's HB is well-populated near the end of the canonical HB (more so than many other clusters with extended blue HB tails), the cluster is providing us with a means of observationally "seeing" where the post-HB evolution pauses for a little.

Independent of how believable the gap in the UIT CMD is, the usable portion of the UIT field does contain the majority of the hot post-HB stars, and does perhaps allow us to observationally identify the transition between an AGB manqué track and an post-early AGB track. AGB manqué evolution is expected to be largely in luminosity, with redward color evolution increasing for cooler, more massive HB stars. The red edge of the group ($m_{1620} - V \approx -1.7$) is thus a conservative upper limit for the HB stars producing AGB manquéstars, and this limit is bluer than the blue end of the primary HB peak. The numbers of post-HB stars help to constrain the tracks further (see §6.2).

As can be seen from Fig. 24, the shape of post-HB evolution tracks does not change drastically with a modest increase in helium abundance to $Y = 0.30$. Increasing helium abundance creates a larger luminosity gap between the blue end of the HB and the AGB manqué stars, greatly increases the number of AGB manqué stars relative to HB stars, and produces bluer manqué stars that are more concentrated in color (Brown et al. 2008).

Because models of M13's HB involving helium-enriched stars predict that the bluest HB stars have $Y \approx 0.38$ (D'Antona & Caloi 2008b), these effects could be tested. Detailed simulations are beyond the scope of this study, but to first order, the number of hot post-HB stars is quite small compared to HB stars in the same color range (17 / 191 = 0.09 for $m_{1620} - V < -1.9$), which argues against large helium enrichment.

6. Population Ratios

One of the primary reasons for this study was to examine evolutionary timescales for stars in different life stages. We first recalculate the HB type $(N_{BHB} - N_{RHB})/(N_{BHB} + N_{VHB} + N_{RHB})$. Here BHB, VHB, and RHB stand for stars bluer, within and redder than the RR Lyrae instability strip.) For M13, $N_{VHB} = 9$, and we have identified five possible RHB stars. Thus we have $\mathrm{HB_{type}} = 0.976 \pm 0.006$.

6.1. The Helium-Sensitive R Ratio

The $R = N_{HB}/N_{RGB}$ ratio compares the evolutionary lifetimes of HB and RGB stars, and is a sensitive helium abundance indicator (e.g. Cassisi et al. 2003). Because of the claim that M13 stars may have high helium abundances (Johnson & Bolte 1998; Caloi & D'Antona 2005), it is particularly important to examine this population ratio. Following the definition of Salaris et al. (2004) and Zoccali et al. (2000), we used V_{ZAHB} (the magnitude of the zero-age HB) as the cutoff for the RGB sample. The determination of the faint limit for the RGB sample is important because the numbers of RGB stars rises quickly with increasing magnitude.

To determine V_{ZAHB}, we applied two methods. For the first, we followed the procedure of Recio-Blanco et al. (2005), using a template cluster of comparable metallicity and a well-studied RR Lyrae population (used to define the reference HB level $\langle V_{RR} \rangle$) to determine a relative magnitude shift. Recio-Blanco et al. used NGC 1904 as the template for clusters near M13's metallicity after first determining $\langle V_{RR} \rangle$ through a comparison with M3. In their comparison of photometry for NGC 1904 and M13 from the WFPC2 camera, they found that M13's sequences are 1.20 mag brighter in V than NGC 1904, with no relative shift in color. The corresponding $\langle V_{RR} \rangle$ value for M13 is therefore predicted to be 14.97 ± 0.07, which results in $V_{ZAHB} = 15.06$.

For the second method, we determined the ZAHB almost exclusively from data on the reddest blue HB stars, under the assumption that they are relatively unevolved and unen-

riched HB stars. (Based on additional arguments in §7.1, we believe this is incorrect.) Our photometry does not have adequate time-coverage for direct determination of $\langle V_{RR} \rangle$. The value determined by Kopacki et al. (2003) (14.83 ± 0.02) was set by comparison to photometry by Rey et al. (2001) that was in turn calibrated to Landolt (1992) standards. Zeropoint differences between our dataset and Kopacki et al. should therefore be small. However, non-variable stars at the blue end of the instability strip have $V = 14.90$ on average. Using this as representative of the average HB level, $V_{ZAHB} = 14.99$.

We find $N_{RGB} = 483$ using the first method, giving $R = 795/483 = 1.65 \pm 0.09$ (error estimate from Poisson statistics). For the second method, $N_{RGB} = 465$ and $R = 1.71 \pm 0.10$. In both cases, M13's R value is about 3σ higher than the theoretical calibration presented in Salaris et al. (2004) for $Y = 0.245$, and in agreement with their measurement of $R = 1.719 \pm 0.197$ using a considerably smaller sample.

This does not account for the effects of HB morphology, however. Theoretical models uniformly predict that blue HB stars have longer evolutionary times than RR Lyrae variables or redder HB stars, which would produce high R values in clusters with blue HB morphologies. Zoccali et al. (2000), for example, conducted an early examination of the effect of HB lifetimes on the R ratio, and Salaris et al. (2004) found that clusters with $\mathrm{HB}_{type} \geq 0.8$ show a larger spread around the mean than clusters with redder morphologies, which implied that the exact morphology of blue HB clusters might be influencing the R ratio. In Sandquist & Hess (2008), we described a method for correcting R for variations in HB lifetimes in a way that is based on observable quantities and is largely independent of chemical composition. The reader should see that article for more details, but we briefly summarize it below.

According to theoretical models, HB lifetimes vary similarly as a function of stellar mass and effective temperature, although the absolute value of the lifetime does depend on composition (see the lefthand panels of Fig. 25). Based on this behavior, we defined a weighting factor for each star in the HB sample:

$$w_i = \frac{t_{HB}(\log T_{eff} = 3.85)}{t_{HB}(\log T_{eff})}$$

The largest portion of the variation in HB lifetimes occurs on the blue tail for $T_{eff} \gtrsim 10^4$ K for stars with low-mass hydrogen envelopes. By choosing $\log T_{eff} = 3.85$ (near the blue edge of the instability strip) as the normalization point, we can correct the blue HB lifetimes back to values representative of the more common variable and red HB stars, and the R value can be realistically compared to values from large studies of clusters with redder HBs (Salaris et al. 2004; Zoccali et al. 2000). The variation of the weighting factors with T_{eff} is shown in the righthand panels of Fig. 25. Although there is some variation in the weighting

factors with composition, they clearly describe the lifetime variation to first order, so that residual uncertainties are at the level of a few percent. Further, the weightings *only* remove the effects of position on the HB, and do not reference the absolute value of the HB lifetime, which depends on composition and physics inputs to the stellar evolution codes (e.g., the $^{12}C(\alpha,\gamma)^{16}O$ reaction rate; Cassisi et al. 2003).

Although color-T_{eff} relationships remain imperfect, it is much more reliable to derive T_{eff} from photometry than it is to derive the stellar mass. For example, the Grundahl u-jump has been found in many clusters with blue HB stars with $T_{eff} \gtrsim 11500$ K (Grundahl et al. 1999). In addition, the canonical HB also seems to have a reasonably well-defined termination near 30000 K. For the purposes of this study of M13, we have used the T_{eff} determinations from Moehler et al. (2003) using Stromgren photometry. Moehler et al. also measured T_{eff} spectroscopically, and while the spectroscopic measurements are in good agreement with the photometric measurements, the spectroscopic measurements are subject to significant model uncertainties at the faint end and appear to deviate systematically from photometric determinations at the red end of the HB. These measurements for M13 do not go all the way to the faint end of the HB, so we have assigned $T_{eff} = 31000$ K to stars at the cutoff in the distribution ($I = 19.5$) based on measurements of NGC 6752 (Moehler et al. 2000), which has similar metallicity and HB extent.

As expected from the analysis above, the use of different sets of models has a small effect on the weighted HB star total. In the case of some model sets (DSEP, Sweigart 1987), we needed to extrapolate the weighting corrections in the range $4.4 \leq \log T_{eff} \leq 4.5$ for an extremely small number of stars. Overall the models agree that the HB sample should be corrected downward by approximately 10%, with Cassisi et al. (2004) ($Y = 0.23, Z = 0.0006$) and Sweigart ($Y = 0.25, Z = 0.001$) models giving $N'_{HB} = 716$, and DSEP ($Y = 0.248$, [Fe/H] $= -1.5$) and Sweigart ($Y = 0.30, Z = 0.001$) models producing a lower $N'_{HB} = 703$. Thus, the corrected ratio is $R \approx 1.47 \pm 0.09$ and 1.51 ± 0.10 for our two methods of determining V_{ZAHB}. (The uncertainty introduced by the choice of models is significantly smaller than the Poisson uncertainties.) These values deviate from theoretical models for $Y = 0.245$ by about 1σ. Based on these arguments, the R ratio appears to rule out a global helium enrichment of $\Delta Y = 0.04$ at a 3σ level (since $dR/dY \approx 10$; Cassisi et al. 2003).

The value of R produced by this analysis rests on the accuracy of the weightings used to correct the HB star total and on the determination of the faint cutoff for the RGB sample. If incorrect weightings were hiding a helium enrichment of $\Delta Y = 0.04$ among M13 HB stars, they would need to have been overestimated by about 28%. We remind the reader that the weightings are corrections *relative* to HB stars near the instability strip and are independent of the absolute value of lifetimes, so we believe that an overestimate of this magnitude would

be difficult to produce. In addition, because we used weightings derived from models with $0.23 < Y < 0.25$, this would *overestimate* the weights for the bluest HB stars if those stars are actually helium-enriched, not underestimate them. If anything, our R measurement is biased slightly too high.

To hide a helium enrichment through a systematic error in the RGB sample, it would be necessary to overestimate the number of stars, which would require a faint limit that was too faint. To produce a measured helium enrichment of $\Delta Y = 0.04$, our faint limit would need to have been at $V = 14.79$, or 0.20 mag brighter than our brightest estimate. Only a gross error in judging the level of the HB could produce an error this big, but the majority of the RR Lyrae stars in the cluster dispute that, having $\langle V \rangle \approx 14.85$ (Kopacki et al. 2003). Even if the RR Lyrae stars are somewhat evolved, they are still *fainter* than the ZAHB level needed to produce a result of $\Delta Y = 0.04$. (The RR Lyrae stars will be discussed more below.) From other indications (such as ΔV_{TO}^{HB}), the HB of M13 is likely to be brighter than average for globular clusters if it is deviant at all. As a result, we don't see a clear reason to dispute the helium abundance implied by the R ratio.

To avoid issues with systematic effects, it is worth doing a *relative* comparison between M13 and M3. We assembled photometry for M3 from Ferraro et al. (1997) and Rood et al. (1999), along with averaged photometry for the large population of RR Lyrae variables from Benkő et al. (2006) and Corwin & Carney (2001). This sample completely covers a $7' \times 7'$ area roughly centered on the cluster core. This contains 602 HB stars, which we subsequently corrected for lifetime effects. Because M3's HB morphology is much more horizontal than M13's, we have used the $V-I$ color to determine lifetime corrections, in part due to questions about the calibration of the B data in this cluster (Valcarce & Catelan 2008). For stars that had no I measurement, we determined an empirical transformation from $B - V$ to $V - I$ using nonvariable HB stars from the Ferraro et al. (1997) data. For a handful of RR Lyrae variables that did not have average brightness information, we assigned the star a color equal to the average color of variables of the same type (RRab or RRc). The details are fairly unimportant because the normalization for the lifetimes is based on stars near the blue edge of the instability strip (near the middle of M3's HB) and because lifetimes are theoretically predicted to vary little except on the blue tail. For M3, the total lifetime correction amounted to just over 1%, with a corrected value of 594 stars.

The cutoff magnitude for the RGB sample ($\langle V_{RR} \rangle$) for M3 can be determined quite accurately, so that we only need to worry about possible zeropoint differences between the variable and non-variable star photometry. We used $V_{ZAHB} = 15.70 \pm 0.03$ from Ferraro et al. (1997), which was also the source of the zeropoint for the HST observations of Rood et al. (1999). The RGB sample brighter than V_{ZAHB} is 444 stars, which gives $R = 1.34 \pm 0.08$.

According to this analysis, the M3 sample is consistent with having lower average helium abundance than M13, but the values differ by slightly more than the error bars and the implied difference in Y is only about 0.015. This is not enough to explain morphological differences in the CMD on the subgiant branch or HB.

This is an interesting and somewhat surprising result that contradicts a number of previous studies of M3 and M13 that indicated that M13 is enriched in helium compared to M3. For example, in their discussion of globular clusters with multiple stellar populations, D'Antona & Caloi (2008) identified M13 as a cluster composed almost entirely of stars enriched in helium by about $\Delta Y = 0.04$. In a later simulation, D'Antona & Caloi (2008b) also model M13's HB population exclusively with helium enriched stars, but in this case with 70% of stars having ranging from $0.27 < Y < 0.35$ and 30% having $Y = 0.38$. For comparison, their interpretation of M3's populations involves 50% of the stars having a near-canonical value of $Y = 0.24$ and 50% having $0.26 < Y < 0.28$. Even if M13's R value is not corrected for lifetime variations, it still falls short of the value expected for the relatively small helium enrichment of $\Delta Y = 0.04$. We will discuss the cluster helium abundance in §7.

6.2. The R_2 Population Ratio and Post-HB Evolution

As the morphology of the HB becomes more blue, the evolutionary tracks of stars after the HB phase start to shift from traditional AGB tracks (starting in a clump at the faint end of the AGB and subsequently following a track paralleling the RGB) to abbreviated AGB tracks (having an evolutionary pause separate from the traditional clump, touching on the traditional AGB at moderate luminosities, and peeling away before reaching the tip) to manqué tracks (retaining a surface temperature thousands of degrees higher than any part of the traditional AGB). M13 contains HB stars that clearly span this range according to the number of traditional AGB, supra-HB, and AGB manqué stars we identified in §5. In view of the continuing difficulties in explaining the blue HBs of clusters like M13, we consider whether the AGB stars can reveal anything about the evolution or structure of the progenitor HB stars.

At the simplest level, the $R_2 = N_{AGB}/N_{HB}$ ratio compares the relative lifetimes in the AGB and HB evolutionary phases. Vargas Álvarez & Sandquist (2007) found that for a sample of clusters with large samples of evolved stars (more than 200 HB stars) that the population ratio R_2 dropped well below the theoretically predicted value of 0.12 (Cassisi et al. 2004) for clusters with a HB type $\gtrsim 0.8$ (mostly bluer than the instability strip). When we include supra-HB and AGB manqué stars in the AGB population, we derive a value $R_2 = 90/795 = 0.113 \pm 0.012$. For the 4 clusters with the reddest morphologies ($\mathrm{HB}_{type} <$

0.2), Sandquist & Bolte (2004) found $\langle R_2 \rangle = 0.106 \pm 0.011$. Clusters with $0.2 < \mathrm{HB}_{type} < 0.8$ had higher values (M5: 0.176 ± 0.018, Sandquist & Bolte 2004; M55: 0.156 ± 0.023, Vargas Álvarez & Sandquist 2007). Values for bluer clusters may be underestimated due to the difficulty of identifying AGB manqué stars using only optical filters. Had we not included AGB manqué and supra-HB stars in the AGB star counts, we would have calculated $R_2 = 61/824 = 0.074 \pm 0.009$, completely consistent with the low values plotted there for M30 and NGC 6752. In the blue HB cluster NGC 2808, Castellani et al. (2006b) were able to identify manqué stars, and found an R_2 value similar to ours. With proper identification of the different types of stars, the R_2 values are consistent with observational values for bluer clusters and with theoretical predictions.

Based on the bimodal distribution of HB stars (approximately 47% of HB stars in the brighter peak, and about 28% in the fainter peak), we might expect to see evidence of an almost bimodal distribution of AGB stars with the manquéand supra-HB stars evolving from the bluest HB stars. The detected AGB manquéand supra-HB population is $N_{manq}/N_{AGB} = 29/90 = 0.32 \pm 0.06$ of the total population. If we assume as a first-order approximation that all AGB stars have equal lifetimes, then this implies that the manquéstars originate in the bluest 32% of the HB stars ($I \gtrsim 17.75$; $V \gtrsim 17.55$). This excludes the bright peak and the majority of the intermediate HB population (see Fig. 15). Taking into account that bluer stars have longer lives (and so are over-represented in the HB population), the red boundary for HB stars producing manquéstars should be further to the red. When this is accounted for using the weighting factors discussed in §6.1, the boundary falls at $I \approx 17.3$ ($V \approx 17.15$; $m_{1620} - V \approx -3$). Both imply the track morphology switches between the two maxima of the HB distribution, but closer to the fainter peak.

7. Discussion

M13 is distinguished by its horizontal branch, and its horizontal branch is notable for two reasons: the fact that the stars are almost exclusively bluer than the instability strip, and the fact that there is a secondary population of stars grouped near the extreme end of the horizontal branch. Below we discuss evidence bearing on each of these points and try to put M13 in context of other globular clusters. However, before we do, we would like to state that this is not intended as a complete survey of the subject, and we apologize for our limited ability to reference the many previous studies.

7.1. The Bimodal Horizontal Branch

Independent of the position of the primary peak of the HB star distribution, the cause of blue HB tails has not been definitively identified. Some studies have identified relationships between HB tails and cluster dynamical parameters such as central density (Buonanno et al. 1997) and total luminosity (Recio-Blanco et al. 2006), although neither of these can clearly explain differences between M3 and M13 because of their structural similarities (see Table 1). While blue tails can plausibly result from a process (such as mass loss or chemical self-enrichment) producing a large dispersion in properties, M13 has a clear secondary peak in its HB distribution and this requires multiple star populations or the action of multiple physical processes. For example, theoretical models predict that varying amounts of mass loss on the RGB from star to star can produce a spectrum of outcomes from normal HB stars to early hot flashers (stars which leave the RGB before the helium flash, but ignite helium shortly afterward) to late hot flashers (stars which ignite helium on the white dwarf cooling curve) to helium white dwarfs (which never ignite helium). To produce a secondary HB peak in this way, some mechanism must be concentrating stars in the CMD, and it is difficult to see how this can be accomplished without almost complete loss of the hydrogen envelope for many stars on the RGB. On the other hand, the self-enrichment hypothesis explains peaks on the HB (not only at the blue end) via discrete populations of stars with different chemical compositions. A peak at the blue end of the HB can be accomplished with a population of stars having extreme helium abundances ($Y > 0.35$) because enriched stars leave the main sequence with lower total mass, and if the mass is low enough they will have almost no envelope by the time they reach the TRGB. He abundances for these hot stars probably can't answer the question directly (due to the action of diffusive and mixing processes), but correlated enrichment of helium and carbon among the hottest stars in ω Cen and NGC 2808 (Moehler et al. 2004, 2007) is not predicted in the self enrichment picture. As yet, there is no clear way of distinguishing between these scenarios for EHB stars. However, clearer understanding of these stars may provide new clues, so we compare M13 with other clusters with blue HB tails below.

Like *some* of the most massive clusters [NGC 2419, NGC 2808, ω Cen, and NGC 6273 (M19)], M13 has a clear second peak at the blue end of the HB in optical filter bands. Even so, there is a range in the way the secondary peak appears. Some of the best comparisons of different clusters (with HBs aligned in the optical) can be found in Piotto et al. (1999), Dalessandro et al. (2008), and Sandquist & Hess (2008). Often there is a gap or edge feature in the HB star distributions as a function of an optical magnitude ($M_V \approx 4.5, M_B \approx 4.2$) and this feature appears to separate blue hook stars from the EHB. In M13 (and also NGC 6752; Sabbi et al. 2004), the secondary peak is almost entirely brighter than the position of the gap. The secondary peak in NGC 2419 reaches its maximum among the blue hook stars,

but appears to straddle the gap. The secondary peak in M19 straddles the position of the gap, but differential reddening prevents the clear identification of a feature. ω Cen shows a sharp edge in the HB distribution at about the position of the gap in NGC 2419, with a much smaller fraction of stars just brighter than the gap. NGC 2808 on the other hand appears to have almost all of its hottest HB stars fainter than the gap, but its population is a considerably smaller fraction of its HB stars. Many other clusters with long blue HB tails do not show a secondary maximum at the blue end of the HB, however. M54 (Momany et al. 2004) and M15 appear to have produced blue hook stars, but there is little or no sign of a secondary maximum. M80 (Ferraro et al. 1998) and M2 (Momany et al. 2004) have HBs with a similar extent to that of M13, but do not show maxima. So clusters are capable of producing EHB populations comprising from nearly 0 up to 30% (for NGC 2419) of the total HB tally, with distinguishing features even among the very bluest HB stars in different clusters.

As emphasized in models (Brown et al. 2001) and observations (Momany et al. 2004), evolution of hot HB stars is mostly in luminosity and this can allow the evolved stars to masquerade as brighter but less evolved HB stars in optical photometry due to steep bolometric corrections. To better characterize the populations at the end of blue end of the HB, ultraviolet observations are needed. In near UV photometry (U, F336W), the effects of luminosity evolution become better separated from color distribution. As can be seen in Fig. 9, far UV photometry (UIT B5, F160BW) mostly flattens the blue end of the HB in magnitude, and should allow the optimum separation of luminosity and color effects. Far UV observations are not very common, and it is even rarer to connect observations in different UV wavelength bands.

A small number of clusters have archival data in the near and far UV as well as optical bands. HST WFPC2 data is available from proposals 5903 (M80; F. Ferraro PI), 6804 (NGC 2808; F. Fusi Pecci PI), and 8709 (NGC 6752, M2; F. Ferraro PI). We processed images using HSTPhot in a manner similar to the M13 images. To compare different clusters, we identified stars at the red end of the Grundahl u jump in U band from HB morphology or with the help of spectroscopic information (NGC 6752, Moni Bidin et al. 2007; NGC 2808, Moni Bidin et al. 2009). The u jump appears to have a common $T_{\rm eff}$ in all clusters (Grundahl et al. 1999), and so we used it to register the CMDs by temperature. In addition, blue HBs have a long segment at nearly constant U magnitude (Ferraro et al. 1997) that includes the u jump, and in the F160BW band the u jump falls near the red end of a fairly flat segment reaching nearly to the end of the HB. Thus, this registration provides a convenient means of comparing the extent of blue HBs in color and magnitude. It also avoids the need to make large and uncertain corrections for reddening in UV bands (Cardelli et al. 1989) or for the time dependence of WFPC2 throughput in the UV (Holtzman et al. 1995).

Fig. 26 shows sets of CMDs shifted so that the red end of the u jump is at (0,0).

A few conclusions can be drawn from simple comparisons. First, the large population of blue hook stars in NGC 2808 falls in a portion of the CMD ($\Delta U > 2, \Delta(U-V) < -1$) that is not occupied by more than a few stars in any other cluster. It is worth remembering that these are not the bluest stars in the Δ F160BW, Δ(F160BW $- V$)) CMD. They are fainter (Δ F160BW$>$ 0.5) and slightly redder than the blue end. This is the origin of the "blue hook" moniker, and it is thought to be the result of a helium-rich atmosphere resulting from flash mixing (Brown et al. 2001).

M13, M2, and M80 have similar morphologies at the blue end of the Δ F160BW, Δ(F160BW $- V$)) CMD, though the distributions of stars differ. The HB sequence dips faintward in the range $-2.4 \lesssim \Delta(\mathrm{F160BW} - V)) \lesssim -2$ before rising again up to (F160BW $- V$)) $= -3$. Most of the stars in the rising portion are also in the Momany U jump (see Fig. 27). The identification between the upturn in F160BW and the Momany U jump is clearest in M13 because of the large population of stars at the end of the HB. Some stars are found to the red in the $(U, U-V)$ CMD for M2 and M80, although these may be blends with main sequence stars in V band[9].

The correlation between stars in the Momany jump and the upturn in F160BW is not perfect, but it suggests that there is a coherent group of stars to be found on the extreme blue HB. The group does not fall at the precise end of the HB though, as we find in each cluster small numbers of stars that are bluer and fainter in the F160BW and U CMDs. This interpretation differs from that of Momany et al. (2004), who stated that the HB sequence appeared to make an almost discontinuous jump in color ($\sim$ 0.3 mag) at constant U magnitude, and extending faintward in U (by $\sim 0.5 - 0.7$ mag) at nearly constant color. The color histograms make it clear that the three clusters have very different distributions, with M2's distribution declining toward the blue end, M80 with a broad but evenly spread group, and M13 with a well-defined peak and a large fraction of the stars in the Momany jump.

While no spectroscopic data exists in the literature for M13 stars in this range, Moehler et al. (2003) examined cooler HB stars (8000 K $\lesssim T_{\rm eff} \lesssim$ 21000 K) and found evidence of strong helium depletion and iron enrichment for $T_{\rm eff} \gtrsim$ 12000 K. We can get additional guidance by contrasting spectroscopic results for NGC 6752 (Moni Bidin et al. 2007) against those for NGC 2808 (Moehler et al. 2004) and ω Cen (Moehler et al. 2007). NGC 6752, ω Cen, and

[9]Main sequence stars contribute very little light in UV bands, and so blends shift almost horizontally to the red in the CMD. Because the F160BW$-V$ color has a longer wavelength baseline than $U - V$, blends don't shift stars as much.

NGC 2808 all have noticeable vertical jump features in $(U, U-V)$ CMDs, but the most obvious jumps occur at larger $T_{\rm eff}$ in NGC 2808 and ω Cen. In NGC 6752, there is consistently helium depletion in the atmospheres of stars hotter than the Grundahl jump at $T_{\rm eff} \approx 11000$ K, including the hottest stars observed. In NGC 2808 and ω Cen, stars with near-solar and super-solar helium abundances (and concurrent carbon enrichment) appear at temperatures above those seen in NGC 6752 ($T_{\rm eff} \approx 31000$ K). Both spectroscopic signatures are consistent with the predictions of "late hot flashers": stars that ignite helium on the white dwarf cooling curve, and initiating convective mixing of the envelope.

We are led to the same conclusion reached by Momany et al. (2004): that the stars in the second U jump are likely to be "early hot flashers". In this case, the existence of a working hydrogen-fusion shell is thought to inhibit convective mixing into the outer envelope during core helium ignition. As a result, no clear spectroscopic signature is expected and none has been found to date. Because helium enrichment of the envelope plays a role in producing blue hook stars (Brown et al. 2001) by reducing atmospheric opacity shortward of the Lyman limit (and reducing redistribution of flux to longer wavelengths), we examined the data for spectroscopically studied stars in the Momany jump within NGC 6752 (Moni Bidin et al. 2007). We found no correlation between measured helium abundances [which covered the range $-3.26 \leq \log(n_{He}/n_H) \leq -1.58$] and U magnitude, which seems to confirm that the envelope is still dominated by hydrogen. The scatter in helium abundance appears to be interesting, however — when Moni Bidin et al. (2009) combined their measurements for M80 and NGC 5986 stars with those from NGC 6752, they found consistent helium depletion for stars hotter than the Grundahl jump at $T_{\rm eff} \approx 11000$ K, but also found stars with larger depletions and generally larger star-to-star scatter in two temperature ranges (13000 K $\lesssim T_{\rm eff} \lesssim$ 18000 K and 25000 K $\lesssim T_{\rm eff} \lesssim$ 31000 K).

Both of the helium depletion features appear to be associated with the U jumps, although the details probably differ. For the Grundahl jump, stars that are hotter than the jump are uniformly brighter in the Stromgren u filter than a canonical ZAHB. By contrast the stars associated with the second U jump in M13 are brighter than the majority of HB stars of similar (but higher or lower) temperature, as seen in the U and F160BW filters. Observationally, the radiative levitation of heavy elements and the downward diffusion of helium almost certainly must be involved because all stars with $T_{\rm eff} \lesssim 11000$ K (excepting blue hook stars) are found to have some degree of surface helium depletion, but the mechanics are still being debated. The transition at 11000 K is associated with the near-disappearance of the surface convection zone, but recent models (Michaud et al. 2008) indicate a need for a low-mass mixed layer near the surface to moderate the build-up of metals. There may be reason to attend to the effects of rotation because a discontinuity in average rotation speeds also appears at around this temperature (with hotter stars largely

being slow rotators; Peterson et al. 1995; Behr 2003).

Based on the evidence above, we considered whether progenitors of extreme HB stars such as early and late hot flashers can be identified on the RGB. Early hot flashers are theoretically expected to only leave the RGB near the tip, while late hot flashers could leave at lower luminosities. While M13 appears able to produce both kinds of hot flashers, the second U jump stars (our early hot flasher candidates) are much more abundant. Thus, we would expect that clusters with similar HB morphologies (like NGC 6752, M2, and M80) to show symptoms of this near the TRGB if anywhere.

Strangely, Sneden et al. (2004) found that M13's known "super O-poor" stars ([O/Fe] < -0.4) have high Na abundances and most appear very close to the RGB tip ($M_V^0 < -2.3$), indicating the possible exposure of heavily processed gas at the surface. For perspective, Carretta et al. (2006) summarize literature data for the well-known anticorrelation between [O/Fe] and [Na/Fe] for stars in 20 clusters, and Carretta et al. (2008) present new spectroscopic data for 19 clusters. The extent of the O-Na anticorrelation varies from cluster to cluster, but it probably requires nuclear processing under conditions that cannot be produced in gas that can be mixed to the surface in low-mass stars. This has led to the supposition that it results from pollution by previous generations of more massive stars. Even so, super O-poor stars are quite rare and, to the best of our knowledge, have not been seen among relatively unevolved turnoff and subgiant branch stars (see Carretta et al. 2006), although this could be due to difficulties in detecting low oxygen abundances among faint stars.

In addition, the cluster NGC 2808 has a large population of blue hook stars and seemingly few or no early hot flasher candidates, and contains super O-poor stars as well (Carretta et al. 2006) but these are fairly uniformly spread down the RGB (although those authors did not observe stars at the tip of the RGB). ω Cen also has a large population of blue hook stars, and appears to have a population of super O-poor stars (Norris & Da Costa 1995). In the cases of NGC 2808 and ω Cen though, there is clear evidence of both self-enrichment and multiple populations, which may complicate the interpretation.

Examination of bright giants in NGC 6752 (Yong et al. 2003; Carretta et al. 2008) have revealed no super O-poor stars. In addition, Mg isotope ratios in M13 (Sneden et al. 2004) and NGC 6752 are correlated with the O depletions among bright giants, but the conditions necessary to process Mg are not expected in RGB stars based on current nuclear reaction rates. The sample of Carretta et al. (2008) hints at the possibility of smaller populations of super O-poor stars in clusters like NGC 3201 and M5, neither of which have extreme HB stars.

Though there is strong evidence of mass loss effects on the extreme BHB, there is still

little to connect this directly to the properties of stars still on the RGB. One outstanding question that deserves theoretical attention involves the position (redder than the extreme end of the HB) and clumping of the early hot flasher candidates in the CMD. Even if helium is enriched overall in the bluest HB stars, some non-standard physics is probably required to produce their observed characteristics because helium-enriched EHB stars should be fainter than ones with primordial helium abundance. We can suggest two types of observations that might help to clarify the situation. First, in clusters with stars concentrated near the blue end of the HB, stars at the TRGB may have chemical peculiarities similar to those in M13 if they are preparing to have early hot helium flashes. If found, this could result from excessive mass loss or from highly helium-enriched stars, but it would connect RGB and extreme HB stars. Second, in clusters with predominantly red HBs, spectra for blue HB stars in a limited range of T_{eff} near the instability strip may reveal their initial helium abundances (Villanova et al. 2009). This would be a direct observational test of whether helium enrichment has produced *any* blue HB stars. While there is circumstantial evidence of helium enrichment in clusters like NGC 6388 and NGC 6441 (Busso et al. 2007), spectroscopic proof should be possible.

7.2. "Second Parameter" Effects on the HB

Because the R ratio seems to rule out previously suggestions of helium enrichment in M13, we discuss the literature on M13 to see if the observations can be reconciled. The main evidence pointing toward a helium enrichment falls into several categories: 1) morphology of the HB, 2) luminosity of the HB and the RR Lyrae variables, and 3) morphology of the subgiant branch.

7.2.1. HB Morphology

M13 and M3 have long been a "second parameter pair" based on the distribution of stars on their HBs — the small difference in [Fe/H] (the "first parameter") between the two clusters is unable to explain the much bluer HB stars in M13. Before discussing further, we emphasize that we are mainly considering the shift in the CMD position of the "most representative" HB stars in the two clusters, and not the differences in the shape of the HB distributions. Our goal is not to model the HB morphology in detail. M13 has an unexplained bimodal HB distribution as well as a significant number of stars between the two peaks, but arguably the brighter peak ($15 < V < 15.5$; slightly bluer than the instability strip) is the most representative based on star numbers. By contrast, M3 has a unimodal distribution with the peak of the distribution falling within the instability strip (Valcarce & Catelan

2008).

Earlier studies (Fusi Pecci et al. 1993; Buonanno et al. 1997) have used $(B-V)_{peak}$ (the dereddened color of the peak of the HB star distribution) as a way of describing the most representative HB stars in clusters, although this indicator starts to lose sensitivity on the steep blue tail. We used our earlier results from histogramming the I magnitudes of HB stars, and then translated the resulting position to the $(B-V)$ color using a fiducial line. We find $I_{peak} \approx 15.25$ and $(B-V)_{peak} \approx -0.05$. For comparison, Buonanno et al. (1997) give $(B-V)_{peak} = 0.30$ for M3. If the clusters have nearly identical chemical compositions, this corresponds to a difference of about $0.06 M_{\odot}$ in HB star mass (Teramo models). Unfortunately, this does not transform to a similar mass difference at the cluster turnoff if common red giant mass loss formulas are applied because they are nonlinear with star mass. If M13 is helium enriched compared to M3 by $\Delta Y = 0.05$, the mass difference is virtually the same. Helium enrichment in M13 does not remove the need for a difference in mean mass between its HB stars and those in M3.

The mass difference can be explained with reasonable assumptions in both the Δt and ΔY hypotheses, and we refer the reader to §1 for a brief summary of recent attempts to model M13's HB. In the Δt hypothesis, M13's stars are older than M3's. In the ΔY hypothesis, helium enrichment allows less massive stars to leave the main sequence earlier, *but* a large amounts of mass loss is still necessary for each star. While this may be correct, the picture is not fully motivated by physical reasoning. As discussed in §5.3.1, the sharp red edge of the bright peak and the population of redward-evolving HB stars may provide new constraints on fits in the ΔY hypothesis. We encourage synthetic HB studies that pay closer attention to these features.

7.2.2. The Luminosity of the HB

The luminosity of the HB is most strongly affected by metallicity and helium abundance ($\delta V_{HB}/\delta Y \approx -4$ mag), and is insensitive to age. However, without accurate and independent measurements of distance and extinction, the luminosity must be determined relative to other cluster stars. Most commonly, the reference landmarks are found among MS stars (such as the turnoff or a fainter point identified with the help of the turnoff) or RGB stars (like the RGB bump). These methods have generally indicated that M13's HB is luminous compared to other clusters, but the reference points usually have the disadvantage of having their own dependencies on composition and age that complicate the interpretation. In the discussion below, we will focus on the $\Delta Y = 0.04$ (Johnson & Bolte 1998) and $\Delta t = 1.7$ Gyr (Rey et al. 2001) hypotheses for explaining differences between M3 and M13, but we must consider the

evolution hypothesis (see §1) at the same time.

When the cluster turnoff is used as a reference, it introduces a dependence on age ($\delta V_{TO}/\delta t \approx 0.075$ mag / Gyr; Caloi & D'Antona 2005) and increases the dependence on helium ($\delta V_{TO}/\delta Y \approx 1.5$ mag; Caloi & D'Antona 2005). We determined $V_{TO} = 18.59 \pm 0.05$, which gives $\Delta V_{TO}^{HB} = 3.69 \pm 0.07$ if we apply our value for V_{HB} at the blue edge of the instability strip. This value is larger than any previously quoted (see Johnson & Bolte 1998 for a summary), and if we use the Kopacki et al. (2003) value for $\langle V_{RR} \rangle$, the value would be higher still (3.76 mag). The larger values of ΔV_{TO}^{HB} depend entirely on whether the RR Lyraes and "reddest blue HB" stars near the instability strip (see §5.3.1) are evolved or not. Both Johnson & Bolte (1998) and Rey et al. (2001) observed much smaller samples in M13, and an examination of their CMDs shows that together they only observed two "reddest BHB" stars among the 55 we identified — understandable considering that most of these stars are in the core of the cluster. As a result, Johnson & Bolte quote a value for V_{HB} that is 0.19 mag fainter than ours. We also note that like the studies of Johnson & Bolte and Rey et al., our photometry for the HB and turnoff regions are on a consistent zeropoint. We see no reason to dispute earlier values of ΔV_{TO}^{HB} for M3, given that M3's HB is well-populated on either side of the instability strip. So if M13's reddest HB stars are not evolved, it has an extreme value for ΔV_{TO}^{HB} (almost 0.2 mag larger than that of M3), and this is consistent with both the Δt and ΔY hypotheses. To find the cause (the HB, TO, or both), we need other reference points.

Ferraro et al. (1997) conducted a similar comparison between M3 and M13 using HST U observations. In U, the subgiant branch and a section of the blue HB become flat, making them excellent magnitude references. The authors found no significant difference between the ΔU_{SGB}^{HB} derived for the two clusters. While this does not directly bear on the luminosity of the HB near the instability strip, it is an indication that the bluer HB of M13 has a normal luminosity compared to M3.

The red giant bump can also be used as a reference point, dependent on helium abundance ($\delta V_{bump}/\delta Y \approx 1.5 - 2$ mag; Riello et al. 2003; Caloi & D'Antona 2005) and age ($\delta V_{bump}/\delta t \approx 0.035$ mag / Gyr; Caloi & D'Antona 2005). The observed value for the difference ΔV_{HB}^{bump} can be put in context using the catalogs of Ferraro et al. (1999) and Di Cecco et al. (2010). To ensure a reliable comparison, we calculated the correction from V_{HB} to $V_{ZAHB} = 14.96$ according to the Ferraro et al. prescription. We therefore derive $\Delta V_{HB}^{bump} = -0.21$, which falls right among those for clusters of similar metallicity (for example, M3 has -0.23 ± 0.07). However, their tabulated value for V_{ZAHB} is 0.14 mag fainter than ours — this is partly a reflection that the photometry they used (Paltrinieri et al. 1998) lacked stars near the instability strip, and partly that they used synthetic HB calculations

to derive the level of the ZAHB relative to the HB stars they did observe. Using the fainter ZAHB, M13's value for ΔV_{HB}^{bump} becomes significantly different from M3's value, and falls at the low end of the distribution for similar clusters. So if the RR Lyraes are showing us the true ZAHB level, neither age nor helium changes are necessary but can't be ruled out because the expected changes are 1σ level. If the ZAHB has a fainter level, rather large differences are needed ($\Delta Y = 0.06 - 0.09$, or $\Delta t = 3.5$ Gyr). The tabulation of Di Cecco et al. (2010) measured values for both M3 and M13 using homogeneous photometry and a template-fitting method for determining V_{ZAHB} for troublesome clusters like M13 that have very blue HBs. Their ΔV_{HB}^{bump} values are in agreement to within the measurement errors.[10]

The brightness of the AGB clump is fairly independent of metallicity (Castellani et al. 1991), but when the magnitude difference with the HB is formed, the dependences on helium abundance and RGB progenitor mass almost completely disappear (Pulone 1992; Cassisi et al. 2001). Although M13 has a sparsely populated AGB clump, there is a fairly clear grouping of 12 stars at $V = 14.19$. Using the bright ZAHB level from the previous paragraph, we have $\Delta V_{HB}^{AGB} = -0.77$. This is slightly smaller than the value for M3 (-0.88 ± 0.10) from Ferraro et al. (1999), but only about 1σ different. If the fainter ZAHB level is applied, the M3 and M13 values agree to within about 0.03 mag. The results might also be affected by likely lower mean HB mass in M13 compared to M3, which affects how the clump is populated and would tend to reduce the luminosity of the clump. We consider this weak evidence in favor of the fainter ZAHB level.

The HB luminosity can be constrained using the end of canonical HB as a reference in clusters with long blue tails. Like NGC 6752, M13's HB appears to terminate essentially at the end of the canonical HB, and we identified blue hook candidates (in §5.2) and second U jump stars (in §7.1) that mark points in the HB near the end. Models show that the difference in magnitude between the termination of the blue HB and the blue end of the instability strip grows substantially larger with increasing helium abundance, mostly because the horizontal part of the HB gets brighter. The faint end of the HB is fairly insensitive to

[10]Caloi & D'Antona (2005) also used the position of the RGB bump relative to the turnoff (ΔV_{TO}^{bump}) as a potential helium indicator, with larger magnitude differences implying higher helium. In their comparison, they found that M13 had a magnitude difference that was 0.14 ± 0.09 larger than that of M3, which they admitted had relatively low significance. Because our photometry of the bump and main sequence constitutes a homogeneous dataset with a much larger number of stars, we checked their quoted bump and turnoff magnitudes (derived from the photometry of Paltrinieri et al. 1998). We find there is a rather large difference in color (0.08 mag) between the Paltrinieri et al. photometry and ours, but the V magnitudes are almost identical to ours. On their own, the RGB bumps of the M13-M3 pair do not give a strong constraint on helium abundance, although Caloi & D'Antona showed that clusters with predominantly blue HBs had larger ΔV_{TO}^{bump} than clusters that have strong populations in the instability strip.

helium abundance because the hydrogen-rich envelopes of the stars are almost gone. If the end of theoretical ZAHBs are shifted in magnitude to fit the end of M13's HB, the bright end is consistent with primordial helium values (see Fig. 28). While the fit is understandably uncertain due to the gap between the HB stars and the blue hook stars in optical filters, the Teramo evolutionary tracks do go nearly parallel to the faint envelope of HB stars (see Fig. 23). The fit seems to rule against helium enrichment among stars within and redder than the primary peak. Evolutionary effects among the reddest HB stars would tend to bias toward an indication of helium enrichment, so this result seems fairly robust. Spectroscopic measurements of stars near the red end of the HB in M13 and NGC 6752 also support the idea that the outer envelopes have *not* been significantly processed through the CNO cycle, and (in NGC 6752) still have primordial helium abundance (Villanova et al. 2009).

Alternately, if the ZAHBs are fit to the red end of the HB, helium-enriched ZAHBs are far too red at the faint end, lending additional credence to models with canonical composition. However, current models of the bluest HB stars do not fully incorporate important physics such as diffusion and radiative levitation, and these effects seem to be responsible for the u jump and the intra-peak HB stars that are brighter than canonical models. As a result, fits to the HB should be treated somewhat skeptically.

Finally, we consider the distance moduli implied by the HB (specifically the RR Lyrae stars) and by the TRGB. Both of these features are in common use as standard candles, and a comparison of the resulting values might also give us clues on whether the HB is unusually bright. The absolute magnitude of the TRGB in I is almost independent of age and chemical composition. From the calibration of Bellazzini et al. (2004), we calculate $M_I^{TRGB} = -4.07$, which gives $(m-M)_I = 14.35$. The distance modulus could be smaller than this if by chance M13 does not contain RGB stars very near the flash stage. To evaluate this possibility, we can use a binomial distribution to calculate the probability that at least one star is within a certain magnitude range of the TRGB. In our cluster-wide sample, there were 271 stars brighter than the RGB bump ($I < 13.6$). Using theoretical RGB luminosity functions that fit M13's population (see §4), stars brighter than that level have an approximately 0.4% chance of being within 0.01 mag of the TRGB, so that a calculation using the binomial distribution predicts a 70% chance of having at least one of the 271 stars within that interval. The probability rises to about 90% that at least one star is within 0.05 mag of the TRGB, so this is probably a minor source of error.

All of the brightest RGB stars are known to be semi-regular variables including the brightest (V11), having an amplitude of about 0.13 mag in V and a timescale for variability of about 30 d (Kopacki et al. 2003). As a result, the variability of the brightest giants is a significant source of error in our determination of I_{TRGB}. Though Kopacki et al. made

observations over 70 d (more than two cycles for most giant variables), it is possible they did not sample the full amplitude of variation. Our CFHT V measurement of V11 (which was used above) was 0.15 mag brighter than the average given by Kopacki et al., while our KPNO observation was only about 0.06 mag brighter (barring zeropoint differences). If we can assume that the I observations are off by similar amounts, this gives $(m-M)_I \approx 14.5$. The range of variation for other bright RGB stars (V17, V24, V38, and V42) overlap that of V11, and all but one give corrected distance moduli within 0.03 mag of the V11 value. V17 gives a significantly brighter value (14.37), but it also has the largest amplitude (0.38 mag) of the red giant variables tabulated by Kopacki et al.. We believe the agreement among 4 of the 5 variables is sufficient to identify the TRGB, which in turn implies $(m-M)_0 = 14.48$ with a very conservative uncertainty of 0.10 mag.

Although there is still considerable discussion of the RR Lyrae M_V−[Fe/H] relation, recent consensus views (e.g. Catelan et al. 2004) imply a mean RR Lyrae value $M_V^{RR} = 0.62$ for M13's metallicity. With $\langle V_{RR} \rangle$ from the Kopacki et al. (2003) observations of M13 RR Lyraes, this gives $(m-M)_V = 14.21$. The disagreement with the TRGB distance modulus can again be relieved if the RR Lyraes in M13 were significantly evolved or were helium enriched ($\Delta Y \approx 0.05$). If we use the TRGB distance modulus and M_V^{RR} to calculate the brightness of the HB, we find $V_{HB} = 15.07$. This is fainter than all of the "reddest BHB" stars but approximately the same brightness as the blue end of the primary peak.

Once again, a comparison with M3 is useful, thanks to that cluster's huge RR Lyrae population. Jurcsik et al. (2003) identified 4 groups of RR Lyraes with different brightness and light curve parameters, with the most abundant group of 50 stars having $\langle V \rangle = 15.67$. Their most evolved group (32 stars), which the authors hypothesized were evolving redward, had $\langle V \rangle = 15.53$. The difference between $\langle V \rangle$ for the most evolved RR Lyraes in M3 and that of M13's RR Lyraes is most consistent with magnitude differences derived from comparing points like the RGB bump and AGB clump (Ferraro et al. 1999).

Evolution is also expected to affect the pulsational properties of stars within the instability strip because the mean density of evolved stars is lower than for unevolved stars, resulting in larger periods. We could expect to discern evolutionary effects in several ways: based on observations derived solely from the light curves (such as the Bailey period-amplitude diagram), period-luminosity relationships (with luminous RR Lyraes having longer periods), and color distributions (with evolved stars likely to be spread more evenly through the instability strip due to their short evolutionary timescale).

If variability information (such as period and variation amplitude) can give unambiguous evolutionary information, it should be preferred because such measurements can generally be made to higher precision than can determinations of average magnitude or color. Fig. 29

shows V amplitude and period data for M13 RR Lyrae stars from Kopacki et al. (2003) in the Bailey diagram. The single known RRab cluster variable (V8) has an even longer period than the "well-evolved" stars in M3 identified by (Cacciari et al. 2005). Because V8 is also the reddest RR Lyrae and evolutionary tracks in this part of the CMD are expected to slope brightward toward the AGB, it would not be surprising if it showed an evolution signature. In M13, the three BL Her stars (Population II Cepheid variables) fall approximately in the part of the CMD where stars that have evolved from the blue HB tail are predicted to pass, and their periods (all greater than a day) also support evolved status. However, V8's $\langle V \rangle$ is fainter than most of the RRc variables. Given the amount of scatter seen in larger samples of RR Lyraes (see below), this can't be considered evidence.

RRc variables are more abundant in M13, so an evolutionary signature among these stars would be more compelling. Four of the RRc variables have periods consistent with the "well-evolved" RRc stars in M3, but with somewhat lower amplitude (one exception falls on the M3 relation). The remaining 4 (V7, V31, V35, V36) have periods consistent with the regular variables in M3 but again with low amplitudes. There is no evidence of separation in average V magnitude between the two groups however, weakening the idea that evolutionary effects can be identified solely from the periods of the RRc variables.

To put M13 in better context, we assembled literature data for other Oosterhoff group II clusters (hereafter, OoII). For a few in this group, the instability strip is heavily populated, leading to an expectation (based on evolution timescales) that a large proportion of the RR Lyraes should be near the ZAHB. Clusters in this category include ω Cen (Kaluzny et al. 2004; Olech & Moskalik 2009), NGC 2419 (Ripepi et al. 2007), NGC 5286 (Zorotovic et al. 2010), M68 (Walker 1994; Clement et al. 1993), and M15 (Corwin et al. 2008; Silbermann & Smith 1995). These clusters have relatively low HB_{type} values (≤ 0.8), and NGC 2419 and M68 have significant red HB populations as well. Both of these factors imply that there are likely to be unevolved stars in the instability strip. This group of OoII clusters, however, is outnumbered by clusters like M13 that have almost exclusively blue HB stars. For example, M2 (Lázaro et al. 2006; Lee & Carney 1999) is a massive cluster that has more RR Lyrae stars than M13, but still has a very small fraction of its stars in the instability strip. For comparison, we compiled data for clusters with only a few RR Lyraes, under the hypothesis that these stars are more likely to have evolved from the blue HB[11]. The Bailey diagrams (V amplitude versus period) for the different samples are shown in Fig.

[11]References for RR Lyraes in "BHB Clusters" are: M9 (Clement & Shelton 1999); M30 (Pietrukowicz & Kaluzny 2004); M55 (Olech et al. 1999); M80 (Wehlau et al. 1990); M92 (Kopacki 2001; Cohen & Matthews 1992); NGC 288 (Kaluzny et al. 1997); NGC 5897 (Wehlau 1990; Clement & Rowe 2001); NGC 5986 (Alves et al. 2001).

29.

M13 RRc variables fall in parts of the Bailey diagram that are commonly occupied by variables in other OoII clusters. In the BHB cluster group and most of the other clusters, a significant fraction of the RRc variables fall near $(A_V, \log P) = (0.45, -0.41)$. This group appears largely independent of cluster metallicity. The main exceptions are NGC 5286, which is more metal rich than M3 and has an analogous group that is much closer in period to M3 RRc variables, and M2, which doesn't have a clear concentration of RRc variables in the Bailey diagram. The second identifiable group of M13 RRc variables overlaps with groups in the BHB Cluster sample and in ω Cen, and has $\log P \approx -0.5$ and $A_V \leq 0.5$. From these diagrams, we conclude that there are not clear evolutionary signatures that be inferred from the Bailey diagram alone.

Strangely, there are proportionately few short period, low amplitude RRc variables in the "protoypical" OoII clusters M15 and M68. In addition, both of these clusters have populations of double-mode RRd variables that largely reside in a small range of color between the RRab and RRc variables (Silbermann & Smith 1995; Walker 1994). Such a distribution is unlikely if most of the stars are evolved BHB stars — evolution accelerates as a star moves redward toward the AGB. Conversely, we find that the shortest period ($\log P \lesssim -0.46$) RRc stars are the bluest RR Lyrae stars in OoII clusters. Many of the known non-radial pulsators in OoII clusters (Kopacki et al. 2003; Olech et al. 1999; Kopacki 2001) are also found within this group.

At best, we find that Bailey diagrams for OoII RRc stars provide some information about average colors. This is somewhat useful for examining the effects of evolution within individual clusters because some color distributions (especially ones biased toward the red) are incompatible with model predictions. However, the RRc don't appear to follow patterns implied by M3, in which "well evolved" stars appear shifted to greater period.

In summary, the majority of the evidence from photometric indicators implies that the M13 RR Lyraes (and nonvariable stars of similar color) are significantly brighter than the ZAHB level. The most notable exception involves the comparison to the RGB bump, while the pulsation properties of the RR Lyraes themselves are somewhat ambiguous. If the reddest HB stars are discounted as significantly evolved, then M13's blue HB appears to fall at approximately the same luminosity level as M3's and the evidence for helium enrichment or age differences from this is removed.

7.2.3. Subgiant Branch Morphology

As mentioned earlier, one of the more unusual aspects of M13's CMD is the steeper slope of its subgiant branch in comparison to M3's. This was interpreted as resulting either from helium enrichment (Johnson & Bolte 1998) or greater age (Rey et al. 2001). Both of the cited papers used the so-called "horizontal method" to compare the ages of clusters with other clusters or isochrones. Higher helium abundance or age tends to shorten the length of the subgiant branch, so that if the turnoffs are aligned in color and fainter main sequence points (usually 0.05 mag redder than the turnoff) are subsequently aligned in magnitude, the relative position of the giant branch reveals the difference. It has been verified repeatedly that there is a difference between M3 and M13, but the cause is unclear.

We can attempt to look at the problem from a different angle by realizing that age and helium enrichment affect the absolute colors of the turnoff and red giant branch in different ways. An increase in helium abundance reduces the opacity of the stellar envelope, making surface temperature higher at both the turnoff and on the red giant branch. On the other hand, increased age makes both the turnoff and red giant branch redder, although the effect on the giant branch is very small.

Because reddening and metal abundance differences have large effects, reliable comparisons of absolute colors can only be done when these are well-determined — M3 and M13 are probably the best example of such a pair. Stetson (1998) discusses them in this respect, but we expand on the arguments here. The reddenings for the two clusters appear to be small and very similar (M13 probably with the larger reddening by $\Delta E(B-V) < 0.01$; Schlegel et al. 1998) and their metallicities appear to agree to within 0.1 dex (with M13 being the more metal poor; Sneden et al. 2004). One additional benefit of using the M3/M13 pair is that the effects of the reddening and metallicity differences on the turnoff should partly cancel, with the metallicity differences leading to an expectation that M13's turnoff should be bluer than M3's by about 0.01 in $B-I$, and less in other optical colors.

A comparison in absolute colors also requires datasets for which the calibration can be done uniformly for both clusters. While we are unable to do this because our deep exposures of M3 and M13 were not taken on the same photometric night, it has been done in the most recent studies, although using different colors. Johnson & Bolte (1998) used $V-I$ and found that M13 was bluer at the turnoff and giant branch by similar amounts ($0.01-0.02$). This implies a tiny helium enrichment ($\Delta Y \approx 0.01$) at most. On the other hand, Rey et al. (2001) used the $B-V$ color and found that the turnoff colors were virtually identical, although M13's red giant branch was still significantly bluer. We examined the standard star photometry of Stetson (2000) for the two clusters (8 November 2007 update), and found that in the $V-I$ color M13 is bluer than M3 on the giant branch and at the turnoff (in agreement

with Johnson & Bolte 1998), while in $B-V$ or $B-I$ colors M13's turnoff is significantly *redder* (even accounting for small differences in reddening) and the giant branches have nearly identical colors (see Fig. 30)[12]. Based only on the Stetson standard stars in $B-V$ and $B-I$ colors, an age difference appears tenable. With the $V-I$ color included, neither helium nor age differences seem capable of explaining the observations because neither is expected to affect one color differently than others. We conclude that current photometric datasets do not paint a consistent picture, and may still be influenced by subtle systematic effects. To make this a stringent test, effort should go into deep and carefully calibrated photometry using filters with a wide wavelength baseline. The $B-I$ color still appears to be a good choice.

8. Conclusions

To our minds, some of the most important questions regarding M13 remain in dispute. One question that we have reopened here is whether the reddest of the blue HB stars in M13 are significantly evolved (and whether they are therefore good representatives of the brightness of the horizontal branch). The weight of the observational and theoretical evidence leans toward the idea that they are significantly evolved, and that the red edge of the primary HB population is a decent indicator of the true HB level.

The distribution of stars on the horizontal branch in M13 is complex, and the most notable questions regard 1) how the color of the primary peak in M13 could have been shifted so far relative to M3's when the gross composition of clusters appear nearly identical, and 2) how a large fraction of M13's RGB stars become blue stars near the end of the canonical HB. Our examination of the luminosity function shows little sign that a large fraction of stars leave the bright RGB before having a core flash, in agreement with the massive cluster NGC 2419 (Sandquist & Hess 2008) but not with NGC 2808 (Sandquist & Martel 2007). We do not find any clear evidence of helium enrichment among the stars of the dominant (redder) HB population, and in fact, the helium abundance indicator R and the relative brightness of the HB argue against significant enrichment. The HB and RGB stars (and different subsets of these) do not show significant signs of radial segregation within the cluster. The small color

[12]While the Stetson standard stars in M3 and M13 are rigorously tied to the system of Landolt standard stars, the observations for the two clusters were taken under varied conditions. M3 and M13 can be observed on the same night using the same equipment, and so it should be possible to get good relative photometry for the pair. We note that Stetson (1998) reported that M13 had a bluer turnoff than M3 by 0.014 mag in $B-I$ (about 0.04 mag when reddening was accounted for) for images of the two clusters taken on the same night under photometric conditions using the same equipment.

difference between the main sequence turnoff and the giant branch of M13 (in comparison to M3) remains unexplained, but careful examination of the absolute colors of both clusters would provide a new test.

Our thorough search of M13's HB population has revealed second U jump and blue hook stars that imply that many of these stars have very low-mass hydrogen-rich envelopes. Far UV observations show that many of the stars in the second U jump are more luminous than stars with similar colors at the end of the HB. The reason is unclear, however. Spectroscopic data on similar stars in NGC 6752 (Moni Bidin et al. 2007) indicate that the excess brightness is not related to enhanced atmospheric helium abundance, so further study is required.

Spectroscopic measurements may help to clarify our understanding of extreme HB stars in a number of ways. We particularly encourage studies of: stars near the red end of the HB in M13 where helium abundances can be accurately determined (Villanova et al. 2009); stars in the extreme HB to look for signs of unusual Mg abundances (a species that appears to be minimally affected by diffusion) that could connect them to giant stars; O, Na, and Mg for stars at the red giant tip of other clusters to determine whether they are super O-poor; relatively unevolved turnoff and subgiant stars in M13 and NGC 2808 to search for large O depletions ([O/Fe]< -0.4) and check whether this is the result of external pollution or not.

We would like to thank D. Pollard for contributions to the paper, S. Cassisi for graciously providing tabulations of CMD positions of HB stars for various degrees of central helium depletion, and the anonymous referee for a careful reading. This work has been funded through AST grants 00-98696 and 05-07785 from the National Science Foundation to E.L.S. and M.B. M.G. was partially supported as part of a Research Experiences for Undergraduates (REU) program at San Diego State University under grant AST 04-53609 from the National Science Foundation.

This research used the facilities of the Canadian Astronomy Data Centre operated by the National Research Council of Canada with the support of the Canadian Space Agency. Some of the data presented in this paper were obtained from the Multimission Archive at the Sapce Telescope Science Institute (MAST). STScI is operated by the Association of Universities for Research in Astronomy, Inc., under NASA contract NAS5-26555. Support for MAST for non-HST data is provided by the NASA Office of Space Science via grant NAG5-7584 and by other grants and contracts.

REFERENCES

Ambika, S., Parthasarathy, M., Aoki, W., Fujii, T., Nakada, Y., Ita, Y., & Izumiura, H. 2004, A&A, 417, 293

Alves, D. R., Bond, H. E., & Onken, C. 2001, AJ, 121, 318

Arellano Ferro, A., Rojas López, V., Giridhar, S., & Bramich, D. M. 2008, MNRAS, 384, 1444

Arp, H. C. 1955, AJ, 60, 317

Barnard, E. E. 1909, ApJ, 29, 72

Barnard, E. E. 1914, ApJ, 40, 173

Barnard, E. E. 1931, Publications of the Yerkes Observatory, 6, 1

Behr, B. B., Djorgovski, S. G., Cohen, J. G., McCarthy, J. K., Côté, P., Piotto, G., & Zoccali, M. 2000, ApJ, 528, 849

Behr, B. B. 2003, ApJS, 149, 67

Bedin, L. R., Piotto, G., Zoccali, M., Stetson, P. B., Saviane, I., Cassisi, S., & Bono, G. 2000, A&A, 363, 159

Bedin, L. R., Piotto, G., Anderson, J., Cassisi, S., King, I. R., Momany, Y., & Carraro, G. 2004, ApJ, 605, L125

Bellazzini, M., Ferraro, F. R., Sollima, A., Pancino, E., & Origlia, L. 2004, A&A, 424, 199

Benkő, J. M., Bakos, G. Á., & Nuspl, J. 2006, MNRAS, 372, 1657

Bergbusch, P. A. 1993, AJ, 106, 1024

Bjork, S. R., & Chaboyer, B. 2006, ApJ, 641, 1102

Bono, G., Caputo, F., & Marconi, M. 1995, AJ, 110, 2365

Bono, G., Caputo, F., Castellani, V., & Marconi, M. 1997, A&AS, 121, 327

Bono, G., Cassisi, S., Zoccali, M., & Piotto, G. 2001, ApJ, 546, L109

Briley, M. M., Cohen, J. G., & Stetson, P. B. 2004, AJ, 127, 1579

Brown, T. M., Sweigart, A. V., Lanz, T., Landsman, W. B., & Hubeny, I. 2001, ApJ, 562, 368

Brown, T. M., Smith, E., Ferguson, H. C., Sweigart, A. V., Kimble, R. A., & Bowers, C. W. 2008, ApJ, 682, 319

Buonanno, R., Corsi, C. E., Buzzoni, A., Cacciari, C., Ferraro, F. R., & Fusi Pecci, F. 1994, A&A, 290, 69

Buonanno, R., Corsi, C., Bellazzini, M., Ferraro, F. R., & Pecci, F. F. 1997, AJ, 113, 706

Busso, G., et al. 2007, A&A, 474, 105

Cacciari, C., Corwin, T. M., & Carney, B. W. 2005, AJ, 129, 267

Caloi, V., & D'Antona, F. 2005, A&A, 435, 987

Cardelli, J. A., Clayton, G. C., & Mathis, J. S. 1989, ApJ, 345, 245

Carretta, E., Bragaglia, A., Gratton, R. G., & Lucatello, S. 2008, arXiv:0811.3591

Carretta, E., Bragaglia, A., Gratton, R. G., Leone, F., Recio-Blanco, A., & Lucatello, S. 2006, A&A, 450, 523

Carretta, E., & Gratton, R. G. 1997, A&AS, 121, 95

Carretta, E., Gratton, R. G., Clementini, G., & Fusi Pecci, F. 2000, ApJ, 533, 215

Carretta, E., Gratton, R. G., Lucatello, S., Bragaglia, A., & Bonifacio, P. 2005, A&A, 433, 597

Carretta, E., Recio-Blanco, A., Gratton, R. G., Piotto, G., & Bragaglia, A. 2007, ApJ, 671, L125

Cassisi, S., Castellani, V., Degl'Innocenti, S., Piotto, G., & Salaris, M. 2001, A&A, 366, 578

Cassisi, S., & Salaris, M. 1997, MNRAS, 285, 593

Cassisi, S., Salaris, M., Castelli, F., & Pietrinferni, A. 2004, ApJ, 616, 498

Cassisi, S., Salaris, M., & Irwin, A. W. 2003, ApJ, 588, 862

Cassisi, S., Castellani, M., Caputo, F., & Castellani, V. 2004, A&A, 426, 641

Castellani, M., & Castellani, V. 1993, ApJ, 407, 649

Castellani, V., Chieffi, A., & Pulone, L. 1991, ApJS, 76, 911

Castellani, M., Castellani, V., & Prada Moroni, P. G. 2006, A&A, 457, 569

Castellani, V., Iannicola, G., Bono, G., Zoccali, M., Cassisi, S., & Buonanno, R. 2006, A&A, 446, 569

Catelan, M., de Freitas Pacheco, J. A., & Horvath, J. E. 1996, ApJ, 461, 231

Catelan, M. 1998, ApJ, 495, L81

Catelan, M., Ferraro, F. R., & Rood, R. T. 2001, ApJ, 560, 970

Catelan, M., Pritzl, B. J., & Smith, H. A. 2004, ApJS, 154, 633

Catelan, M. 2009, Ap&SS, 18

Cho, D.-H., Lee, S.-G., Jeon, Y.-B., & Sim, K. J. 2005, AJ, 129, 1922

Clement, C. M., Ferance, S., & Simon, N. R. 1993, ApJ, 412, 183

Clement, C. M., & Rowe, J. 2000, AJ, 120, 2579

Clement, C. M., & Rowe, J. F. 2001, AJ, 122, 1464

Clement, C. M. & Shelton, I. 1999, ApJ, 515, L85

Clement, C. M., & Shelton, I. 1999, AJ, 118, 453

Cohen, J. G., & Matthews, K. 1992, PASP, 104, 1205

Cohen, J. G., & Meléndez, J. 2005, AJ, 129, 303

Cohen, R. L., Guhathakurta, P., Yanny, B., Schneider, D. P., & Bahcall, J. N. 1997, AJ, 113, 669

Conlon, E. S., Dufton, P. L., & Keenan, F. P. 1994, A&A, 290, 897

Corwin, T. M., Borissova, J., Stetson, P. B., Catelan, M., Smith, H. A., Kurtev, R., & Stephens, A. W. 2008, AJ, 135, 1459

Corwin, T. M., & Carney, B. W. 2001, AJ, 122, 3183

Corwin, T. M., Carney, B. W., & Nifong, B. G. 1999, AJ, 118, 2875

Cudworth, K. 1979, AJ, 84, 1005

Cudworth, K. M., & Monet, D. G. 1979, AJ, 84, 774

Dalessandro, E., Lanzoni, B., Ferraro, F. R., Vespe, F., Bellazzini, M., & Rood, R. T. 2008, ApJ, 681, 311

D'Antona, F., & Caloi, V. 2008, in Proc. of IAU Symp. 246, Dynamical Evolution of Dense Stellar Systems, ed. E. Vesperini, M. Gierzs, & A. Sills (Dordrecht: Kluwer), 156

D'Antona, F., & Caloi, V. 2008, MNRAS, 390, 693

D'Cruz, N. L., Dorman, B., Rood, R. T., & O'Connell, R. W. 1996, ApJ, 466, 359

D'Cruz, N. L., et al. 2000, ApJ, 530, 352

Denisenkov, P. A., & Denisenkova, S. N. 1989, Astronomicheskij Tsirkulyar, 1538, 11

Di Cecco, A., et al. 2010, ApJ, 712, 527

Dieball, A., Knigge, C., Zurek, D. R., Shara, M. M., & Long, K. S. 2005, ApJ, 625, 156

Dieball, A., Knigge, C., Zurek, D. R., Shara, M. M., Long, K. S., Charles, P. A., & Hannikainen, D. 2007, ApJ, 670, 379

Dinescu, D. I., Girard, T. M., & van Altena, W. F. 1999, AJ, 117, 1792

Dolphin, A. E. 2000, PASP, 112, 1383

Dolphin, A. E. 2000, PASP, 112, 1391

Dorman, B. 1992, ApJS, 81, 221

Dorman, B., Rood, R. T., & O'Connell, R. W. 1993, ApJ, 419, 596

Dotter, A., Chaboyer, B., Jevremović, D., Baron, E., Ferguson, J. W., Sarajedini, A., & Anderson, J. 2007, AJ, 134, 376

Edmonds, P. D., & Gilliland, R. L. 1996, ApJ, 464, L157

Fabbian, D., Recio-Blanco, A., Gratton, R. G., & Piotto, G. 2005, A&A, 434, 235

Fekadu, N., Sandquist, E. L., & Bolte, M. 2007, ApJ, 663, 277

Ferraro, F. R., Carretta, E., Corsi, C. E., Fusi Pecci, F., Cacciari, C., Buonanno, R., Paltrinieri, B., & Hamilton, D. 1997, A&A, 320, 757

Ferraro, F. R., Paltrinieri, B., Fusi Pecci, F., Rood, R. T., & Dorman, B. 1997, MNRAS, 292, L45

Ferraro, F. R., Paltrinieri, B., Fusi Pecci, F., Cacciari, C., Dorman, B., & Rood, R. T. 1997, ApJ, 484, L145

Ferraro, F. R., Paltrinieri, B., Fusi Pecci, F., Rood, R. T., & Dorman, B. 1998, ApJ, 500, 311

Ferraro, F. R., Messineo, M., Fusi Pecci, F., de Palo, M. A., Straniero, O., Chieffi, A., & Limongi, M. 1999, AJ, 118, 1738

Fusi Pecci, F., Ferraro, F. R., Bellazzini, M., Djorgovski, S., Piotto, G., & Buonanno, R. 1993, AJ, 105, 1145

Fusi Pecci, F., Ferraro, F. R., Corsi, C. E., Cacciari, C., & Buonanno, R. 1992, AJ, 104, 1831

Grundahl, F., Vandenberg, D. A., & Andersen, M. I. 1998, ApJ, 500, L179

Grundahl, F., Catelan, M., Landsman, W. B., Stetson, P. B., & Andersen, M. I. 1999, ApJ, 524, 242

Haft, M., Raffelt, G., & Weiss, A. 1994, ApJ, 425, 222

Hargis, J. R., Sandquist, E. L., & Bolte, M. 2004, ApJ, 608, 243

Harris, W. E. 1996, AJ, 112, 1487

Holtzman, J. A., Burrows, C. J., Casertano, S., Hester, J. J., Trauger, J. T., Watson, A. M., & Worthey, G. 1995, PASP, 107, 1065

Itoh, N., Hayashi, H., Nishikawa, A., & Kohyama, Y. 1996, ApJS, 102, 411

Johnson, C. I., Kraft, R. P., Pilachowski, C. A., Sneden, C., Ivans, I. I., & Benman, G. 2005, PASP, 117, 1308

Johnson, J. A., & Bolte, M. 1998, AJ, 115, 693

Jurcsik, J., Benkő, J. M., Bakos, G. Á., Szeidl, B., & Szabó, R. 2003, ApJ, 597, L49

Kadla, E. I. 1966, Izvestiya Glavnoj Astronomicheskoj Observatorii v Pulkove, 181, 93

Kalirai, J. S., et al. 2001, AJ, 122, 257

Kaluzny, J., Olech, A., Thompson, I. B., Pych, W., Krzemiński, W., & Schwarzenberg-Czerny, A. 2004, A&A, 424, 1101

Kaluzny, J., Krzeminski, W., & Nalezyty, M. 1997, A&AS, 125, 337

Kinman, T., Castelli, F., Cacciari, C., Bragaglia, A., Harmer, D., & Valdes, F. 2000, A&A, 364, 102

Kopacki, G. 2001, A&A, 369, 862

Kopacki, G., Kolaczkowski, Z., & Pigulski, A. 2003, A&A, 398, 541

Landolt, A. U. 1992, AJ, 104, 340

Langer, G. E., Hoffman, R., & Sneden, C. 1993, PASP, 105, 301

Lázaro, C., Ferro, A. A., Arévalo, M. J., Bramich, D. M., Giridhar, S., & Poretti, E. 2006, MNRAS, 372, 69

Lee, J.-W., & Carney, B. W. 1999, AJ, 117, 2868

Lee, Y.-W., Demarque, P., & Zinn, R. 1994, ApJ, 423, 248

Ludendorff, H. 1905, Publikationen des Astrophysikalischen Observatoriums zu Potsdam, 50, 1

McLaughlin, D. E., & van der Marel, R. P. 2005, ApJS, 161, 304

Michaud, G., Richer, J., & Richard, O. 2007, ApJ, 670, 1178

Michaud, G., Richer, J., & Richard, O. 2008, ApJ, 675, 1223

Miller Bertolami, M. M., Althaus, L. G., Unglaub, K., & Weiss, A. 2008, A&A, 491, 253

Moehler, S., Dreizler, S., Lanz, T., Bono, G., Sweigart, A. V., Calamida, A., Monelli, M., & Nonino, M. 2007, A&A, 475, L5

Moehler, S., Heber, U., Lemke, M., & Napiwotzki, R. 1998, A&A, 339, 537

Moehler, S., Landsman, W. B., Sweigart, A. V., & Grundahl, F. 2003, A&A, 405, 135

Moehler, S., Sweigart, A. V., Landsman, W. B., & Heber, U. 2000, A&A, 360, 120

Moehler, S., Sweigart, A. V., Landsman, W. B., Hammer, N. J., & Dreizler, S. 2004, A&A, 415, 313

Momany, Y., Piotto, G., Recio-Blanco, A., Bedin, L. R., Cassisi, S., & Bono, G. 2002, ApJ, 576, L65

Momany, Y., Bedin, L. R., Cassisi, S., Piotto, G., Ortolani, S., Recio-Blanco, A., De Angeli, F., & Castelli, F. 2004, A&A, 420, 605

Moni Bidin, C., Moehler, S., Piotto, G., Recio-Blanco, A., Momany, Y., & Méndez, R. A. 2006, A&A, 451, 499

Moni Bedin, C., Moehler, S., Piotto, G., Momany, Y., & Recio-Blanco, A. 2007, A&A, 474, 505

Moni Bidin, C., Moehler, S., Piotto, G., Momany, Y., & Recio-Blanco, A. 2009, A&A, 498, 737

Norris, J. E., & Da Costa, G. S. 1995, ApJ, 447, 680

Nemec, J. M. 2004, AJ, 127, 2185

Olech, A., Kaluzny, J., Thompson, I. B., Pych, W., Krzeminski, W., & Shwarzenberg-Czerny, A. 1999, AJ, 118, 442

Olech, A., & Moskalik, P. 2009, A&A, 494, L17

Pace, G., Recio-Blanco, A., Piotto, G., & Momany, Y. 2006, A&A, 452, 493

Paltrinieri, B., Ferraro, F. R., Carretta, E., & Fusi Pecci, F. 1998, MNRAS, 293, 434

Papadakis, I., Hatzidimitriou, D., Croke, B. F. W., & Papamastorakis, I. 2000, AJ, 119, 851

Parise, R. A., et al. 1994, ApJ, 423, 305

Peterson, R. C. 1983, ApJ, 275, 737

Peterson, R. C., Rood, R. T., & Crocker, D. A. 1995, ApJ, 453, 214

Pietrinferni, A., Cassisi, S., Salaris, M., & Castelli, F. 2006, ApJ, 642, 797

Pietrinferni, A., Cassisi, S., Salaris, M., Percival, S., & Ferguson, J. W. 2009, ApJ, 697, 275

Pietrukowicz, P., & Kaluzny, J. 2004, Acta Astronomica, 54, 19

Pilachowski, C. A., Sneden, C., Kraft, R. P., & Langer, G. E. 1996, AJ, 112, 545

Piotto, G., Zoccali, M., King, I. R., Djorgovski, S. G., Sosin, C., Rich, R. M., & Meylan, G. 1999, AJ, 118, 1727

Piotto, G., et al. 2005, ApJ, 621, 777

Piotto, G., et al. 2007, ApJ, 661, L53

Pollard, D. L., Sandquist, E. L., Hargis, J. R., & Bolte, M. 2005, ApJ, 628, 729

Pulone, L. 1992, Memorie della Societa Astronomica Italiana, 63, 485

Rey, S.-C., Yoon, S.-J., Lee, Y.-W., Chaboyer, B., & Sarajedini, A. 2001, AJ, 122, 3219

Recio-Blanco, A., et al. 2005, A&A, 432, 851

Recio-Blanco, A., Aparicio, A., Piotto, G., de Angeli, F., & Djorgovski, S. G. 2006, A&A, 452, 875

Riello, M., et al. 2003, A&A, 410, 553

Ripepi, V., et al. 2007, ApJ, 667, L61

Rood, R. T., et al. 1999, ApJ, 523, 752

Sabbi, E., Ferraro, F. R., Sills, A., & Rood, R. T. 2004, ApJ, 617, 1296

Salaris, M., Riello, M., Cassisi, S., & Piotto, G. 2004, A&A, 420, 911

Sandage, A. 1981, ApJ, 244, L23

Sandquist, E. L., & Bolte, M. 2004, ApJ, 611, 323

Sandquist, E. L. & Hess, J. R., 2008, AJ, 136, 2259

Sandquist, E. L., & Martel, A. R. 2007, ApJ, 654, L65

Sarajedini, A., et al. 2007, AJ, 133, 1658

Savedoff, M. P. 1956, AJ, 61, 254

Schlegel, D. J., Finkbeiner, D. P., & Davis, M. 1998, ApJ, 500, 525

Silbermann, N. A., & Smith, H. A. 1995, AJ, 110, 704

Simon, N. R., & Clement, C. M. 1993, ApJ, 410, 526

Sirianni, M., et al. 2005, PASP, 117, 1049

Smith, G. H. 2005, The Observatory, 125, 244

Smith, G. H., & Briley, M. M. 2006, PASP, 118, 740

Smith, G. H., Briley, M. M., & Harbeck, D. 2005, AJ, 129, 1589

Smith, G. H., Shetrone, M. D., Bell, R. A., Churchill, C. W., & Briley, M. M. 1996, AJ, 112, 1511

Smith, H. A., & Wehlau, A. 1985, ApJ, 298, 572

Sneden, C., Kraft, R. P., Guhathakurta, P., Peterson, R. C., & Fulbright, J. P. 2004, AJ, 127, 2162

Stecher, T. P., et al. 1997, PASP, 109, 584

Stetson, P. B. 1987, PASP, 99, 191

Stetson, P. B. 1992, JRASC, 86, 71

Stetson, P. B. 1998, Bulletin d'information du telescope Canada-France-Hawaii, 38, 1

Stetson, P. B. 2000, PASP, 112, 925

Straniero, O., Chieffi, A., & Limongi, M. 1997, ApJ, 490, 425

Strom, S. E., Strom, K. M., Rood, R. T., & Iben, I., Jr. 1970, A&A, 8, 243

Sweigart, A. V. 1987, ApJS, 65, 95

Thompson, H. M. A., Keenan, F. P., Dufton, P. L., Ryans, R. S. I., Smoker, J. V., Lambert, D. L., & Zijlstra, A. A. 2007, MNRAS, 378, 1619

Valcarce, A. A. R., & Catelan, M. 2008, A&A, 487, 185

VandenBerg, D. A., Bergbusch, P. A., & Dowler, P. D. 2006, ApJS, 162, 375

Vargas Álvarez, C. A., & Sandquist, E. L. 2007, AJ, 134, 825

Villanova, S., Piotto, G., & Gratton, R. G. 2009, A&A, 499, 755

Walker, A. R. 1994, AJ, 108, 555

Wallerstein, G. 1970, ApJ, 160, 345

Wallerstein, G. 2002, PASP, 114, 689

Wehlau, A. 1990, AJ, 99, 250

Wehlau, A., & Butterworth, S. 1990, AJ, 100, 686

Wehlau, A., Butterworth, S., & Hogg, H. S. 1990, AJ, 99, 1159

Wehlau, A., & Hogg, H. S. 1984, AJ, 89, 1005

Whitney, J. H., et al. 1995, AJ, 110, 1722

Yi, S., Demarque, P., & Kim, Y.-C. 1997, ApJ, 482, 677

Yong, D., Aoki, W., & Lambert, D. L. 2006, ApJ, 638, 1018

Yong, D., Grundahl, F., D'Antona, F., Karakas, A. I., Lattanzio, J. C., & Norris, J. E. 2009, ApJ, 695, L62

Yong, D., Grundahl, F., Lambert, D. L., Nissen, P. E., & Shetrone, M. D. 2003, A&A, 402, 985

Zinn, R. J., Newell, E. B., & Gibson, J. B. 1972, A&A, 18, 390

Zinn, R. 1974, ApJ, 193, 593

Zoccali, M., Cassisi, S., Bono, G., Piotto, G., Rich, R. M., & Djorgovski, S. G. 2000, ApJ, 538, 289

Zoccali, M., Cassisi, S., Piotto, G., Bono, G., & Salaris, M. 1999, ApJ, 518, L49

Zorotovic, M., et al. 2010, AJ, 139, 357

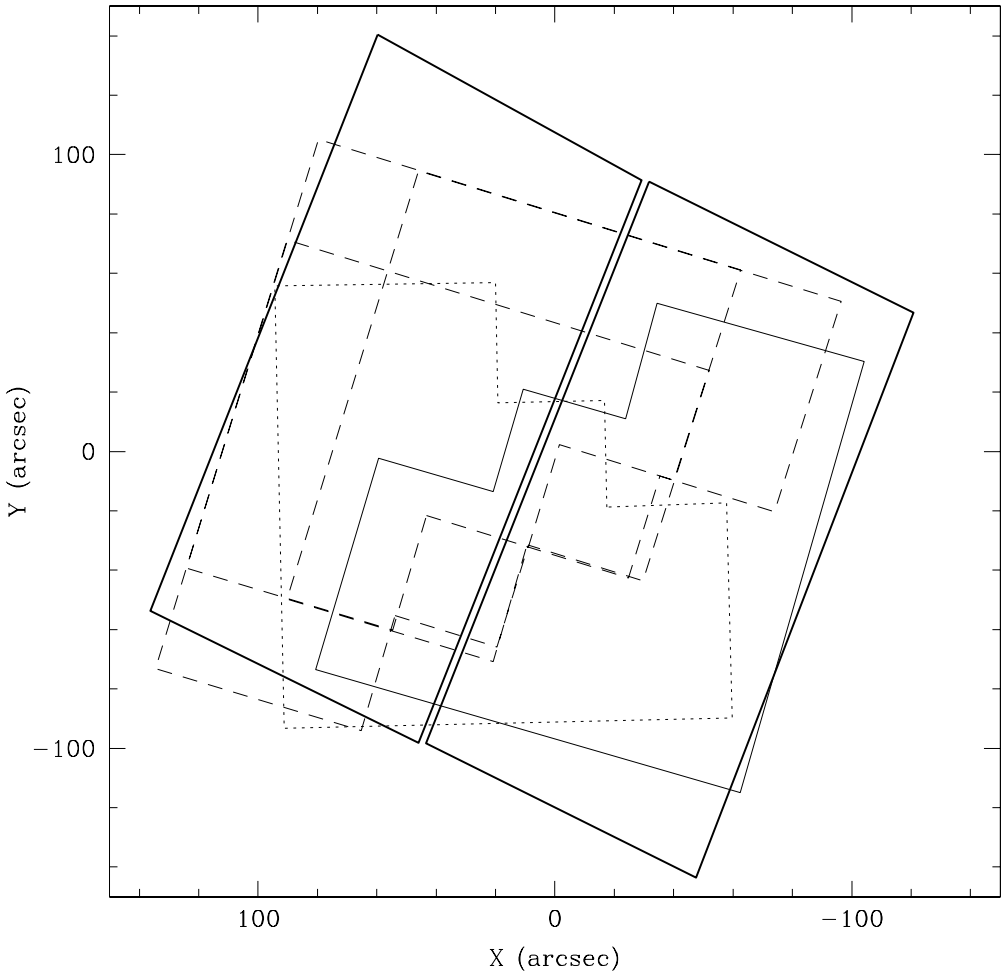

Fig. 1.— Outlines of the observed HST fields for M13. The HST proposal 5903 field with a dotted border, the proposal 8278 field with a solid border, and the proposal 8174 fields with a dashed border. (Three overlapping fields were observed as part of proposal 8174.) The ACS fields of the two WFC chips are shown with a dark solid line (WFC1 on the left).

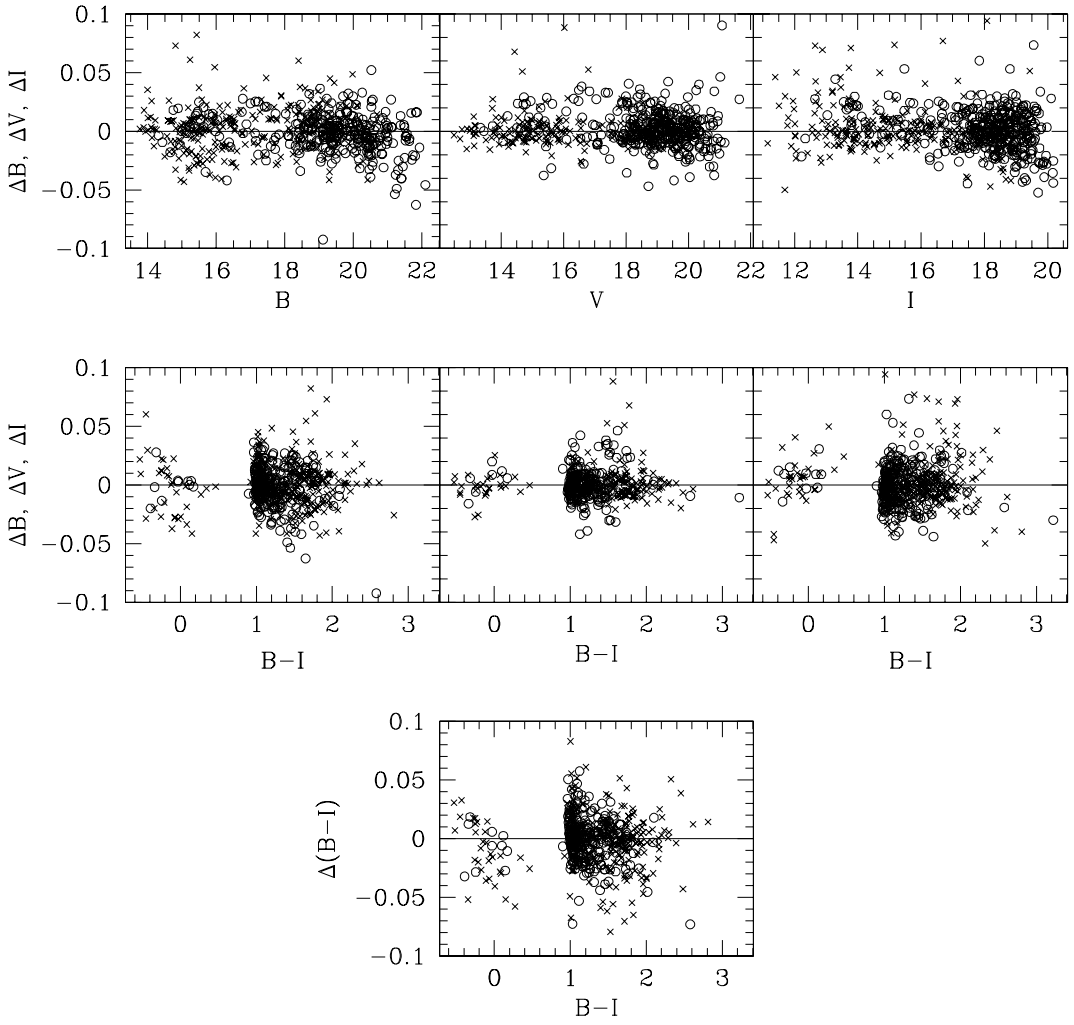

Fig. 2.— Photometric residuals between our calibrated photometry and the standard magnitudes of (Stetson 2000) in the sense of this study minus Stetson's. Stars measured on chip 11 of the CFHT field are shown with open circles, and stars from chip 12 are shown with crosses.

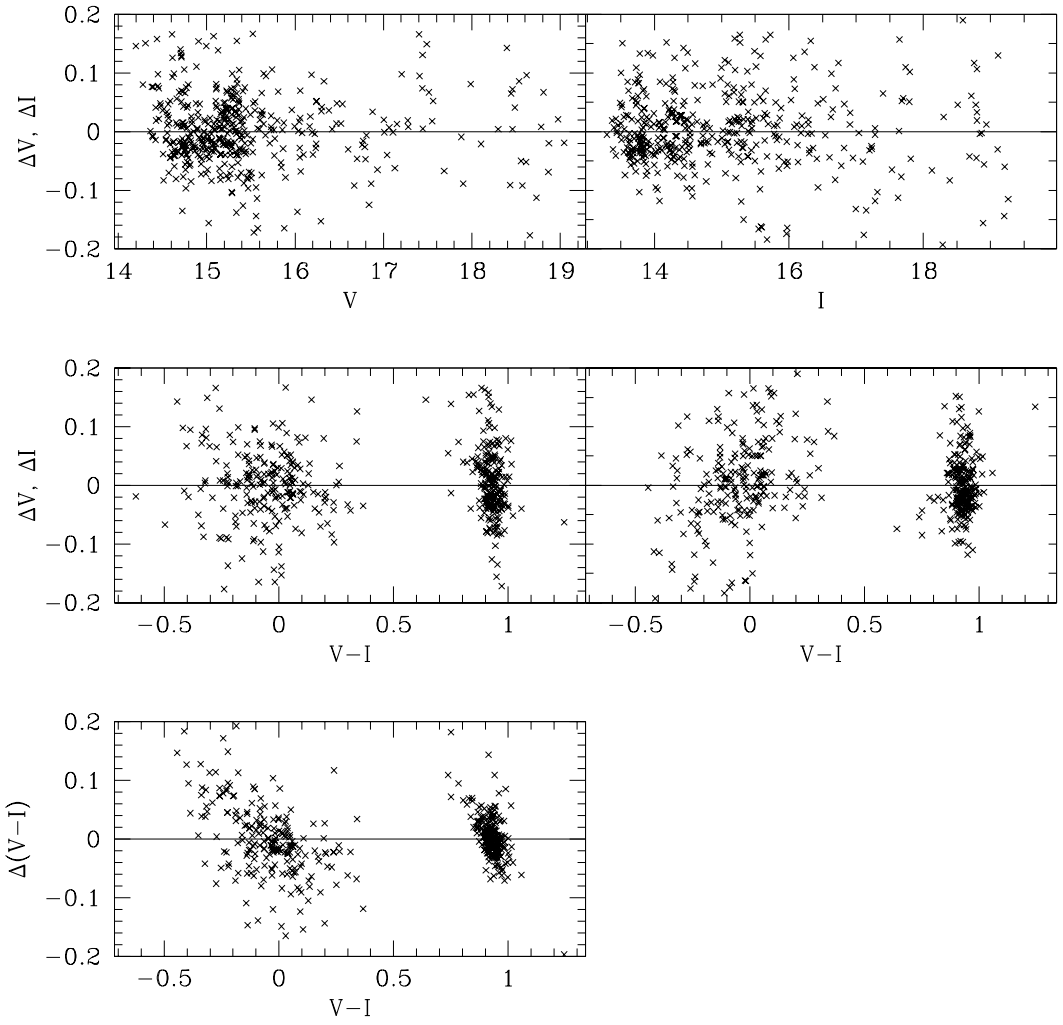

Fig. 3.— Photometric residuals between our calibrated CFHT photometry and the ACS photometry calibrated to the standard system (in the sense of CFHT minus ACS).

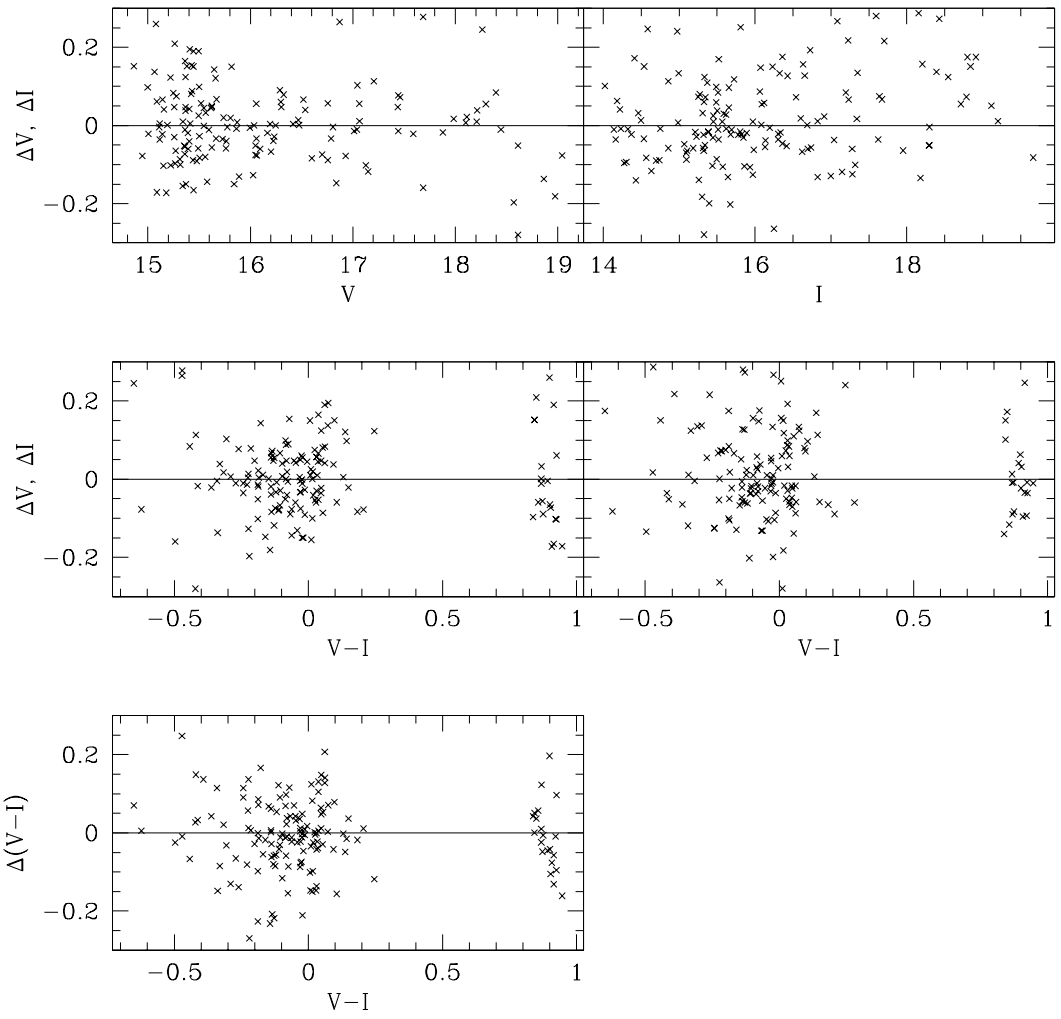

Fig. 4.— Photometric residuals between our calibrated CFHT photometry and the WFPC2 photometry (F555W and F814W filters) calibrated to the standard system (in the sense of CFHT minus WFPC2).

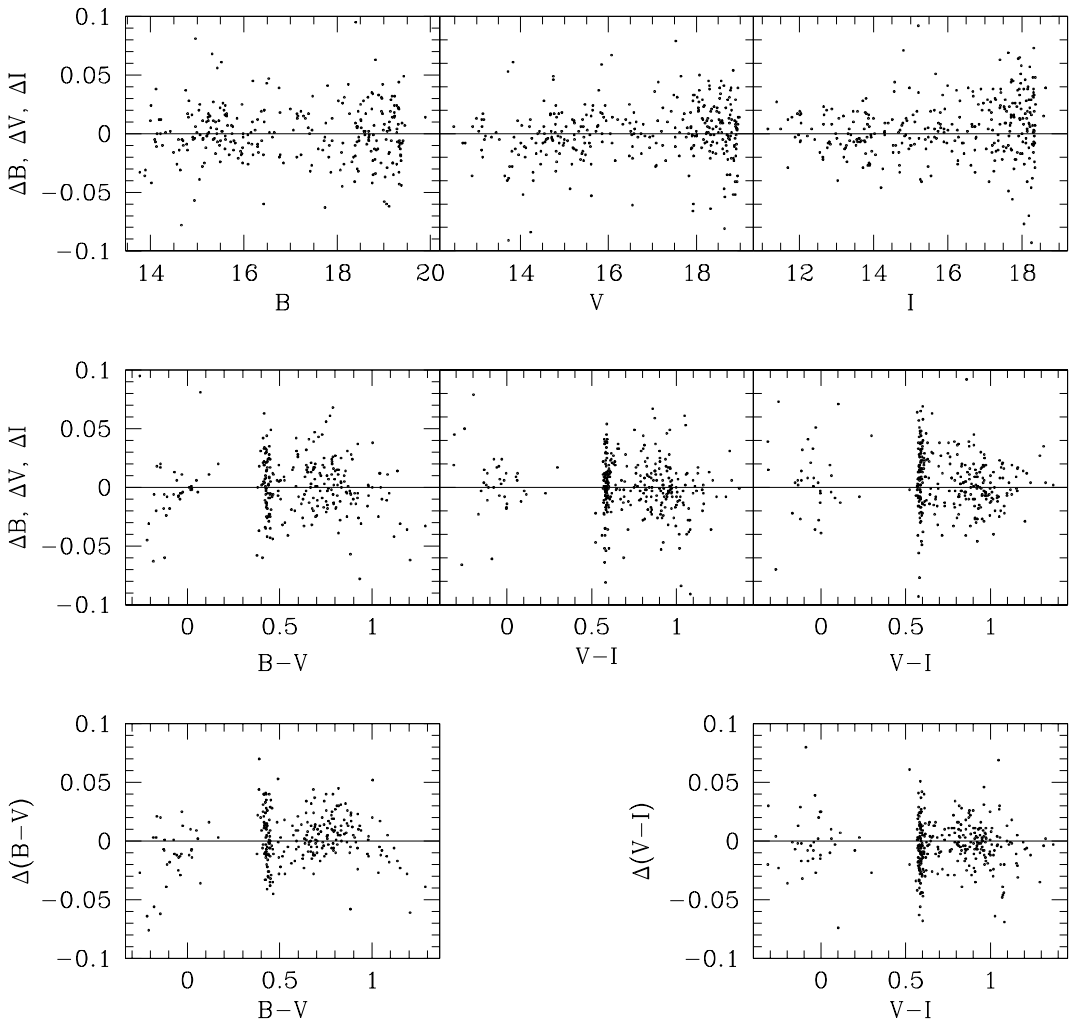

Fig. 5.— Photometric residuals between our calibrated KPNO photometry and the standard magnitudes of Stetson (2000).

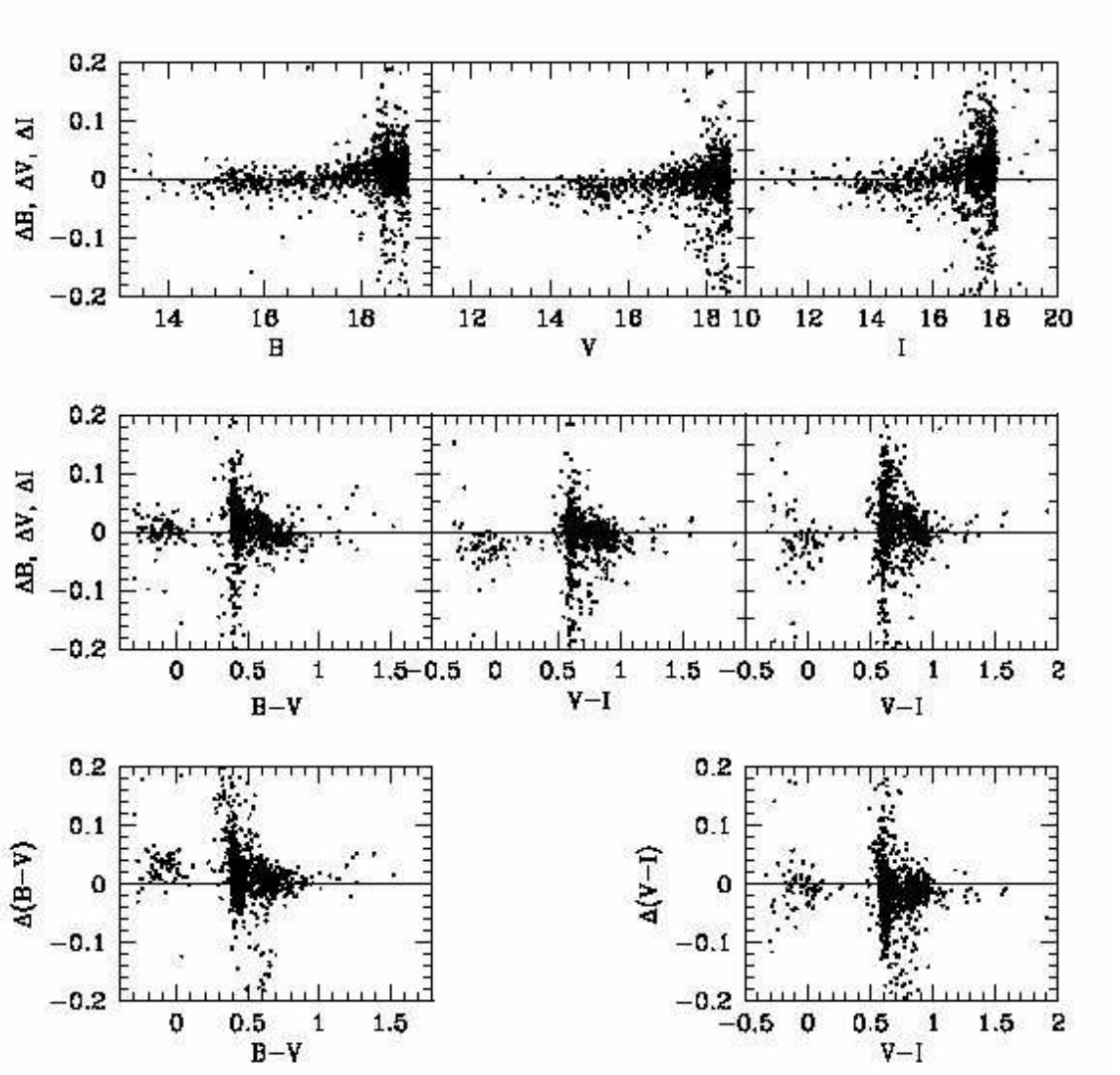

Fig. 6.— Photometric residuals between our calibrated KPNO and CFHT photometry (chip 11) in the sense of KPNO minus CFHT. The sample has been restricted to stars brighter than the main sequence turnoff (with the exception of faint HB stars).

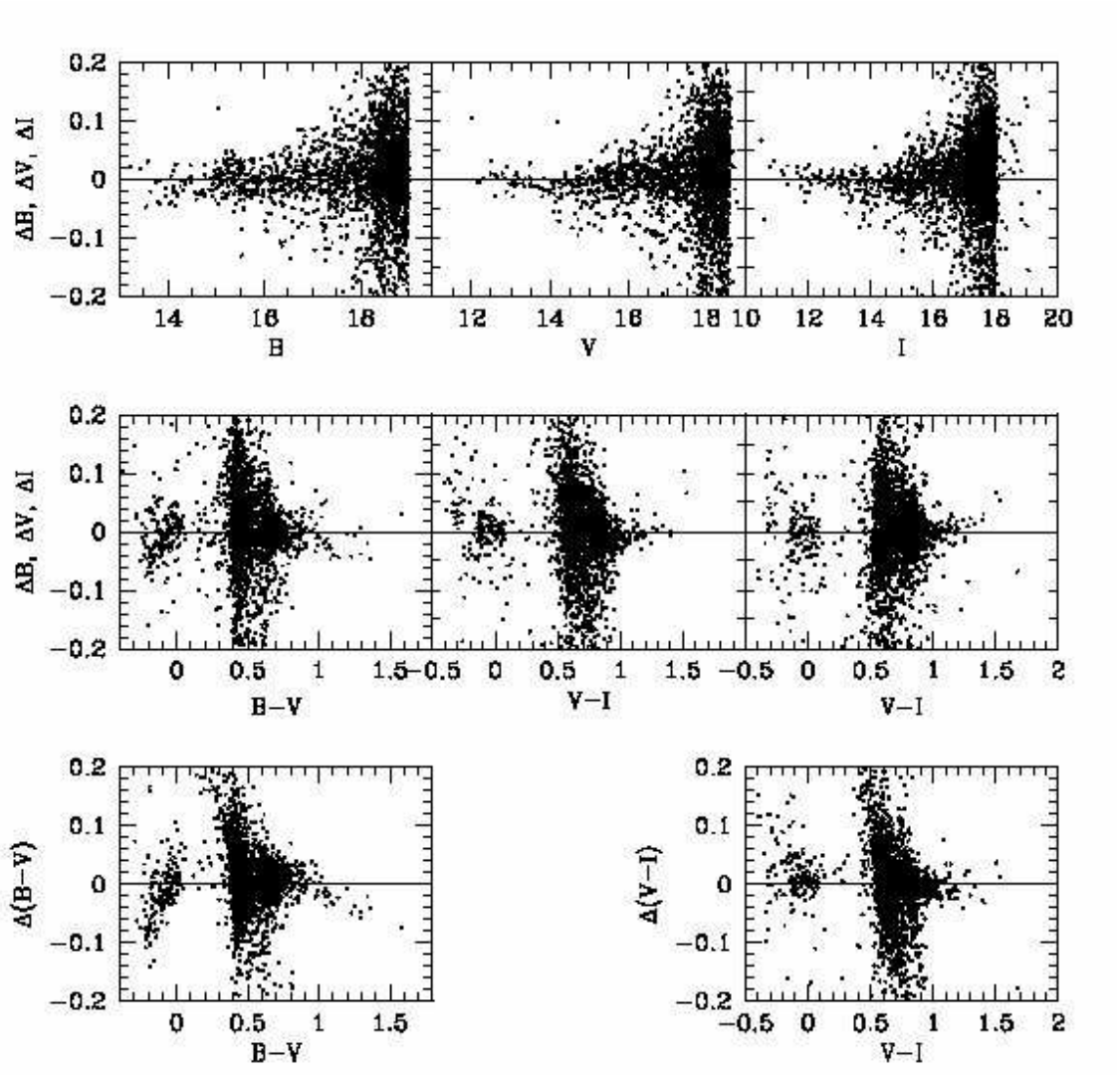

Fig. 7.— Photometric residuals between our calibrated KPNO and CFHT photometry (chip 12) in the sense of KPNO minus CFHT. The sample has been restricted to stars brighter than the main sequence turnoff (with the exception of faint HB stars).

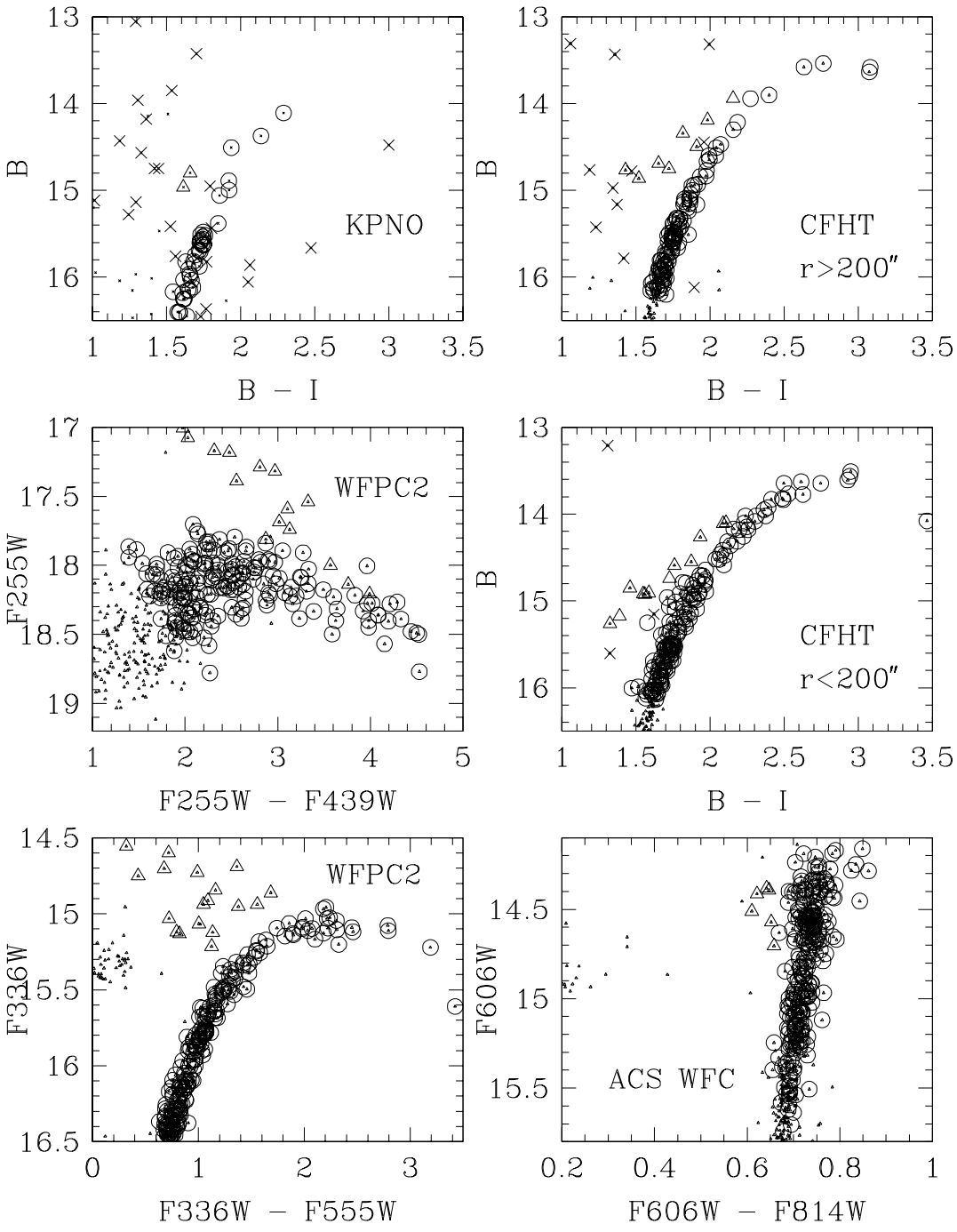

Fig. 8.— Color-magnitude diagrams used in the identification of bright RGB stars. RGB stars have ◯, AGB stars have △, and known field stars have × symbols.

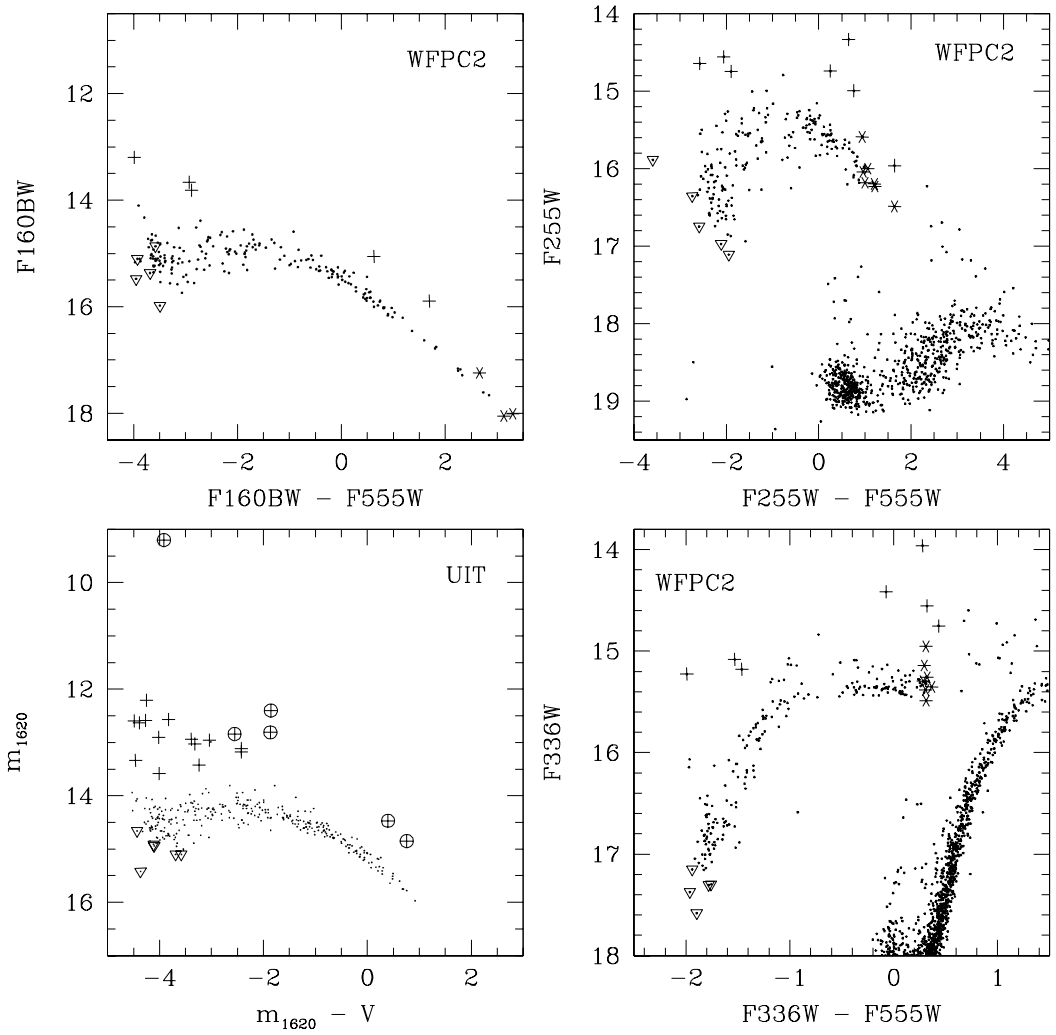

Fig. 9.— Ultraviolet color-magnitude diagrams used in the identification of HB stars. Variable HB stars have $*$ symbols, AGB manqué and supra-HB stars are + symbols, "UV-bright" stars have $\bigcirc$ symbols, and the hottest HB stars have $\bigtriangledown$ symbols. In the UIT panel, the V magnitude comes from the images with the highest available resolution (ACS, CFHT, or KPNO).

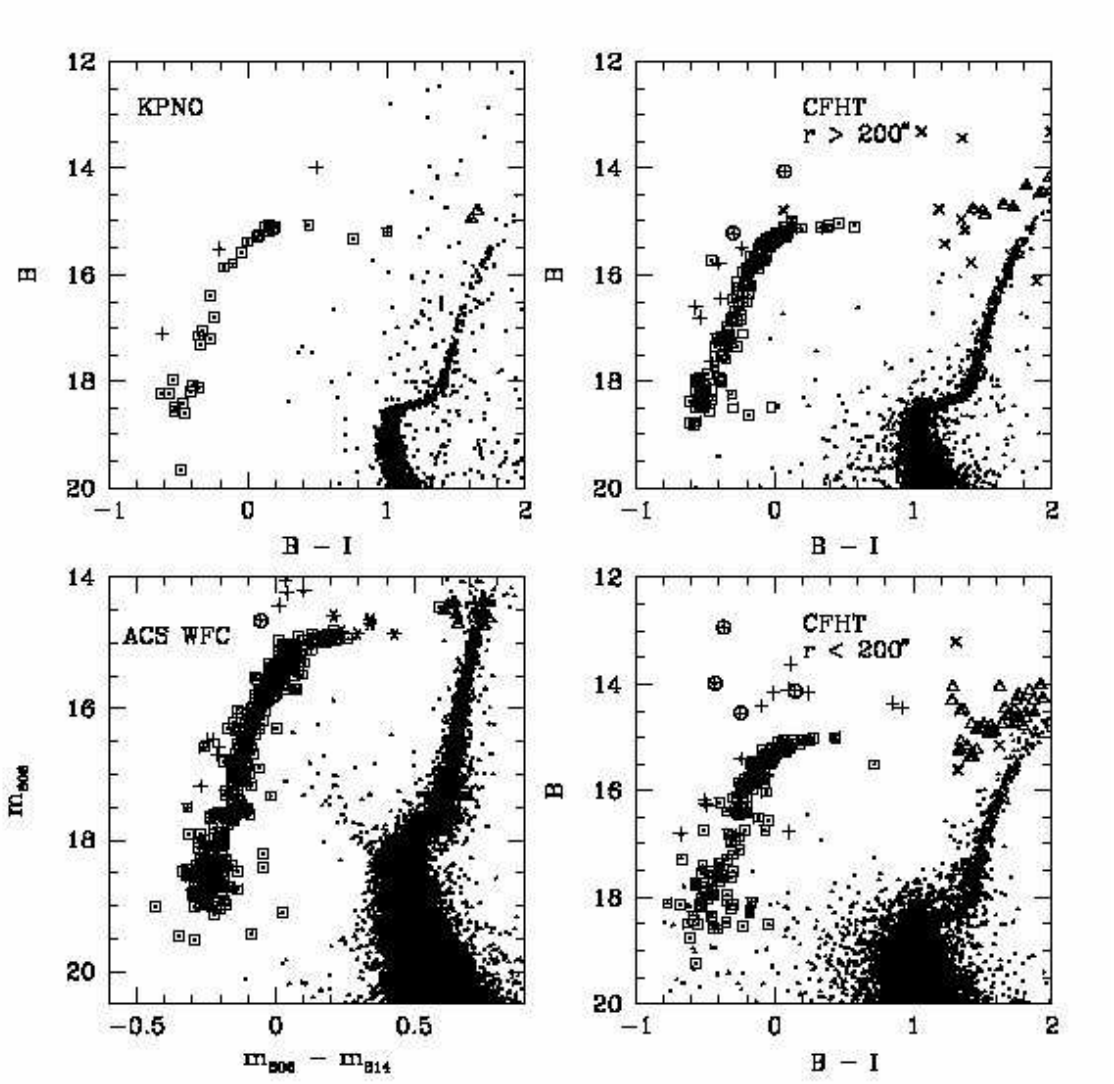

Fig. 10.— Optical color-magnitude diagrams used in the identification of HB stars. Symbols are the same as in the right panels of Fig. 9, with the exceptions that AGB stars are shown with △ symbols, and unevolved non-variable HB stars are shown with □ symbols.

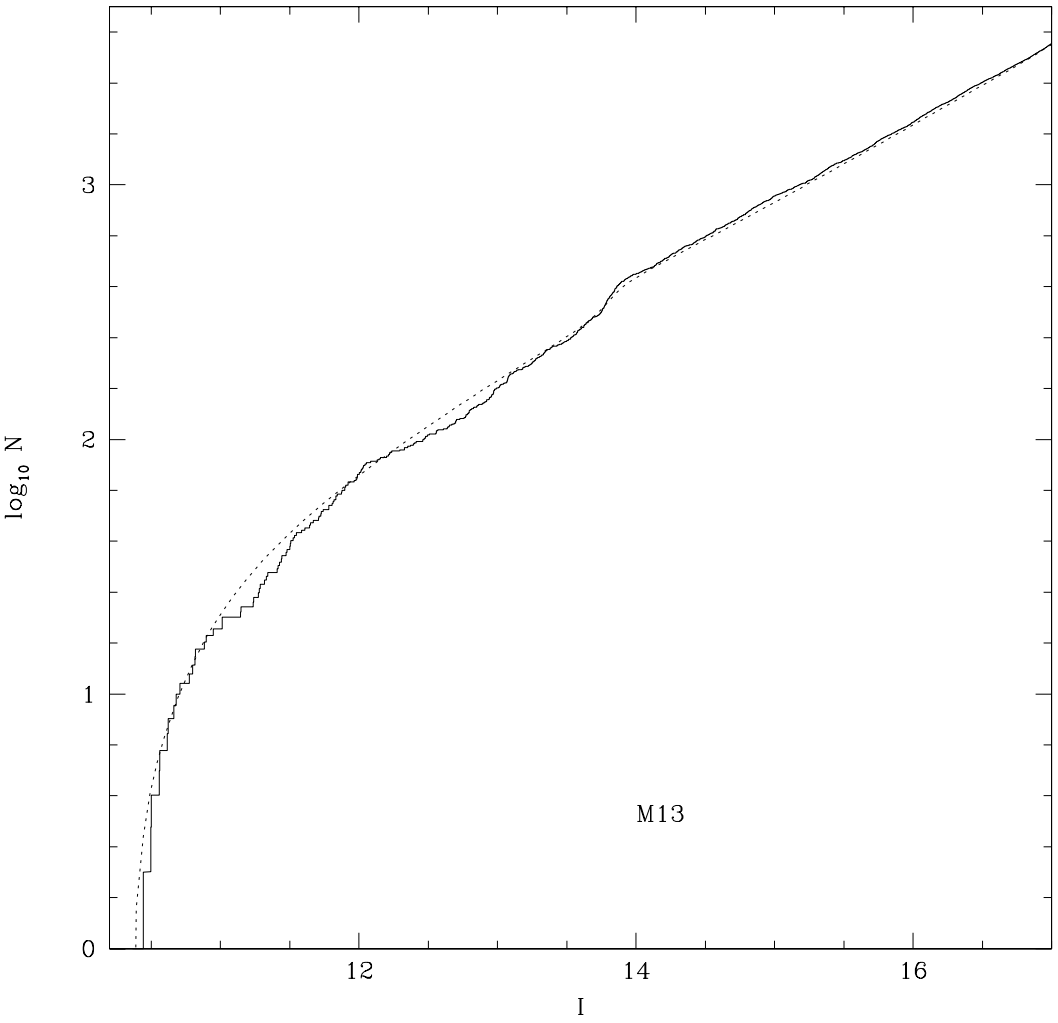

Fig. 11.— Comparison of the cumulative luminosity function of M13 RGB stars (*solid line*) with theoretical predictions from a Victoria-Regina model (*dotted line*; VandenBerg et al. 2006) with [Fe/H]= -1.41 and [α/Fe] = $+0.3$. The theoretical model has been shifted horizontally to match at the tip of the RGB, and vertically normalized to the RGB sample at $I = 13.7$, just brighter than the RGB bump

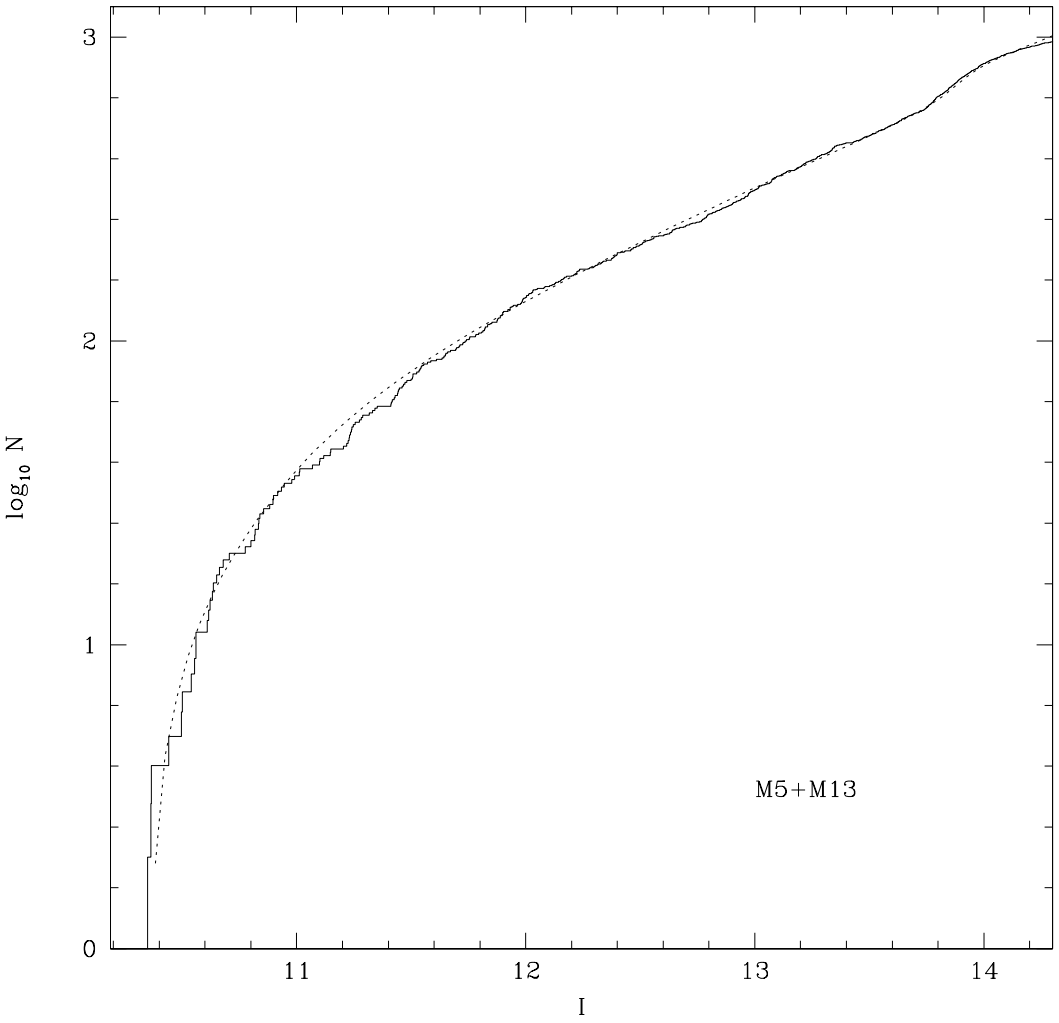

Fig. 12.— Comparison of the combined cumulative luminosity function of M13 and M5 RGB stars (*solid line*) with theoretical predictions from the Victoria-Regina model (*dotted line*; VandenBerg et al. 2006) with [Fe/H]= −1.41 and [α/Fe] = +0.3. The theoretical model has been shifted horizontally to match at the tip of the RGB, and vertically normalized to the RGB sample at $I = 13.7$, just brighter than the RGB bump

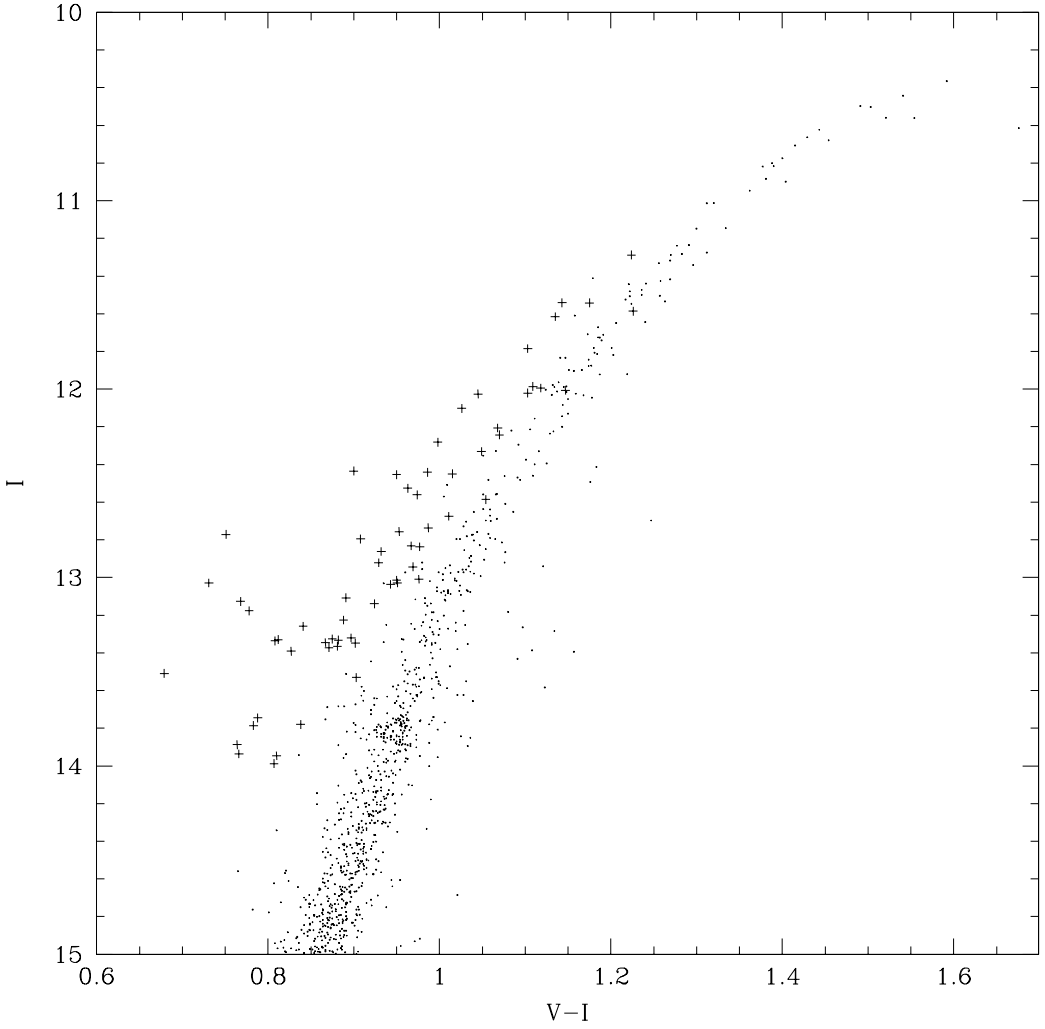

Fig. 13.— Combined color-magnitude diagram for bright giant stars (AGB stars are identified with crosses) from all photometry sources.

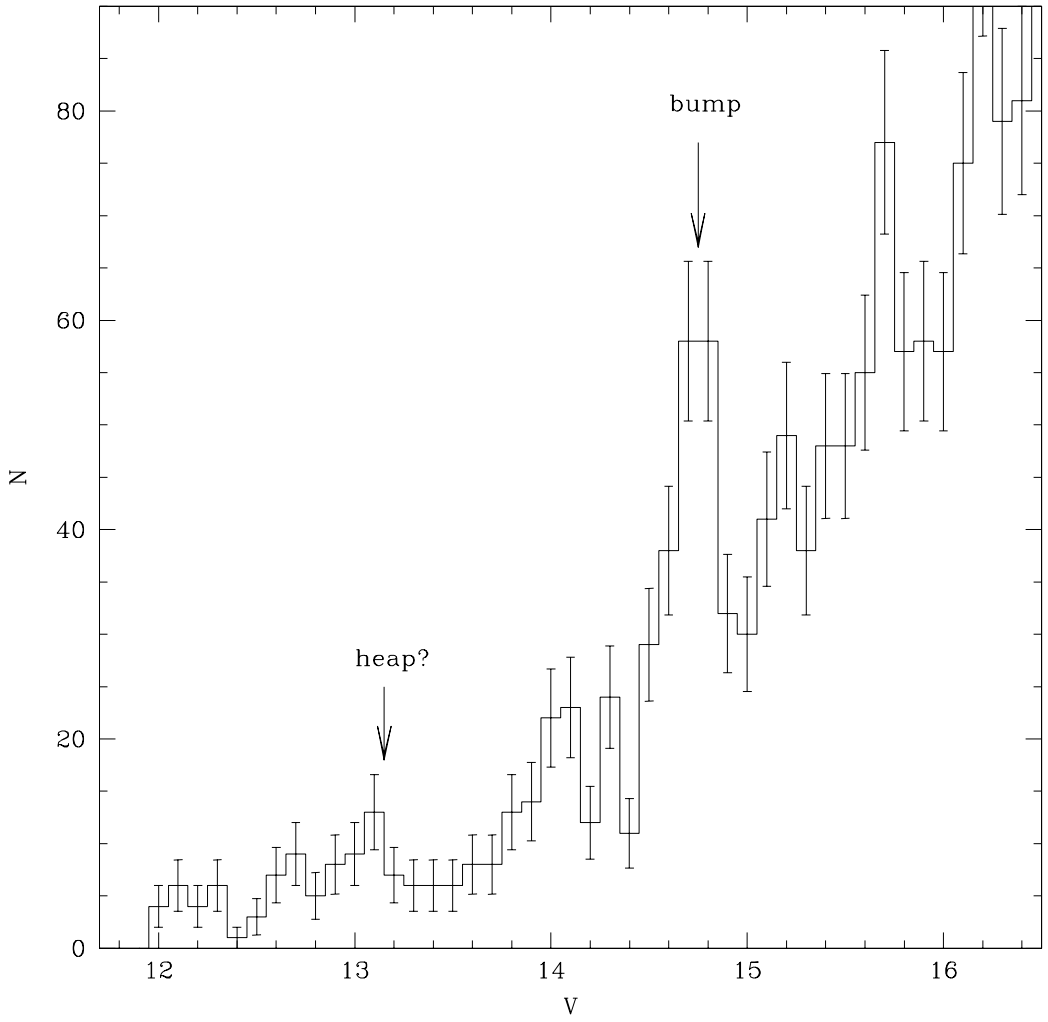

Fig. 14.— The differential luminosity function of M13 RGB stars with the bump and possible hump identified. Error bars are based on Poisson statistics.

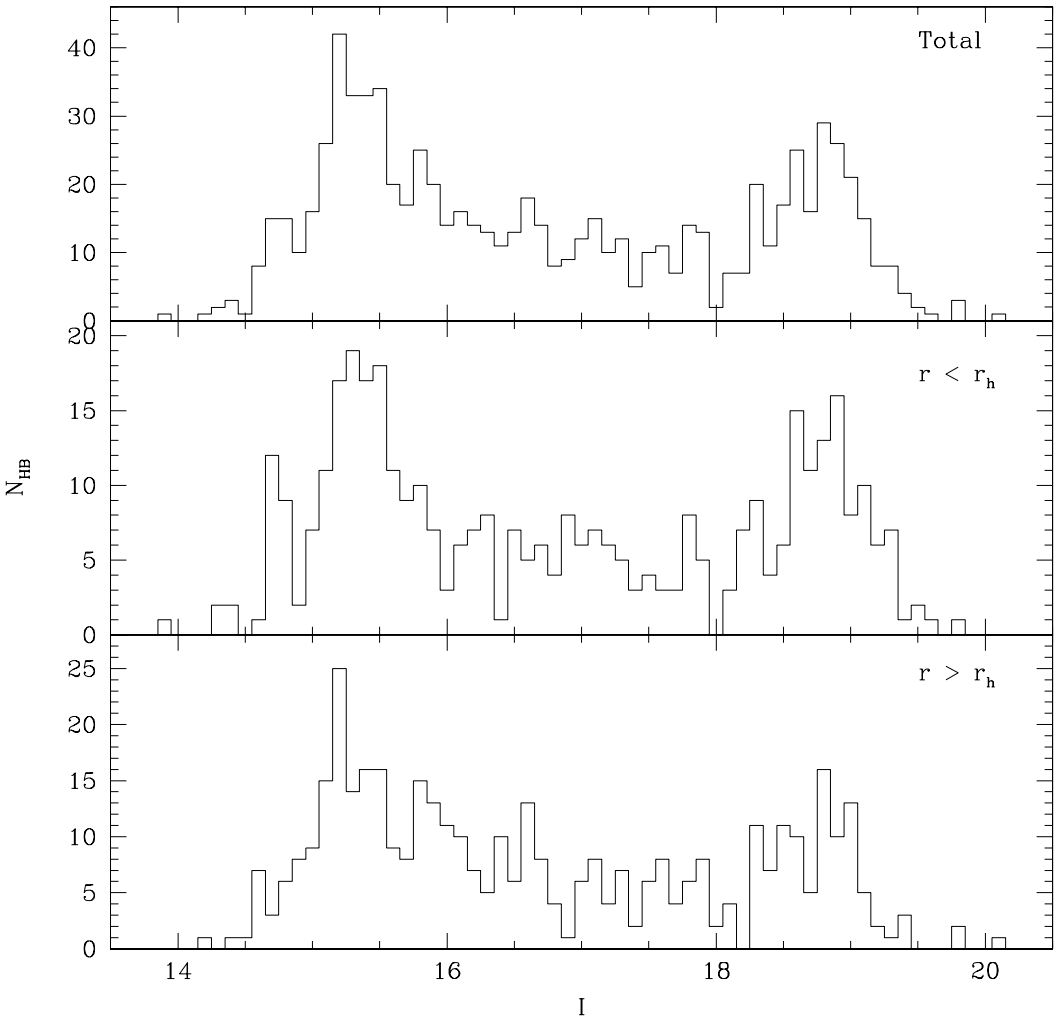

Fig. 15.— I-band Distribution of horizontal branch stars in M13. *Top panel:* the total sample. *Middle panel:* stars within 1 half-light radius (94″). *Bottom panel:* stars outside 1 half-light radius.

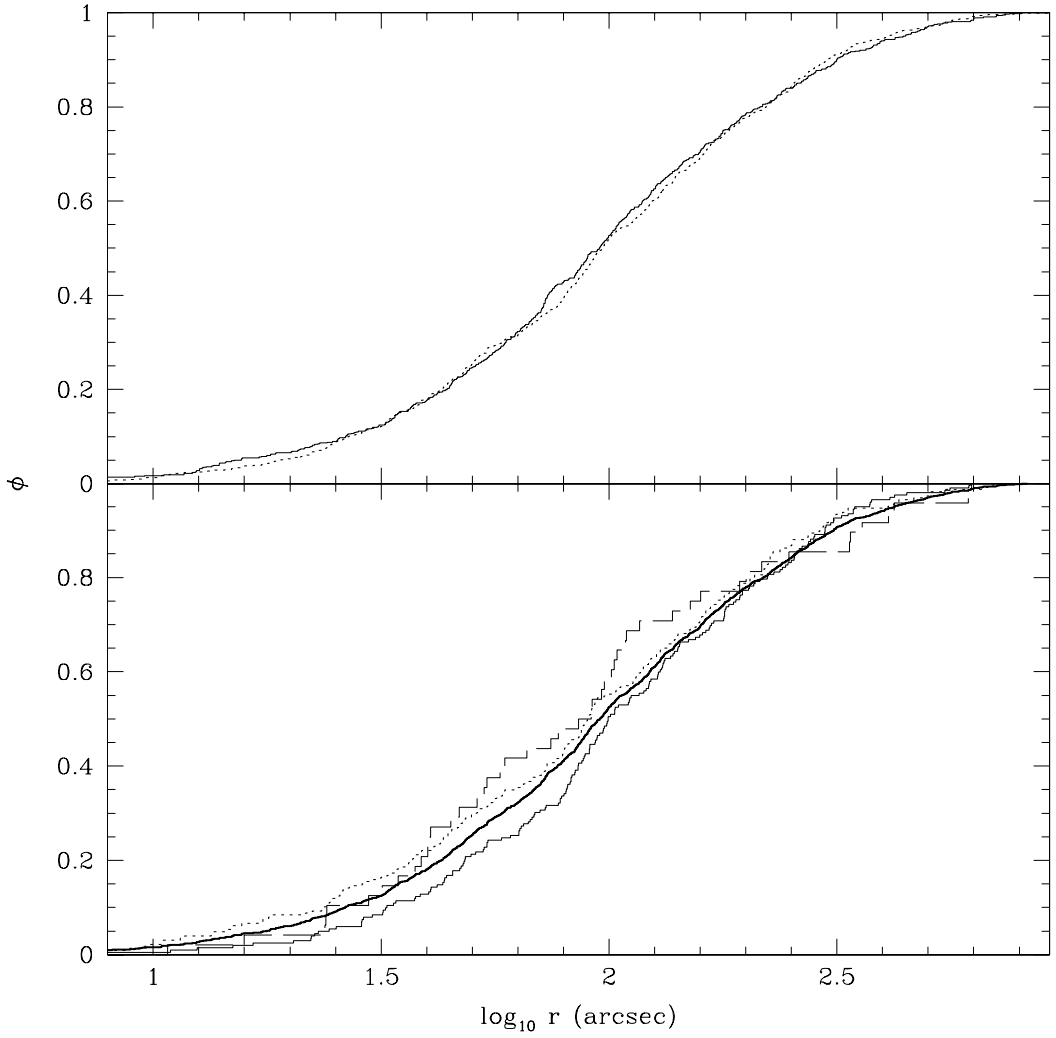

Fig. 16.— Cumulative radial distribution of star populations. *Top panel:* red giant stars (*solid line*), and horizontal branch stars (*dotted line*). *Bottom panel:* horizontal branch stars divided by magnitude into faint peak ($I < 18$; *dotted line*), intermediate stars ($16.25 < I < 18$; *solid line*), red HB stars ($I \lesssim 14.9$; *dashed line*, and combined RGB/HB population (*dark solid line*).

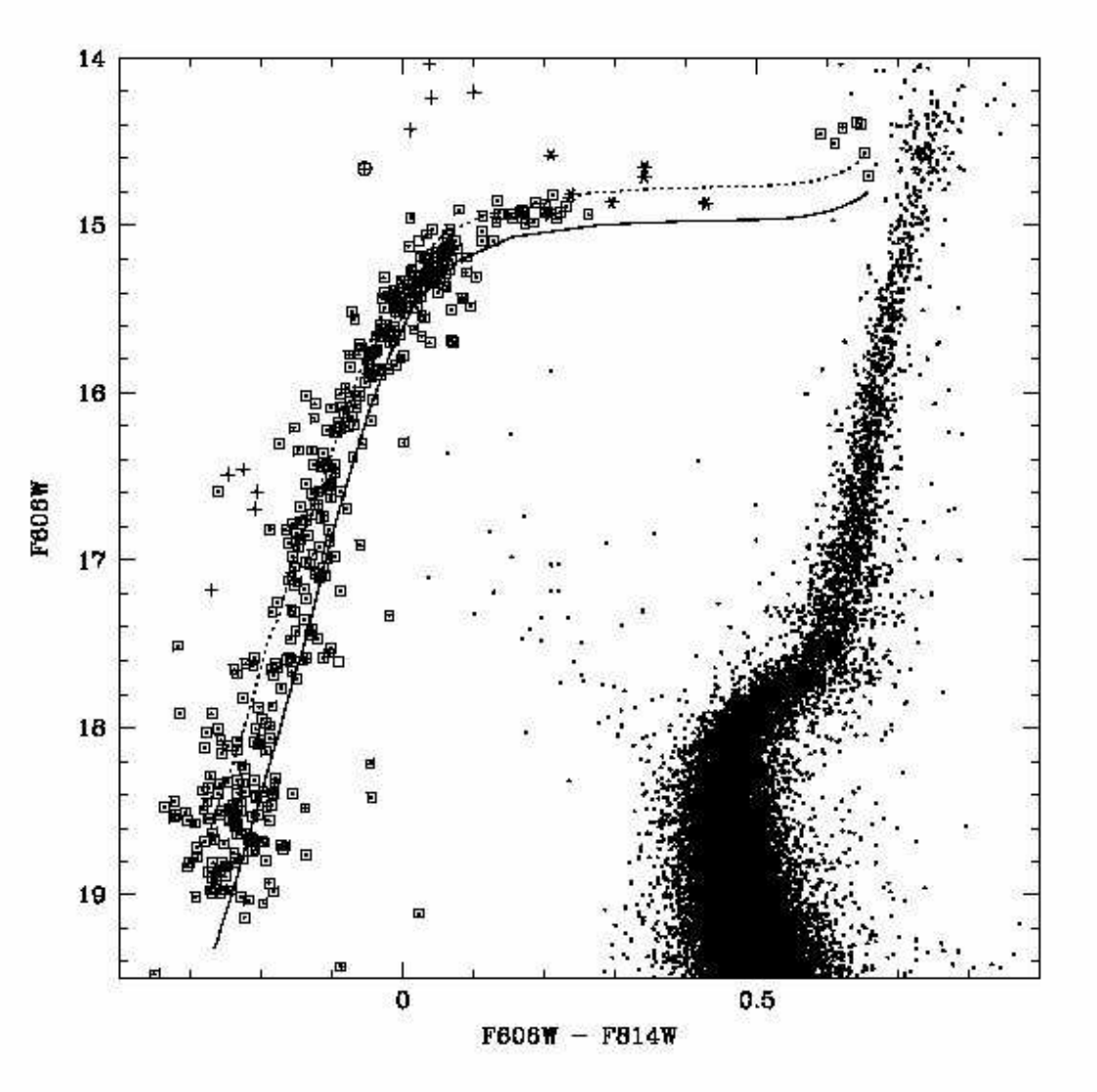

Fig. 17.— Zoomed color-magnitude diagram from ACS data. Symbols are as in Fig. 10. The ZAHB (*solid line*) and the $Y_c = 0.10$ locuses (*dotted line*) are shown for α-enhanced Teramo HB models having $Z = 0.001$ and $Y = 0.246$, with $(m - M)_{606} = 14.55$ and $\mathrm{E}(F606W - F814W) = 0.02$ assumed. The AGB clump falls just above the bright end of the plot.

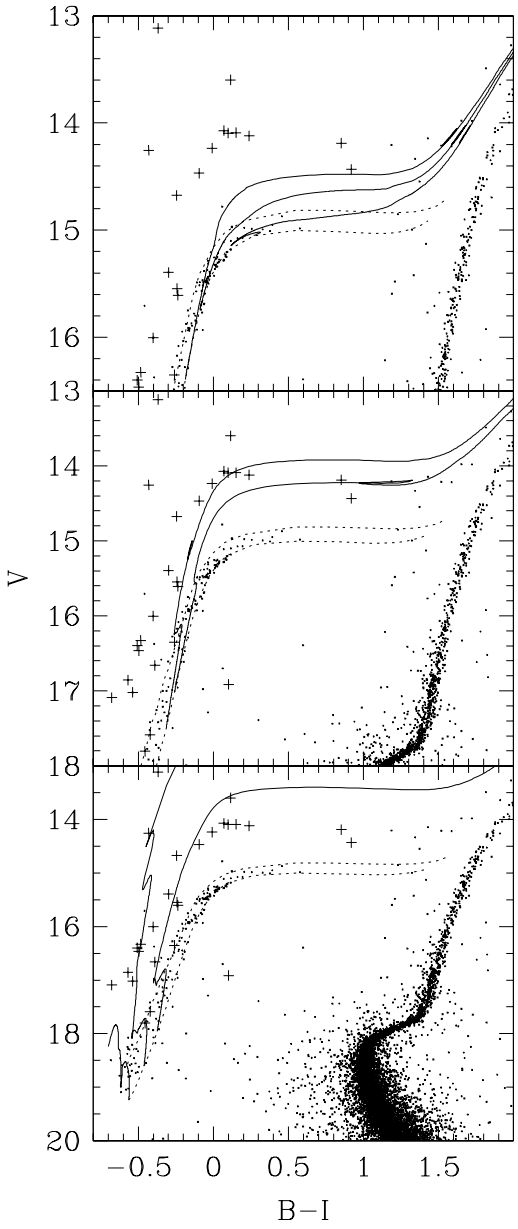

Fig. 18.— Comparison of ground-based CFHT and KPNO photometry ($r > 200''$) with Teramo (Pietrinferni et al. 2006) HB models. In all panels theoretical values are shifted by 14.45 in V and 0.02 in $B-I$ to fit the envelope of HB stars. *Left panels:* Comparison with evolution tracks having [Fe/H]= -1.62 and [α/Fe] $\sim +0.4$ ([M/H] = -1.27, $Z = 0.001$). The ZAHB and the $Y_c = 0.10$ locuses are shown with dotted lines. The tracks are for 0.4912, 0.50, and 0.52 $M_\odot$ (*bottom panel*), 0.54 and 0.56 $M_\odot$ (*middle panel*), and 0.58, 0.6, and 0.63 $M_\odot$ (*top panel*).

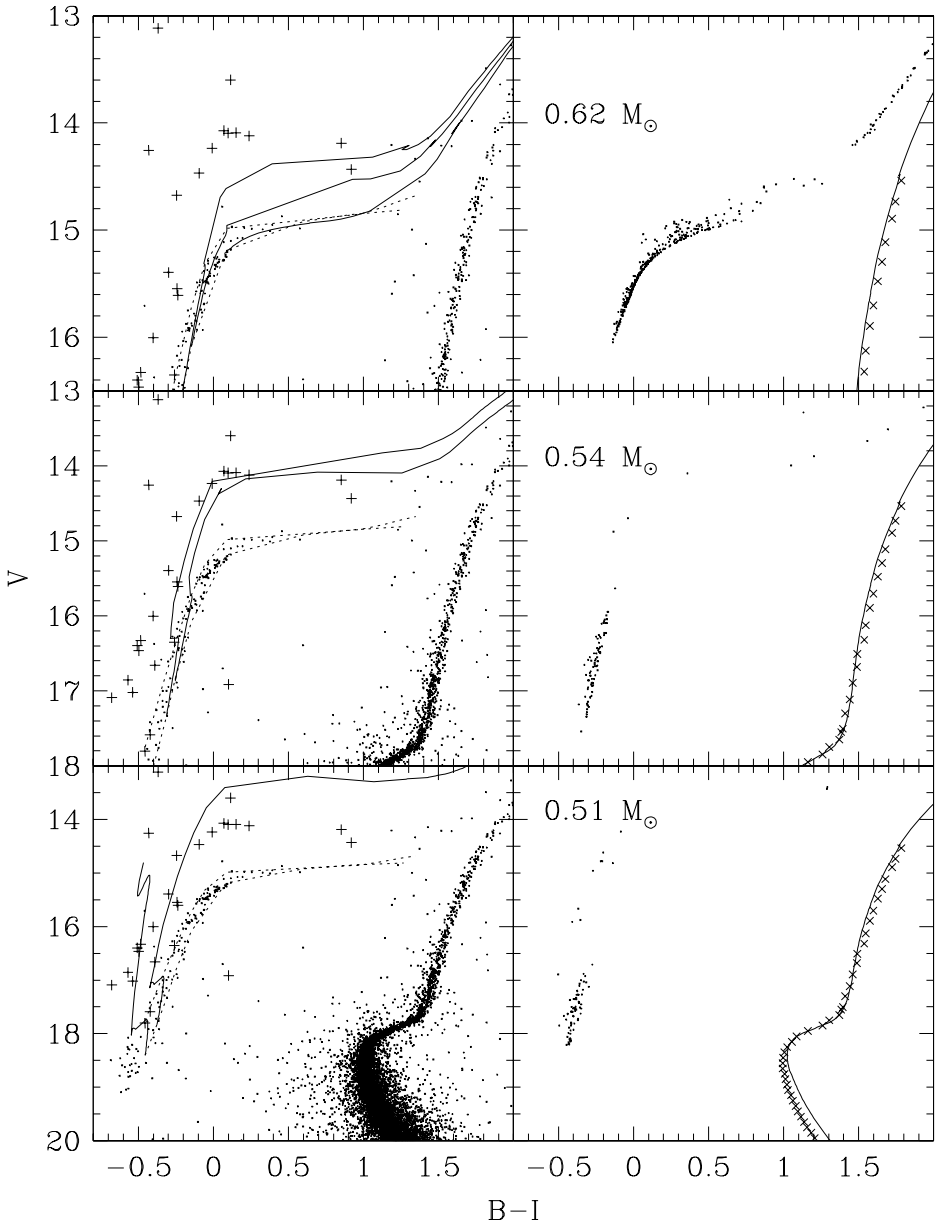

Fig. 19.— Comparison of ground-based CFHT and KPNO photometry ($r > 200''$) with DSEP HB models. In all panels theoretical values are shifted by 14.28 in V and 0.02 in $B-I$ to fit the envelope of HB stars. *Left panels:* Comparison with evolution tracks having [Fe/H]$= -1.5$ and $[\alpha/\mathrm{Fe}] = +0.4$. The ZAHB and the $Y_c = 0.05$ locuses are shown with dotted lines. The tracks are for 0.50 and 0.52 $M_\odot$ (*bottom panel*), 0.54 and 0.56 $M_\odot$ (*middle panel*), and 0.58, 0.6, and 0.65 $M_\odot$ (*top panel*). *Right panels:* Example synthetic horizontal branch populations having the same initial composition and a mass dispersion of 0.01 $M_\odot$, The number of synthetic HB stars roughly corresponds to the number in the total sample (see Fig. 15). Also included (*solid line*) is an isochrone for the same composition and an age of 14 Gyr. Crosses show our mode fits to MS data, and individual stars that represent the mean HB line.

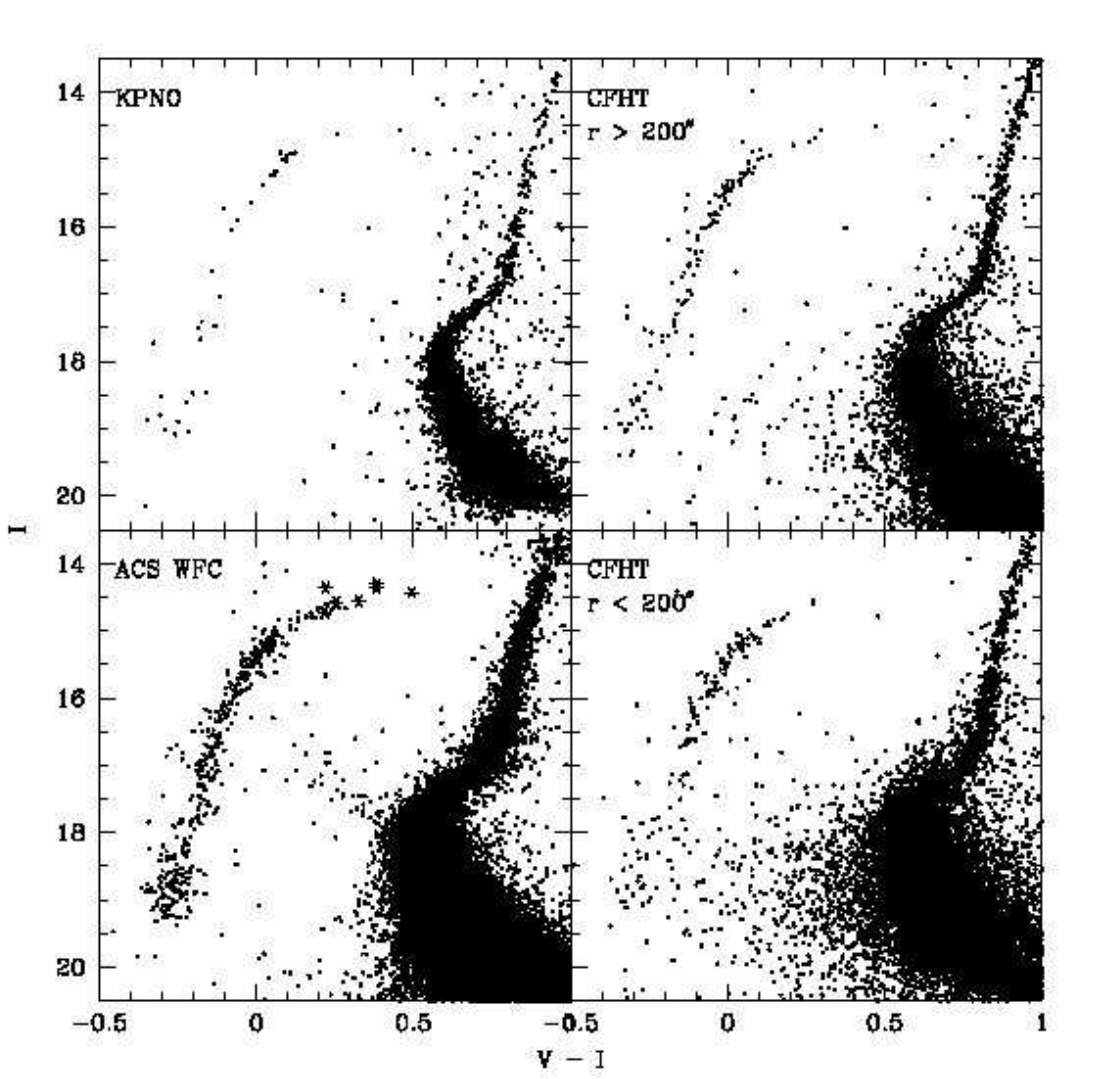

Fig. 20.— $(I, V-I)$ color-magnitude diagram for HB stars from all photometry sources. RR Lyrae stars (shown with $*$ symbols) are found within the ACS field, and the photometry used is not averaged over the oscillation period.

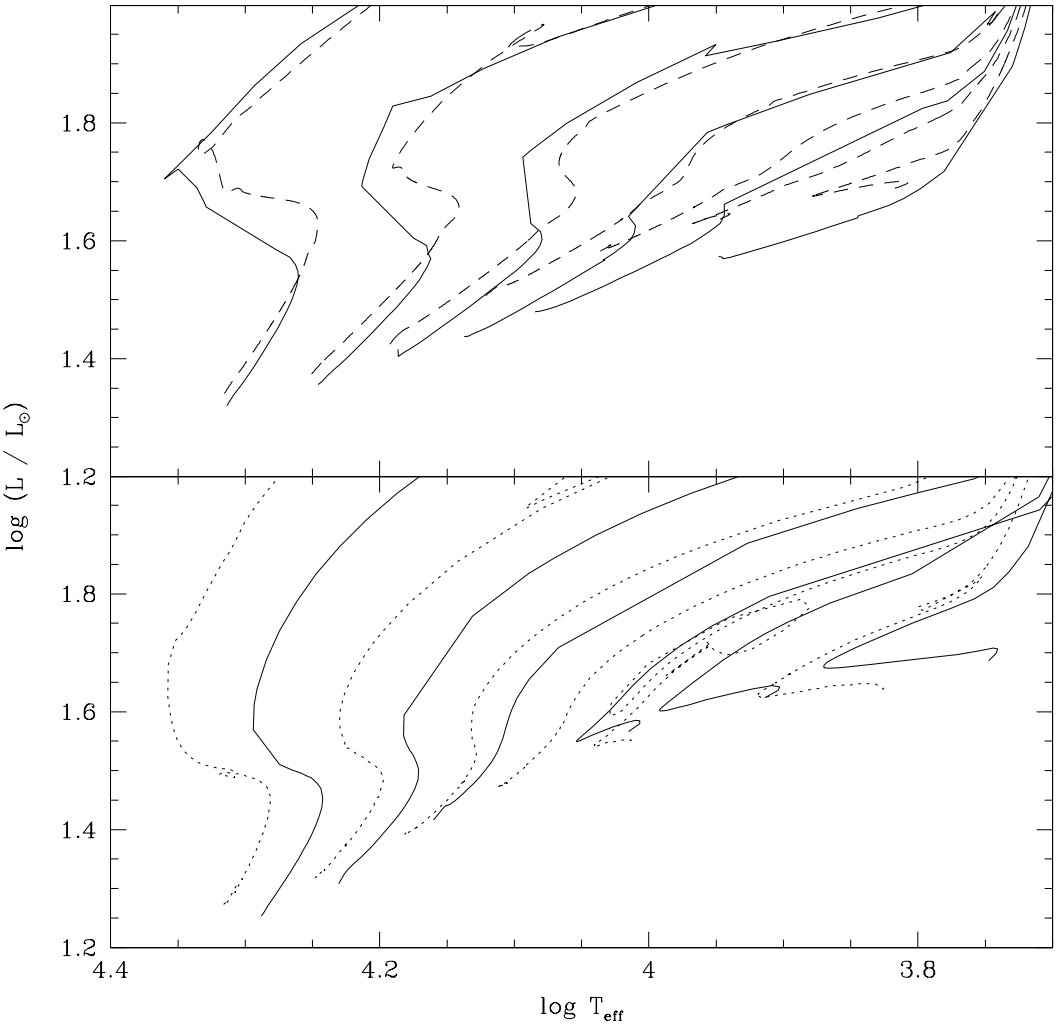

Fig. 21.— HR diagrams for HB stars from theoretical models. *Top panel:* Models from Dotter et al. (2007) (*solid line*) for $Z = 0.00107$, $[\alpha/\mathrm{Fe}] = +0.4$ and from Pietrinferni et al. (2006) (*dashed line*) for $Z = 0.001$ (0.52, 0.54, 0.56, 0.58, 0.6, 0.65 $M_{\odot}$ for both sets.) *Bottom panel:* Models from Dorman et al. (1993) for $[\mathrm{Fe/H}] = -1.48$, $[\mathrm{O/Fe}] = 0.63$ (*solid line*; 0.52, 0.54, 0.56, 0.59, 0.61, 0.65 $M_{\odot}$) and from Yi et al. (1997) for $Z = 0.001$ (*dotted line*; 0.52, 0.54, 0.56, 0.58, 0.60, 0.64 $M_{\odot}$).

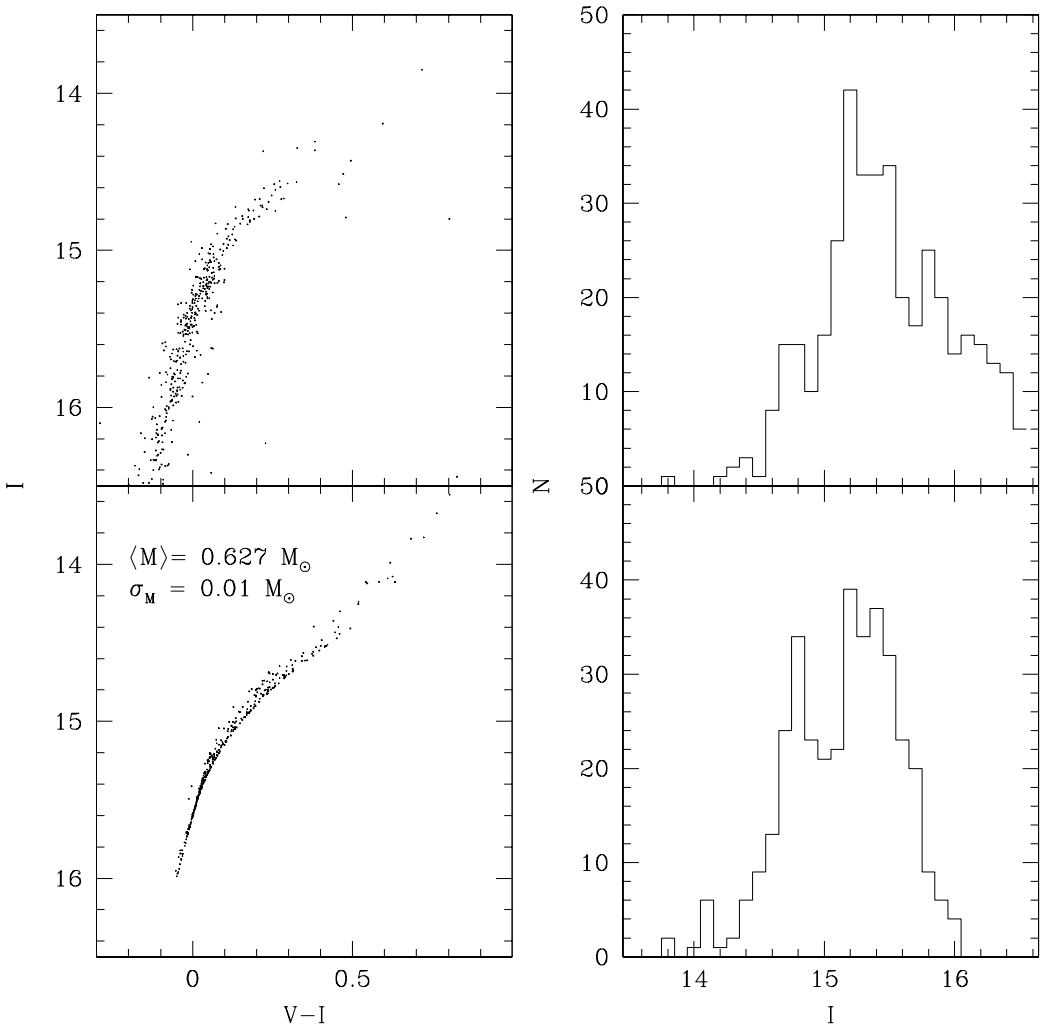

Fig. 22.— Comparison of observations (*upper panels*) with DSEP models (*lower panels*; assuming $(m - M)_I = 14.28$) of the primary peak on M13's HB. *Left panels:* $(I, V - I)$ color-magnitude diagrams. *Right panels:* I-band distributions.

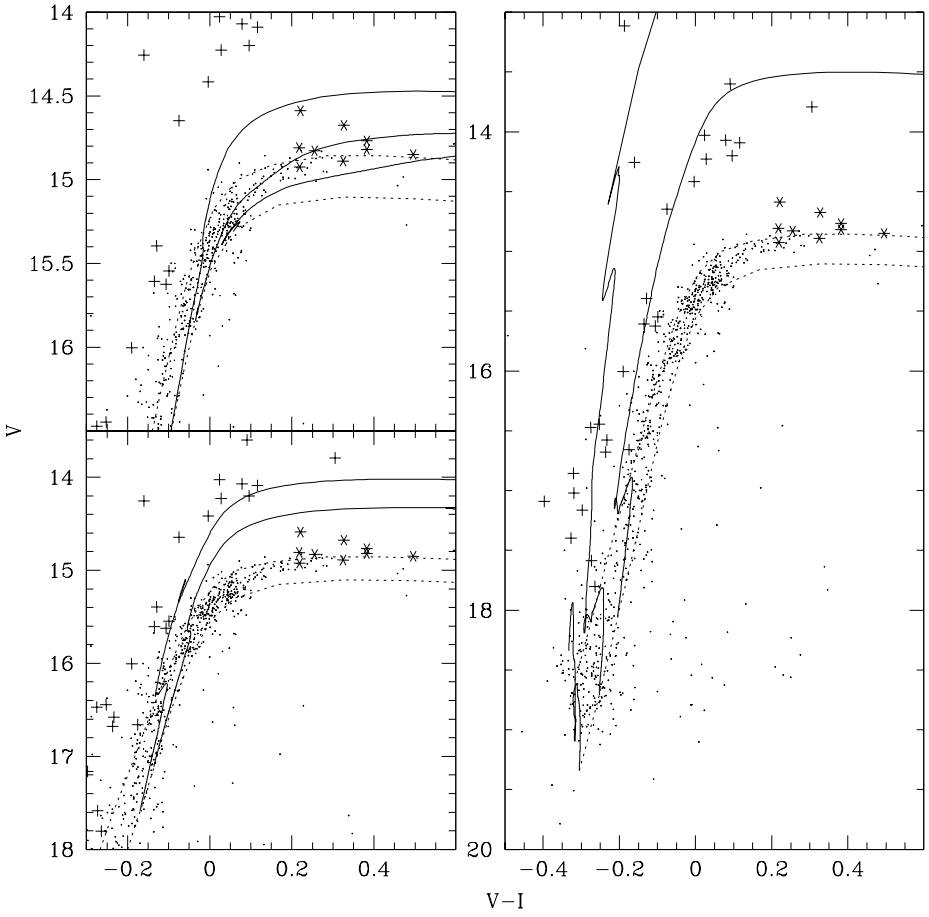

Fig. 23.— Comparison of mastered photometry with Teramo (Pietrinferni et al. 2006) HB models. In all panels theoretical values are shifted by 14.55 in V and 0.01 in $V - I$ to fit the envelope of HB stars, and have [Fe/H]= -1.62, $Y = 0.246$, and [α/Fe] $\sim +0.4$ ([M/H] = -1.27, $Z = 0.001$). The ZAHB and the $Y_c = 0.05$ locuses are shown with dotted lines. Evolution tracks are shown for 0.57, 0.60, and 0.62 $M_\odot$ (*upper left panel*), 0.54 and 0.56 $M_\odot$ (*lower left panel*), and 0.4912, 0.50, and 0.52 $M_\odot$ (*right panel*).

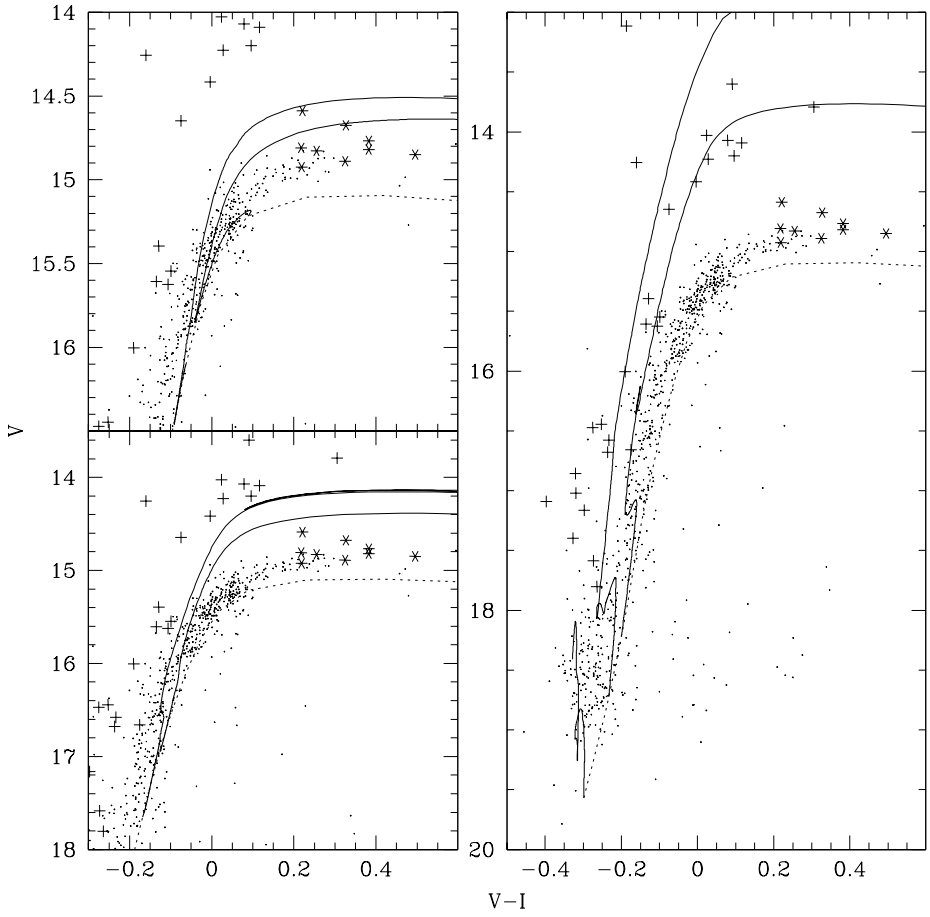

Fig. 24.— Comparison of mastered photometry with Teramo (Pietrinferni et al. 2006) helium enriched ($Y = 0.30$, $Z = 0.000924$) HB models. In all panels theoretical values are shifted by 14.75 in V and 0.01 in $V - I$ to fit the envelope of HB stars. The ZAHB locus is shown with a dotted line. Evolution tracks are shown for 0.57 and 0.61 $M_{\odot}$ (*upper left panel*), 0.54 and 0.56 $M_{\odot}$ (*lower left panel*), and 0.481, 0.50, and 0.52 $M_{\odot}$ (*right panel*).

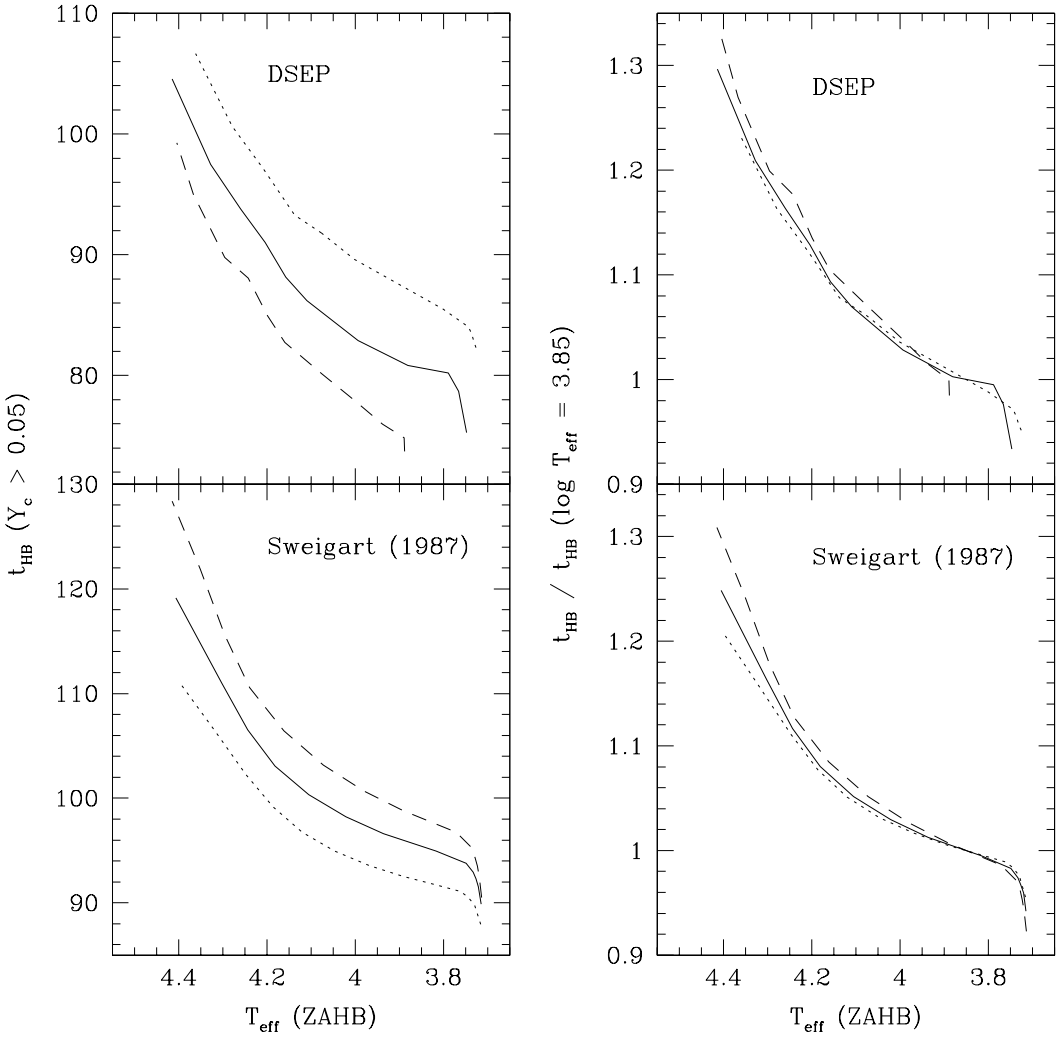

Fig. 25.— HB lifetimes as a function of T_{eff} from DSEP (Dotter et al. 2007) models for (from top to bottom) [Fe/H] $= -1.0, -1.5$, and -2.0 ([α/Fe] $= 0.2$), and Sweigart models $Y = 0.30, 0.25$, and 0.20 ($Z = 0.001$).*Left panels:* lifetimes in Myr. *Right panels:* lifetimes normalized to the stars reaching the zero-age HB at $\log T_{eff} = 3.85$. (For the DSEP model with [Fe/H] $= -2.0$, the most massive models do not reach that temperature, and were normalized at $\log T_{eff} = 3.89$.)

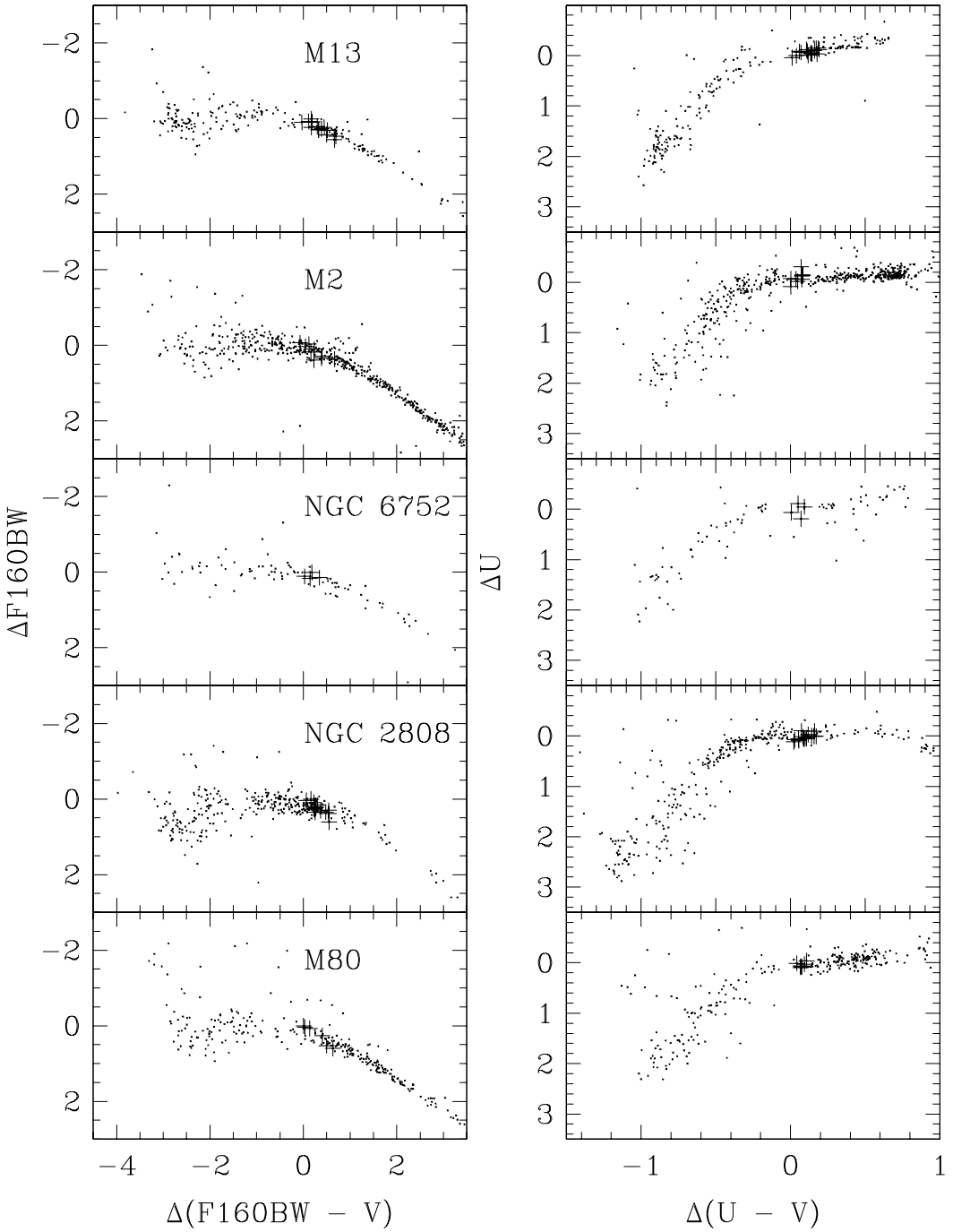

Fig. 26.— CMDs of 5 globular clusters with blue HB tails in the F160BW and F336W (calibrated to U) filters from HST. Crosses show stars identified at the red end of the Grundahl u jump, and all CMDs have been shifted so that the bluest of these stars is at (0,0).

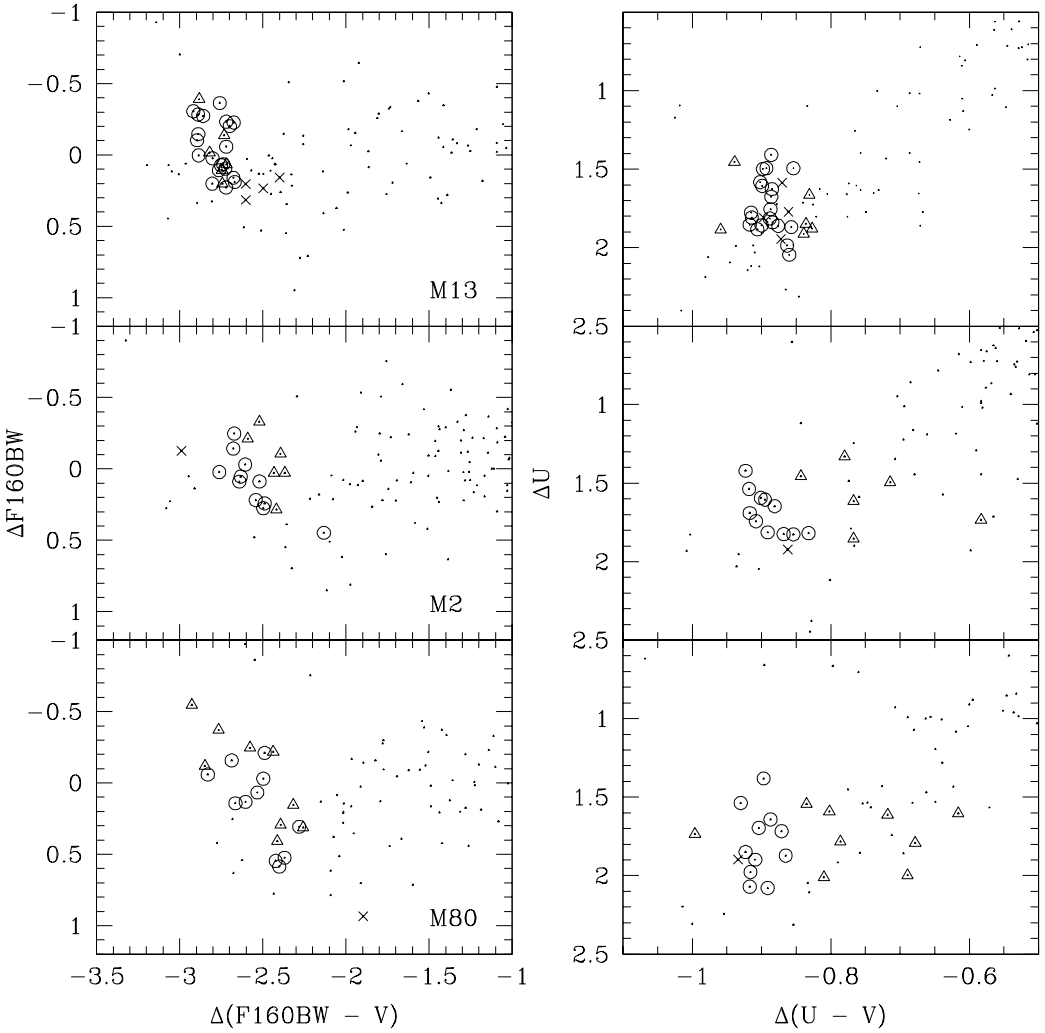

Fig. 27.— Similar to Fig. 26, but zoomed on the blue end of the HB. △ show are stars that were identified in the jump feature in the F160BW filter, × were ones identified in the F336W (U) filter, and ◯ ones that were identified in both.

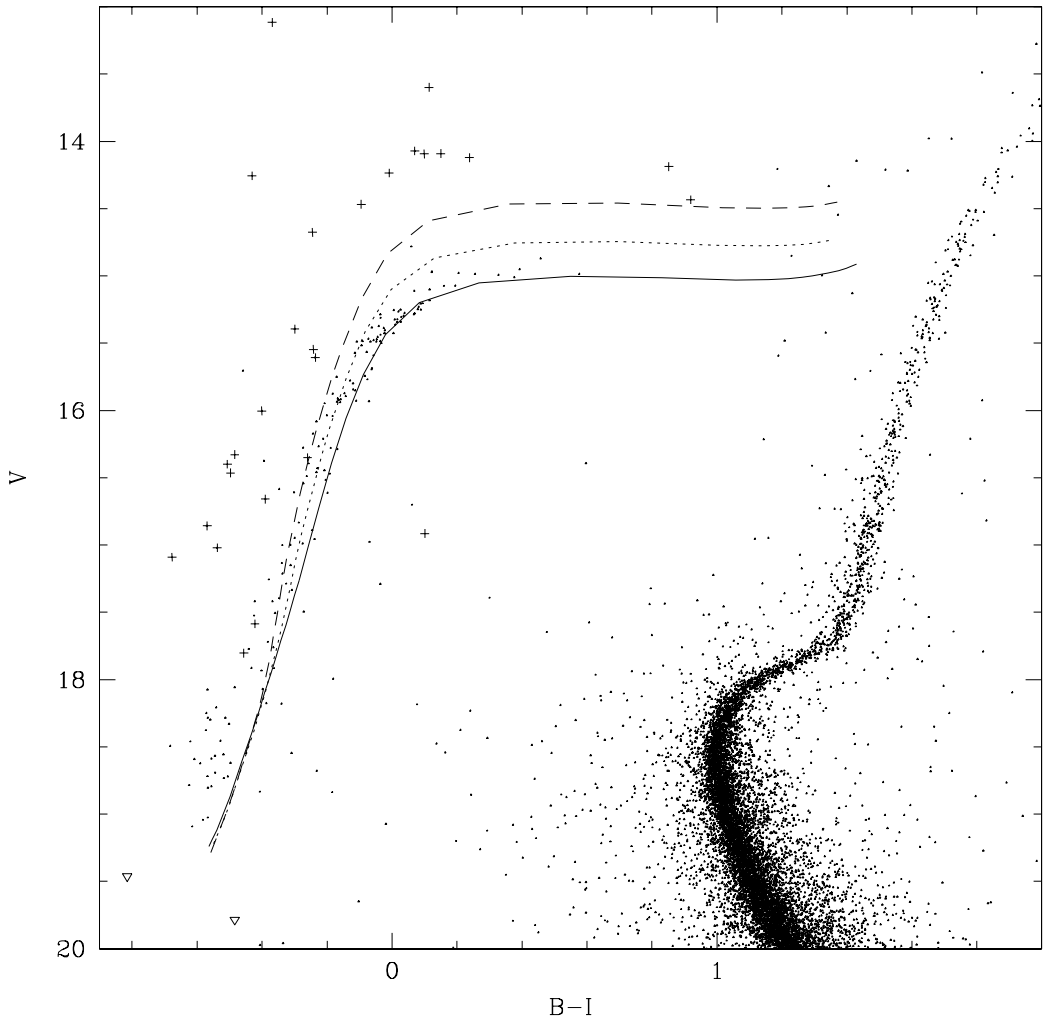

Fig. 28.— Comparison of ground-based CFHT and KPNO photometry ($r > 200''$) with Teramo (Pietrinferni et al. 2006) ZAHB models for $Y = 0.246$ (*solid line*), 0.30 (*dotted line*), and 0.35 (*dashed line*). All ZAHB curves have been shifted by 0.02 in $B - I$, but by 14.45, 14.40, and 14.30 mag respectively in V. Blue hook candidates are shown with $\bigtriangledown$ symbols.

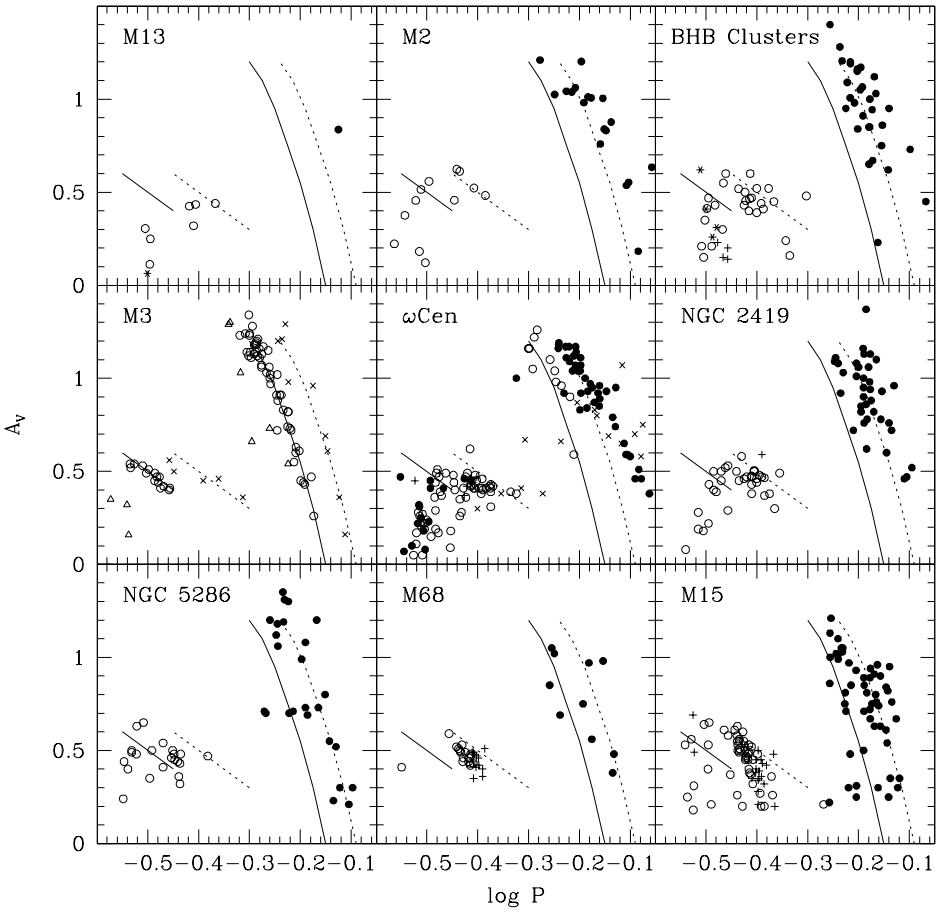

Fig. 29.— Comparison of period-amplitude values for RR Lyrae stars in M3 (Cacciari et al. 2005), M13 (Kopacki et al. 2003), and other Oosterhoff II group clusters. For M3, stars identified as "evolved" (long period / high amplitude) are shown with $\times$, and small amplitude variables are shown with $\triangle$ (among the RRab stars, these are suspected Blazhko variables). For other clusters, fundamental mode pulsators are shown with $\bullet$, first harmonic pulsators have as $\bigcirc$, double-mode pulsators have $+$ (and are plotted with the dominant first overtone period), and non-radial pulsators have $*$. Solid lines are mean relations for regular M3 variables, and dotted lines are mean relations for "evolved M3 variables" (Cacciari et al. 2005). In ω Cen, stars are segregated by magnitude: for $\langle V \rangle > 14.6$, RRab stars have $\bigcirc$ and RRc stars have $\bullet$; for $14.4 < \langle V \rangle < 14.6$, RRab stars have $\bullet$ and RRc stars have $\bigcirc$; and for $\langle V \rangle < 14.4$, all RRab stars have $\times$.

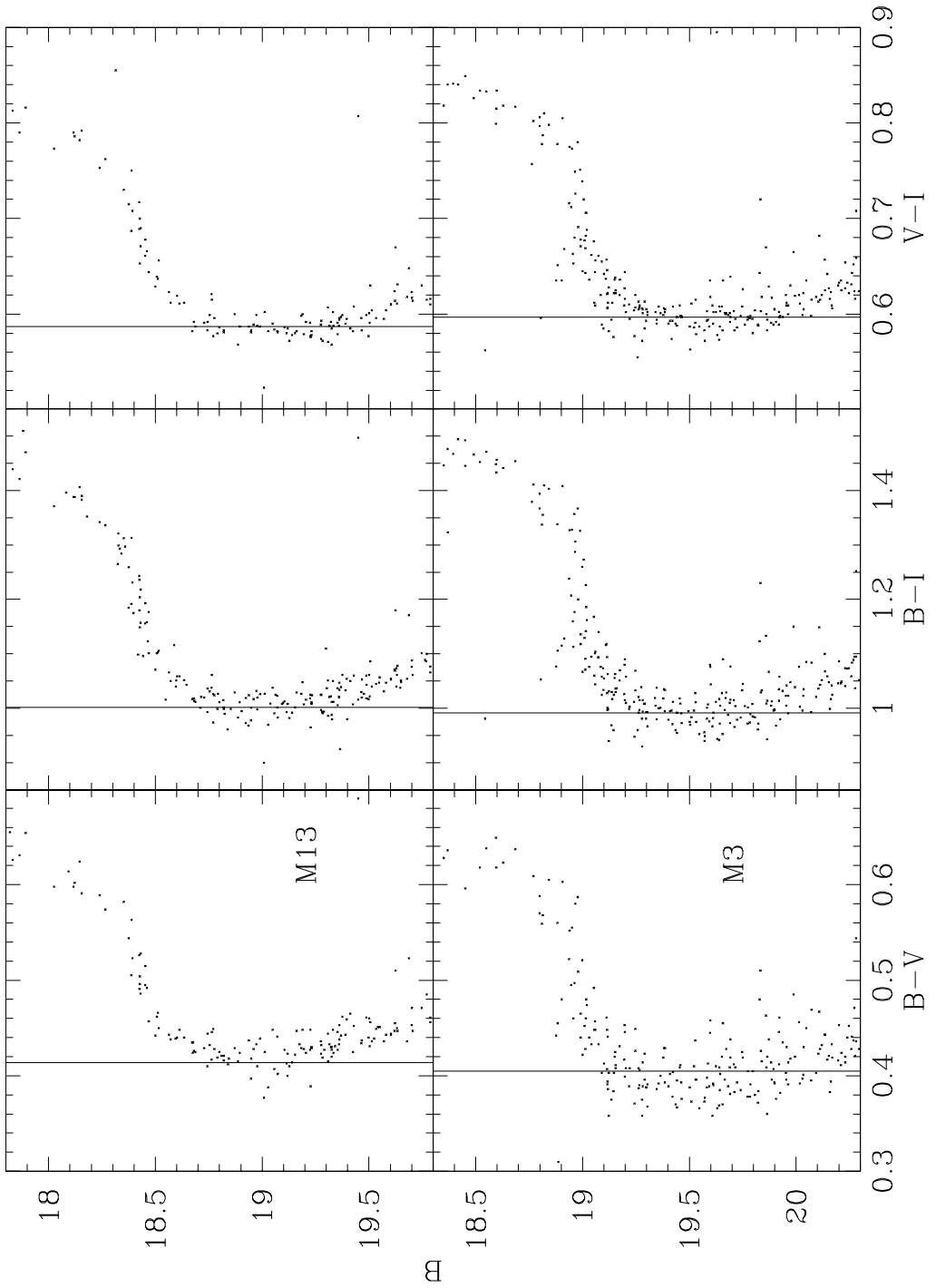

Fig. 30.— Stetson standard star values for M13 and M3 at the cluster turnoff in different optical colors. The vertical lines are the median color values of stars within about 0.2 mag of the cluster turnoff in brightness.

Table 1. Characteristics of M13 and M3

	M13	M3
$[Fe/H]_{CG97}$ [a]	-1.39	-1.34
R_a (kpc) [b]	21.5 ± 4.7	13.4 ± 0.8
R_p (kpc) [b]	5.0 ± 0.5	5.5 ± 0.8
e [b]	0.62 ± 0.06	0.42 ± 0.07
Ψ (deg)[b]	54 ± 5	55 ± 2
L_Z (kpc km s^{-1})[b]	-376 ± 145	705 ± 123
E_{tot} (10^5 km^2 s^{-2})[b]	-0.476 ± 0.088	-0.649 ± 0.022
M_{V_t}[c]	-8.66	-8.65
$\log \rho_0$ ($L_{V_\odot}$pc^{-3})	3.33	3.51
c[c]	2.11	1.56
r_c (pc)[c]	1.7	1.3
r_c ($''$)	46	26
r_h (pc)[c]	3.5	3.7
r_h ($''$)[c]	94	73
d (kpc)[c]	7.7	10.4
E$(B-V)$[d]	0.017	0.013

[a]Carretta & Gratton (1997)

[b]Dinescu et al. (1999)

[c]McLaughlin & van der Marel (2005); power-law models were used for $M_{V,t}$ values

[d]Schlegel et al. (1998)

Table 2: Description of HST data

Proposal ID	Principal Investigators	Filters
5903	Ferraro	F160BW,F255W,F336W,F439W,F555W
8174	van Altena	F555W,F785LP
8278	Bailyn	F555W,F814W
10775	Sarajedini	F606W, F814W

Table 3. Star Cross-Identifications

ID	L ID	K ID	B ID	Flag[a]	Other	Notes
V5	806a	0	0	0	0	RR1; blend in KPNO
V7	344	432	0	0	0	RR1
V8	206	389	0	0	0	RR0; reddest RRLyr
V9	806b	0	0	0	0	RR1
V25	0	0	0	0	0	RR1; evolved? bad sampling?; SIMBAD L630 ID is wrong (nearby RGB)
V31	807	0	1043	0	0	RR1; av affected by blending; BARN201 (blend)
V34	918	0	0	0	0	RR1
V35	571	0	0	0	0	RR1; gap in ACS
V36	0	0	0	0	0	RR2

Note. — Table 3 is published in its entirety in the electronic edition of the Astronomical Journal. A portion is shown here for guidance regarding its form and content. Sources for IDs: L: Ludendorff (1905); K: Kadla (1966); A: Arp (1955); B: Barnard (1931)

[a]UIT Photometry Flag. 0: No UIT detection; 1: Optimal photometry with no likely blending effects; 2: Photometry probably minimally affected by neighbors; 3: Photometry contamination of uncertain magnitude; 4: Photometric contamination certain; 5: Blending of two UIT sources.

Table 4. HB Star Photometry

ID	$\Delta\alpha$	$\Delta\delta$	B	V	I	Source	m_{1620}	σ_{1620}	Flag	F160BW	σ_{160}	F255W	σ_{255}	F336W	σ_{336}	P_{PM}
V5	57.711	1.414	15.252	14.690	14.308	ACS			0			16.180	0.042	15.487	0.004	
V7	−52.404	−67.743	15.283	14.944	14.726	ACS			0			16.196	0.181	15.352	0.005	87
V8	−106.089	25.345	99.999	14.922	14.428	ACS			0							99
V9	58.994	3.471	15.003	14.745	14.363	ACS			0	18.010	0.118	16.231	0.071	15.297	0.003	
V25	14.847	−5.506	14.753	14.589	14.368	ACS			0	17.240	0.100	15.590	0.042	14.954	0.003	
V31	57.728	78.754	99.999	14.890	14.565	ACS			0							99
V35	91.867	−28.731	15.070	14.833	14.579	ACS			0			16.487	0.191	15.143	0.003	
V36	−0.226	10.760	14.834	14.676	14.349	CFHT			0	17.209	0.083	15.999	0.060	15.257	0.004	

Note. — Table 4 is published in its entirety in the electronic edition of the Astronomical Journal. A portion is shown here for guidance regarding its form and content.

Table 5. AGB Star Photometry

ID	$\Delta\alpha$	$\Delta\delta$	B	V	I	Source	m_{1620}	σ_{1620}	Flag	F160BW	σ_{160}	F255W	σ_{255}	F336W	σ_{336}	P_{PM}
1	−612.315	557.213	17.108	17.398	17.725	KPNO	12.83	0.03	1							
2	−403.576	148.486	15.225	15.395	15.524	CFHT	12.84	0.03	1							99
3	−233.816	112.551	16.444	16.659	16.834	CFHT	13.42	0.04	1							
4	−222.956	29.858	14.766	14.144	13.336	CFHT			0							99
5	−184.247	134.084	15.793	16.004	16.194	CFHT	12.96	0.02	1							

Note. — Table 5 is published in its entirety in the electronic edition of the Astronomical Journal. A portion is shown here for guidance regarding its form and content.

Table 6. RGB Star Photometry

ID	$\Delta\alpha$	$\Delta\delta$	B	V	I	Source	F255W	σ_{255}	F336W	σ_{336}	P_{PM}
1	−707.261	7.295	14.373	13.365	12.236	KPNO					99
2	−556.761	489.164	15.380	14.515	13.533	KPNO					99
3	−543.549	−318.220	15.149	14.304	13.285	CFHT					99
4	−468.740	−80.657	15.734	14.968	14.024	CFHT					99
5	−439.069	44.185	15.543	14.739	13.785	CFHT					99

Note. — Table 6 is published in its entirety in the electronic edition of the Astronomical Journal. A portion is shown here for guidance regarding its form and content.

Table 7. Bright Nonmember Star Photometry

ID	$\Delta\alpha$	$\Delta\delta$	B	V	I	Source	P_{PM}
K178	−785.649	−294.677	14.410	13.740		PM	0
K180	−763.792	−269.343	12.280	11.070		PM	0
K185	−725.361	−382.757	15.380	14.700		PM	0
K190	−702.285	186.036	15.784	14.926	14.078	KPNO	0
K196	−664.843	556.797	15.468	14.764	14.019	KPNO	12

Note. — Table 7 is published in its entirety in the electronic edition of the Astronomical Journal. A portion is shown here for guidance regarding its form and content. ID Notes: L: Ludendorff (1905); K: Kadla (1966); CM: Cudworth & Monet (1979); SA, SB: Savedoff (1956); F: this paper.

Table 8. HB Star Distribution

Sample	$I < 16.25$ f_{P1}	$16.25 < I < 18$ f_I	$I > 18$ f_{P2}	$f_{P1} - f_{P2}$
Total	365	197	222	
	0.47 ± 0.02	0.25 ± 0.02	0.28 ± 0.02	0.18 ± 0.02
$r < r_c/2$	25	10	21	
	0.45 ± 0.07	0.18 ± 0.05	0.38 ± 0.06	0.07 ± 0.09
$r < r_c$	82	36	61	
	0.46 ± 0.04	0.20 ± 0.03	0.34 ± 0.04	0.12 ± 0.05
$r_c/2 < r < r_h$	145	80	99	
	0.45 ± 0.03	0.25 ± 0.02	0.30 ± 0.03	0.14 ± 0.04
$r_h < r < 3.5r_h$	157	94	87	
	0.46 ± 0.03	0.28 ± 0.02	0.26 ± 0.02	0.21 ± 0.04
$r > 3.5r_h$	38	13	15	
	0.58 ± 0.06	0.20 ± 0.05	0.23 ± 0.05	0.35 ± 0.08

Table 9. Kolmogorov-Smirnov Test Results for Comparisons with Victoria-Regina RGB Models

M13 Sample				Combined M13 + M5 Sample			
I Cutoff	D	P	N	$I - I_{TRGB}$ Cutoff	D	P	N
13.4	0.080	0.10	232	3.3	0.036	0.46	545
13.2	0.078	0.19	193	3.1	0.040	0.44	460
13.0	0.068	0.45	159	2.9	0.052	0.23	397
12.8	0.098	0.16	130	2.7	0.039	0.69	329
12.6	0.110	0.13	109	2.5	0.048	0.56	273
12.4	0.102	0.25	97	2.3	0.046	0.69	234
12.2	0.093	0.43	86	2.1	0.049	0.72	200
12.0	0.126	0.19	73	1.9	0.073	0.30	171
11.8	0.118	0.40	55	1.7	0.097	0.12	148
11.6	0.139	0.34	44	1.5	0.083	0.40	114
11.4	0.130	0.66	30	1.3	0.087	0.48	91
11.2	0.161	0.58	22	1.1	0.091	0.59	70